الجـــمـــهـــوريـة الجـــــــــزائـريـــة الديمـــــقـراطـيـــة الـشـــعـبـيـــة
**PEOPLE'S DEMOCRATIC REPUBLIC OF ALGERIA**
وزارة التـعـــليـــــم العـــالي و البـــحث العـــلـــمـــي
**Ministry of Higher Education and Scientific Research**
جـــامعة أبي بـكـــر بـلـقـايـد – تـــلمســان –

Abou Bekr Belkaid University – Tlemcen –
Faculty of TECHNOLOGY

**Student Center i2E - University of Tlemcen**

# MASTER'S THESIS

Submitted in Partial Fulfillment of the Requirements for the Degree of Master

**Field** : Mechanical Engineering

**Specialty** : Renewable Energy

**by** : **BEKKAYE Aymen**

**BEKHTI Adem**

**Title**

## Analysis , sizing and manufacturing of an indirect circulation solar air collector for drying agri – food products

Publicly defended on July 6, 2026, before the examination committee composed of:

| | | | |
|---|---|---|---|
| Mr. SAIM Rachid | Pr | University of Tlemcen | President |
| Mr. YOUSFI Sidi Mohammed | MCB | University of Tlemcen | Examiner |
| Ms. OUARRAD Somia | MCB | Expert I2E TLEMCEN | Examiner |
| Mr. KHELLIL Salim | Expert | Environmental consulting firm | Socio-economic Representative |
| Mr. GUELLIL Hocine | MCA | University of Tlemcen | Supervisor |
| Ms. KHALDI Souheyla | MCA | University of Tlemcen | Supervisor |
| Mr. KORTI .A. Nabil | Pr | University of Tlemcen | Co-supervisor |
| Ms. SARI HASSOUN Hind | MAA | University of Tlemcen | Co-supervisor |

Academic year: 2025/ 2026

# Acknowledgments

*First and foremost, I would like to express my deepest gratitude to* ***Allah*** *Almighty, whose infinite mercy, guidance, and blessings granted me the strength, patience, and perseverance to complete this dissertation. Without His grace, this achievement would not have been possible.*

*I would like to express my profound gratitude to my supervisors* ***Mr. Guellil Hocine and Mr. Korti .A. Nabil, Ms. SARI HASSOUN Hind, and Ms. KHALDI Souheyla****, for their invaluable guidance, unwavering support, constructive criticism, insightful advice, and constant encouragement throughout every stage of this research. Their expertise, patience, and dedication have not only contributed significantly to the successful completion of this dissertation but have also enriched my academic and personal development.*

*We would also like to express our sincere gratitude to* ***Mr. SAIM R.****, Professor at the University of Tlemcen, for kindly agreeing to preside over the thesis defense committee.*

*We also extend our sincere thanks to* ***Mr. YOUSFI Sidi Mohammed.****,* ***Ms. OURRAD S.****,* ***Mr. BENRAMDANE M.*** *Lecturers at the University of Tlemcen, and* ***Mr. BENDAHOU M.*** *Technical Director at ALZINC for honoring us by accepting to be a member of the defense committee..*

*My sincere gratitude is also extended to* ***Professor BENRAMDANE Mohammed****, Head of the Department, for his continuous support, encouragement, and dedication to promoting academic excellence. His leadership and commitment to providing a stimulating academic environment have been greatly appreciated throughout my studies.*

*I would also like to express my heartfelt appreciation to all the professors and staff members of the Department of Mechanical engineering for their dedication, professionalism, and for the valuable knowledge, they generously shared throughout my academic journey. Their efforts have played a fundamental role in my education and personal growth.*

*My deepest and most heartfelt gratitude goes to my beloved parents and my family for their unconditional love, endless sacrifices, unwavering faith in my abilities, and continuous encouragement. Their support has been the cornerstone of every success I have achieved and the driving force behind my perseverance.*

# *Dedication*

***In the Name of Allah, the Most Compassionate, the Most Merciful***

*I dedicate this dissertation, first and foremost, to my beloved parents, whose unconditional love, endless sacrifices, unwavering encouragement, and sincere prayers have been the foundation of every step I have taken. Their faith in me has been my greatest source of strength and inspiration, and this achievement is as much theirs as it is mine.*

*I also dedicate this work with deep love and appreciation to my family, especially the* ***Bekkaye Family*** *and the* ***Mahboub Family****, whose affection, encouragement, and constant support have accompanied me throughout my academic journey. Their presence in my life has been a continuous source of motivation and confidence, for which I will always remain profoundly grateful.*

*Finally, I dedicate this humble work to everyone who has inspired me to pursue knowledge with determination, integrity, and perseverance.*

***May this dissertation serve as a humble expression of my gratitude, respect, and appreciation to all those who have stood by my side throughout this journey.***

*Bekkaye Aymen*

# *Dedication*

*I dedicate this humble work to everyone who believed in me and supported me throughout my academic journey.*

*To my beloved parents, my father and my mother, whose unconditional love, endless sacrifices, patience, and constant encouragement have always been my greatest source of strength and motivation. No words can truly express my deep gratitude, respect, and appreciation for everything you have done for me. May God bless you with good health, a long life, and reward you abundantly for your unwavering support.*

*To all my family members, thank you for your love, trust, and continuous support throughout every stage of my life.*

*To everyone who encouraged and supported me, whether near or far, and contributed in one way or another to the completion of this work.*

*I dedicate this humble achievement to all of you with sincere gratitude and appreciation.*

*Bekhti Adem*

# ملخص

تقدم هذه الدراسة عملاً تجريبياً لمقارنة مجمّعين شمسيين للهواء غير مباشري الجريان ، ومصممين لتجفيف الأغذية الزراعية: المجمّع الشمسي التقليدي ذو اللوح المسطح (PSC)، ومجمّع شمسي مبتكر مزود بأنابيب ألومنيوم مرنة (SCT) تم تطويره لتعزيز انتقال الحرارة. أُجريت الاختبارات التجريبية في مختبر (ETAP) بجامعة تلمسان تحت مستويات إشعاع شمسي ومعدلات تدفق هواء مختلفة. وأظهرت النتائج تفوق المجمّع المزود بأنابيب مرنة (SCT) على المجمّع التقليدي (PSC)، حيث حقق متوسط زيادة في درجة حرارة الهواء قدره 2.30 درجة مئوية، وكفاءة حرارية أعلى بنسبة 5.98%.

بناءً على ذلك، تم ربط المجمّع بغرفة تجفيف لتشكيل نظام تجفيف شمسي متكامل يعمل بالحمل القسري غير المباشر. وأُجريت البحوث التجريبية في ظل ظروف مناخية حقيقية بجامعة تلمسان خلال شهر يونيو 2026 لكلا التصميمين (PSC و SCT). وأكدت النتائج التجريبية موثوقية النظام: حيث سجل المجمّع المبتكر (SCT) درجة حرارة للهواء الخارج بلغت 71.3 درجة مئوية، مقارنة بـ 54.8 درجة مئوية للمجمّع التقليدي (PSC)، ما يمثل زيادة في درجة الحرارة بمقدار 16.5 درجة مئوية، كما حقق كفاءة حرارية قصوى بلغت 55.4%، في حين حقق المجمّع التقليدي (PSC) نسبة 33.8%. وتثبت هذه النتائج أن دمج أنابيب الألومنيوم المرنة في مجمّعات الهواء الشمسية يعد حلاً بسيطاً، واقتصادياً، وفعالاً لتعزيز الأداء الحراري لمجمّعات الهواء الشمسية وتحسين الكفاءة العامة لأنظمة التجفيف الشمسية.

**الكلمات المفتاحية:** مجمّع هواء شمسي، التجفيف الشمسي، لوح ماص مستوٍ، أنابيب ألومنيوم مرنة، الكفاءة الحرارية، الطاقة المتجددة.

# Abstract

This work presents an experimental study comparing two indirect forced-convection solar air collectors designed for agricultural food drying: a conventional flat-plate solar collector (PSC) and an innovative solar collector equipped with flexible aluminum tubes (SCT), developed to enhance heat transfer. Experimental tests were conducted at the ETAP Laboratory of the University of Tlemcen under various solar radiation levels and airflow rates. The results showed that the SCT outperformed the PSC, providing an average air temperature increase of 2.30 °C and a 5.98% higher thermal efficiency.

The collector was subsequently coupled with a drying chamber to form a complete indirect forced-convection solar drying system. Experimental investigations were carried out under real climatic conditions at the University of Tlemcen during June 2026 for both configurations (PSC and SCT). The experimental results confirmed the reliability of the system: the SCT achieved an outlet air temperature of 71.3 °C, compared with 54.8 °C for the PSC, corresponding to a temperature gain of 16.5 °C, and reached a maximum thermal efficiency of 55.4%, whereas the PSC achieved 33.8%.

These findings demonstrate that integrating flexible aluminum tubes into solar air collectors is a simple, cost-effective, and efficient solution for enhancing the thermal performance of solar air collectors and improving the overall efficiency of solar drying systems.



**Keywords:** solar air collector, solar drying, smooth absorber plate, flexible aluminum tubes, thermal efficiency, renewable energy.

## Résumé

Ce travail présente une étude expérimentale comparant deux capteurs solaires à air à circulation indirecte destinés au séchage agroalimentaire : un capteur plan conventionnel (PSC) et un capteur innovant à tubes flexibles en aluminium (SCT), conçu pour améliorer les échanges thermiques. Des essais expérimentaux ont été réalisés au niveau du laboratoire ETAP au sein de l'Université de Tlemcen sous différentes conditions de rayonnement solaire et de débit d'air. Les résultats ont montré que le SCT surpasse le PSC, avec une élévation de température de l'air plus élevée de 2,30 °C et un rendement thermique supérieur de 5,98 %.

Le capteur a ensuite été couplé à une chambre de séchage afin de constituer un système complet de séchage solaire indirect à convection forcée. Des essais en conditions climatiques réelles ont été réalisés à l'Université de Tlemcen durant le mois de juin 2026 pour les deux configurations (PSC et SCT). Les résultats expérimentaux confirment la fiabilité du système : le SCT atteint une température de sortie d'air de 71,3 °C (contre 54,8 °C pour le PSC, soit un gain de 16,5 °C) et un rendement thermique maximal de 55,4 % (contre 33,8 % pour le PSC).

Ces résultats prouvent que l'intégration de tubes flexibles en aluminium est une solution simple, économique et efficace pour optimiser les capteurs solaires à air et les systèmes de séchage solaire.



**Mots-clés :** capteur solaire à air, séchage solaire indirect, absorbeur tubulaire, tubes flexibles en aluminium, transfert thermique, rendement thermique, énergie solaire.

# TABLE OF CONTENTS

**GENERAL INTRODUCTION ..... 3**

## CHAPTER I : LITERATURE REVIEW ON SOLAR DRYING AND SOLAR AIR COLLECTORS

**I.1 Introduction ..... 6**

**I.2 Energy Context and Solar Potential in Algeria ..... 6**

**I.3 Fundamentals of Agro-Food Product Drying ..... 7**
I.3.1 Definition of Drying ..... 7
I.3.2 Heat and Mass Transfer Mechanisms ..... 8
I.3.3 Operating Parameters Influencing Drying Kinetics ..... 9
I.3.4 Solar Drying Systems ..... 10

**I.4 Solar Air Collectors (SAC) ..... 12**
I.4.1 Justification for the Selection of an Indirect-Circulation Solar Air Collector ..... 12
I.4.2 General Operating Principle and Components ..... 13
I.4.3 Design Parameters and Operating Conditions ..... 15
I.4.4 Techniques for Enhancing Thermal Performance ..... 16

**I.5 Literature Review: ..... 16**

**I.6 Conclusion: ..... 33**

## CHAPTER II: EXPERIMENTAL PROCEDURES

**II.1 Introduction : ..... 35**

**II.2 Presentation of the Experimental Setup : ..... 35**

**II.3 Description of the Solar Collector : ..... 39**
II.3.1 Construction of the Structure ..... 39
II.3.2 Fan Installation: ..... 40
II.3.3 Absorber Preparation: ..... 40
II.3.4 Glazing Installation ..... 41
II.3.5 Thermocouple positions ..... 41
II.3.6 Final Assembly ..... 41

**II.4 Construction of an Artificial Heat Source ..... 42**

**II.5 Measurement Instruments** ..... **43**
II.5.1 Measurement of Solar Radiation ..... 43
II.5.2 Air Velocity Measurement ..... 44
II.5.3 Temperature Measurement ..... 45
II.5.4 Voltage and Current Controller ..... 46

**II.6 Experimental Procedure** ..... **46**

**II.7 Assembly and Experimental Evaluation of the Solar Drying System** ..... **48**

**II.8 Theoretical analysis:** ..... **50**
II.8.1 The energy Qout: ..... 50

**II.9 Conclusion** ..... **50**

## CHAPTERIII: PARAMETRIC COLLECTOR ANALYSIS

**III.1. Introduction:** ..... **52**

**III.2 Plate solar collector PSC:** ..... **53**
III.2.1 Thermal Behavior of PSC: ..... 53
III.2.2 Thermal efficiency Behavior of PSC: ..... 58

**III.3 Solar air collector with a metallic tubular absorber (SCT)** ..... **62**
III.3.1 Comparative Thermal Performance of Flat-Plate and Tube-Integrated Absorbers ..... 63

**III. 4 Summary of key performance indicators for both configurations** ..... **72**

**III.4 Conclusion** ..... **74**

## CHAPTER IV: THERMAL CAPTURE ANALYSIS

**IV.1 Introduction** ..... **77**

**IV.2 Description of the Experimental Setup** ..... **77**

**IV.3 Experimental Results** ..... **78**
IV.3.1 Diurnal Variation of Solar Irradiance: ..... 78
IV.3.2 Ambient Temperature Evolution: ..... 80

**IV.4 Thermal performance and temperature profile of the solar collector:** ..... **81**
IV.4.1 Diurnal Variation of Collector Component Temperatures: ..... 81
IV.4.2 Comparative Analysis of Temperature Gain and Thermal Efficiency for PSC and SCT Configurations: ..... 84

**IV.5 Conclusion:** ..... **88**

**GENERAL CONCLUSION :** ..... **91**

# LIST OF FIGURES

## Chapter I

Fig I. 1 Typical Drying Curve for Convective Drying ..... 8
Fig I. 2 Types of solar dryers ..... 12
Fig I. 3 Schematic cross-section of a solar air collector (steady-state regime) ..... 13
Fig I. 4 Schematic cross-section of a solar air collector with indirect circulation ..... 14
Fig I. 5 Schematic comparison of the main air circulation configurations in solar air collectors ..... 15
Fig I. 6 Experimental setup used for the validation studies.[11] ..... 17
Fig I. 7 schematic diagram: (1 transparent cover, 2 absorber plate, 3 baffles,4 air duct, 5 iron support, 6 aspirator, 7 bottom plate, 8 in- sulation, 9 inlet, 10 outlet. And Different cases[12]. ..... 18
Fig I. 8 Change in the temperature difference in terms of hours of the day at different mass flows for all cases[12]. ..... 19
Fig I. 9 Proposed design concept of double pass solar air heater with diamond shaped fins.[13] ..... 20
Fig I. 10 Experimental setup components: (a) SAH with Fin Arrangements, (b) Weather Monitoring Station, (c) Outdoor Installation of the SAH Unit, and (d) Data Acquisition System with Data Logger.[14] ..... 21
Fig I. 11 Heat transfer coefficient variation for different mass flow rates.[14] ..... 21
Fig I. 12 (a) Geometry of LHTESS, (b) Computational mesh domain.[15] ..... 22
Fig I. 13 Detailed photographs of the (a) designed collector, (b, c) absorber plate,and (d) thermal energy storage unit.[16] ..... 23
Fig I. 14 (a–c) Illustrative design of fin arrangements with varying inclination angles (30◦, 45◦, and 60◦); (d) indoor experimental setup.[17] ..... 24
Fig I. 15 THPP for different geometries/configurations used in SACs.[18] ..... 26
Fig I. 16 Finned tubes and actual experimental configurations[19]. ..... 27
Fig I. 17 Collectors with cans and with baffles.[20] ..... 27
Fig I. 18 Flexible aluminum air ducts used in the system, a) original and b) painted versions.[21] ..... 28
Fig I. 19 Schematic of the compact indirect sola dryer. The diagram shows key components: (1) glass cover, (2) absorber plate, (3) C-fins, (4) back insulation, (5) dryer chamber, (6) product trays, (7) DC fan [22] ..... 29

Fig I. 20 (a) Schematic diagram of the dryer; (b) Interior of the dryer; (c) Measurement of the product temperature; (d) Dryer under load.[23] ..... 31
Fig I. 21 (a) Schematic diagram of the mixed Mode dryer and indirect Mode dryer [24] ..... 32

## Chapter II

Fig II. 1 Experimental setup of a flat-plate solar collector 45° inclined ..... 37
Fig II. 2 Inlet flat-plate solar collector External face ..... 38
Fig II. 3 Inlet flat-plate solar collector Internal face (4 fans) ..... 38
Fig II. 4 Outlet flat-plate solar collector ..... 38
Fig II. 5 Solar collector diagram ..... 39
Fig II. 6 Internal view of the collector showing the matte black absorber plate and the fans. . 40
Fig II. 7 flexible aluminum tubes ..... 41
Fig II. 8 Solar collector with and without flexible aluminum tubes ..... 42
Fig II. 9 Artificial heat source ..... 43
Fig II. 10 Solarimetre ..... 44
Fig II. 11 Digital Thermo-Anemometer ..... 44
Fig II. 12 Automatic Weather Station ..... 45
Fig II. 13 Type K thermocouple ..... 45
Fig II. 14 Temperature recorder ..... 45
Fig II. 15 Digital Multimeter and Voltage and amperage controller ..... 46
Fig II. 16 Experimental Setup Used in the Laboratory ..... 47
Fig II. 17 Experimental Setup of the Solar Drying System. ..... 49
Fig II. 18 mint leaves ..... 49
Fig II. 19 banana slices ..... **Erreur ! Signet non défini.**

## ChapterIII

Fig III. 1 Temperature Evolution (Tin to Tp1) of PSC as a Function of Time at mass flow rate $\dot{m}$ = 0.015 kg/s and solar irradiance I = 323.55 W/m²) ..... 53
Fig III. 2 Temporal evolution of temperature at a mass flow rate of $\dot{m}$= 0.015 kg/s under different solar irradiance levels (283.7, 323.55, 447.35 and 772.16 W/m²). ..... 55
Fig III. 3 Temporal evolution of temperature at a solar irradiance I= 323.55 W/m² under different mass flow rate (0.01, 0.015, 0.02, 0.025 kg/s ) ..... 57
Fig III. 4 a) Temporal evolution of Thermal efficiency at $\dot{m}$= 0.015 kg/s under different solar irradiance levels (283.7, 323.55, 447.35 and 772.16W/m²), b) Thermal efficiency as a function of irradiance at constant mass flow ..... 59

Fig III. 5 a) Temporal evolution of Thermal efficiency at constant solar irradiance I=323.550 W/m² under different mass flow levels, b) Thermal efficiency as a function of mass flow at constant solar irradiant ..... 61
Fig III. 6 Temporal evolution of the absorber average temperature for the PSC and SCT collectors under two solar irradiation levels (278.15 W/m² and 447.35 W/m²) at a constant mass flow rate of ṁ = 0.015 kg/s ..... 63
Fig III. 7 Temporal evolution of the air temperature rise (ΔT = Tout − Tin) across the PSC and SCT collectors under two solar irradiation levels (278.15 W/m² and 447.35 W/m²) at a constant mass flow rate of ṁ = 0.015 kg/s ..... 64
Fig III. 8 Temporal evolution of the thermal efficiency ηth for the PSC and SCT collectors under two solar irradiation levels (278.15 W/m² and 447.35 W/m²) at a constant mass flow rate of ṁ = 0.015 kg/s. ..... 66
Fig III. 9 Temporal evolution of the absorber average temperature TP for the PSC and SCT collectors under two mass flow rate levels (ṁ = 0.01 kg/s and 0.015 kg/s) at a constant solar irradiation I= 447.35 W/m² ..... 67
Fig III. 10 Temporal evolution of ΔT=Tout-Tin for the PSC and SCT collectors under two mass flow rate levels (ṁ = 0.01 kg/s and 0.015 kg/s) at a constant solar irradiation I= 447.35 W/m² ..... 69
Fig III. 11 Temporal evolution of the thermal efficiency ηth for the PSC and SCT collectors under two mass flow rate levels (ṁ = 0.01 kg/s and 0.015 kg/s) at a constant solar irradiation I= 447.35 W/m² ..... 71

## Chapter IV

Fig IV. 1 Temporal variation of solar irradiance on June 18th, and 22nd, 2026. ..... 78
Fig IV. 2 Ambient temperature profiles for June 17th, 18th, and 22nd, 2026. ..... 80
Fig IV. 3 Temporal evolution of absorber plate, outlet air and ambient temperatures for the PSC on June 18, 2026. ..... 81
Fig IV. 4 Temporal evolution of absorber plate, outlet air, and ambient temperatures for the SCT on June 18, 2026. ..... 83
Fig IV. 5 Daily variation of the temperature difference (ΔT) between PSC and SCT configurations. ..... 85
Fig IV. 6 Temporal variation of thermal efficiency for both SCT and PSC configurations. ... 87

# LIST OF TABLES

## Chapter I

Table I. 1 Optimal Solar Drying Conditions for Typical Algerian Agro-Food Products [6–9]10
Table I. 2 Typical Design Parameters of a Solar Air Collector [10] ..... 16
Table I. 3 comparative results [18] ..... 25
Table I. 4 Energy and Exergy Performance Results [22] ..... 30
Table I. 5 Thermal and Exergetic Performance Results [23] ..... 30
Table I. 6 Thermal Behavior of the Solar Collector [24] ..... 32

## Chapter III

Table III. 1 Comparative Thermal Performance of PSC and SCT Collectors Under Low and High Solar Irradiance Conditions ..... 64
Table III. 2 Comparison of air temperature rise ΔT between PSC and SCT configurations under low and high solar irradiance ..... 65
Table III. 3 Comparison of thermal efficiency ηth between PSC and SCT configurations under low and high solar irradiance ..... 66
Table III. 4 Comparison of thermal efficiency ηth between PSC and SCT configurations under low and high mass flow rate. ..... 72

# Nomenclature

**Latin Symbols:**

Ac: Sensor surface [ $m^2$]

Ap : Absorber plate area[ $m^2$]

Aw: Water activity [0 to 1]

C*p* : Specific heat capacity of the fluid [J/(kg·K)]

$F_R$:Heat removal factor

h or hc : Heat transfer coefficient [W/$m^2$.K]

hm : Mass transfer coefficient

I or G : Solar irradiance (incident radiation) [W/$m^2$]

ṁ : Mass flow rate of the fluid [kg/s]

Pélec : Electric power [W]

Q or Qout : Useful thermal energy output of the collector [W]

Qloss : Thermal losses [W]

Qtot : Total solar energy received by the collector [W]

Re : Reynolds number

t: Time[min]

T : Temperature [°C ]

Tin : Air temperature at collector inlet [°C]

Tout: Air temperature at collector outlet [°C]

Tp: Mean absorber plate temperature [°C]

Tp1: Absorber temperature – lower section [°C]

Tp2: Absorber temperature – middle section [°C]

Tp3:  Absorber temperature – upper section [°C]

ΔT:  Difference in air temperature between the inlet and outlet of the chamber [°C]

X: Moisture content [kg water / kg dry matter]

**Greek Symbols:**

η: Efficiency (general) [%]

ηc  : Collector thermal efficiency [ %]

ηex,evap: Process exergy efficiency[ %]

ηth : Thermal (energy) efficiency of the collector  [%]

**Abbreviations & Acronyms:**

BA13: Standard gypsum board (plasterboard, 13 mm thickness)

CFD: Computational Fluid Dynamics

COP: Coefficient of Performance

DC: Direct Current

DPSAH: Double Pass Solar Air Heater

ETAP: Energétique et Thermique Appliquées (Research Laboratory, University of Tlemcen)

kWh/m² Solar Energy per Unit Area [kWh/m²]

LHTESS : Latent Heat Thermal Energy Storage System

MW: Megawatt [ MW]

PCM : Phase Change Material

PSC : Plate Solar Collector (conventional flat-plate design)

PVT : Photovoltaic-Thermal Collector

SAC : Solar Air Collector

SAH : Solar Air Heater

SCT : Solar air Collector with Tubes (tube-integrated absorber design)

SI : Sustainability Index

THPP: Thermo hydraulic Performance Parameter

UV : Ultraviolet Radiation

WER : Waste Exergy Ratio

# GENERAL INTRODUCTION

## General Introduction

Today, humanity faces a dual challenge: meeting a constantly growing global energy demand while reducing the greenhouse gas emissions responsible for climate change. In this context, renewable energies are increasingly establishing themselves as an essential alternative to fossil fuels, whose reserves are dwindling and whose exploitation generates considerable environmental impacts. Algeria, a country whose economy has historically relied on hydrocarbons, is gradually becoming aware of the need to diversify its energy mix. With an annual sunshine duration that can reach 3,900 hours on the high plateaus and in the Sahara, and a global horizontal solar radiation exceeding 5.6 kWh/m²/day in the Far South,

The country possesses one of the most generous solar potentials in the world. The Tlemcen region, in the northwest of the country, benefits from an annual irradiation of 1,800 to 2,000 kWh/m² and 2,600 to 2,800 hours of sunshine per year, making it a particularly favorable site for the deployment of solar thermal systems. In parallel with this energy challenge, the Algerian agri-food sector faces considerable post-harvest losses, estimated at nearly 50% for fruits and vegetables due to a lack of sufficient storage and processing infrastructure.

In this context, solar drying appears to be a solution that is both economically accessible and ecologically responsible, allowing for the valorization of local agricultural production while reducing dependence on conventional energy sources. Solar air collectors, due to their simple design, low operating cost, and versatility of application, represent the technological core of these drying systems. It is within this perspective that this thesis is framed, the objective of which is to design, manufacture, and experimentally evaluate a single-pass solar air collector intended to be integrated into an indirect solar drying system for processing agri-food products. Particular attention is paid to improving the thermal performance of the collector by integrating flexible aluminum tubes onto the absorbing surface, aiming to increase the convective exchange area and promote turbulence in the air flow.

This work is structured around four complementary chapters: The first chapter lays the theoretical and bibliographical foundations of the study. It provides a state-of-the-art overview of solar drying and solar air collectors, analyzing the Algerian energy context, the

heat and mass transfer mechanisms involved in agri-food drying, and the main techniques for improving the thermal performance of solar collectors identified in recent scientific literature.

The second chapter is dedicated to the description of the experimental setup. It presents in detail the design and fabrication of the solar air collector within the ETAP laboratory at the University of Tlemcen, the measurement instruments deployed, the artificial radiation source used for laboratory tests, as well as the experimental protocol implemented for the two studied configurations: the plane absorber collector (PSC) and the collector equipped with aluminum tubes (SCT).

The third chapter presents the experimental results obtained under controlled laboratory conditions. It provides a comparative analysis of the thermal performance of the two collector configurations (PSC) and (SCT) by studying the influence of incident solar radiation and mass air flow rate on the absorber temperature, the air temperature rise, and the thermal efficiency of each system.

The fourth and final chapter is dedicated to experimental validation under real outdoor conditions. The collector is coupled to a drying chamber and subjected to natural weather conditions during measurement campaigns conducted over three days in June 2026. A thorough comparative thermodynamic analysis of the two configurations is presented, integrating the diurnal evolution of solar irradiance, the temperature profiles of the components and the instantaneous thermal efficiency.

# CHAPTER I

# LITERATURE REVIEW ON SOLAR DRYING AND SOLAR AIR COLLECTORS

## I.1 Introduction

Before presenting the fundamental principles of solar drying and the technical characteristics of the solar air collector investigated in this study, it is essential to place this work within its energy, environmental, and socio-economic context. This chapter first outlines Algeria's energy situation and the growing role of renewable energy in the country's energy transition strategy. It then highlights the country's abundant solar resource, with particular emphasis on the selected study site. Finally, it discusses the challenges associated with post-harvest losses of agricultural products and emphasizes the importance of solar drying as a sustainable solution for their preservation and valorization.

## I.2 Energy Context and Solar Potential in Algeria

Algeria is currently at a critical turning point in its energy transition. Its economy relies heavily on hydrocarbons, which accounted for 47% of government revenues and 86% of export earnings between 2019 and 2023, while more than 99% of the country's energy production and consumption is supplied by fossil fuels. Faced with the gradual depletion of these resources and the growing demands of the global energy transition, the Algerian government has adopted an ambitious renewable energy development program, revised in 2015 and elevated to the status of a national priority in 2016. The program aims to install 22,000 MW of renewable energy capacity by 2030 to meet domestic energy demand, with the objective of generating 27% of the country's electricity from renewable sources. Within this strategy, solar energy occupies a central position. Given that Algeria's renewable energy potential is overwhelmingly dominated by solar radiation, the country considers solar energy a major opportunity and a key driver of economic and social development [1].

This ambition is supported by one of the world's most abundant solar resources. The annual sunshine duration exceeds 2,000 hours across almost the entire country and can reach up to 3,900 hours on the High Plateaus and in the Sahara Desert. Meanwhile, the annual solar energy received on a horizontal surface of one square meter is approximately 3 kWh/m²/day in the northern regions and exceeds 5.6 kWh/m²/day in the Great South. The Tlemcen region, located in northwestern Algeria, benefits from an annual global horizontal irradiation of approximately 1,800–2,000 kWh/m² and a yearly sunshine duration ranging from 2,600 to 2,800 hours. These favorable climatic conditions make the region particularly well suited for the deployment of solar thermal systems for industrial and agro-industrial applications [2].

It is precisely in this sector that the potential for harnessing solar energy is both the most immediate and the least exploited. The Algerian agri-food sector faces considerable post-harvest losses. Across Africa, fruits and vegetables experience the highest loss rates, reaching approximately 50% of total production, a situation that also characterizes Algeria due to the lack of adequate storage and processing infrastructure. Although conventional industrial dryers powered by natural gas, fuel oil, or electricity effectively extend the shelf life of agricultural products, they involve high energy consumption and significant environmental impacts, making them incompatible with the country's objectives of energy efficiency and sustainable development.

Solar drying therefore emerges as an affordable and sustainable alternative, suitable for both rural micro-entrepreneurs and small and medium-sized enterprises (SMEs). It offers an attractive return on investment while enabling shared management through agricultural cooperatives. Consequently, harnessing Algeria's abundant solar resource for agro-food drying represents a technical, economic, and social solution to the challenges of sustainable rural development [3].

## I.3 Fundamentals of Agro-Food Product Drying

### I.3.1 Definition of Drying

Drying is a unit operation that consists of removing, totally or partially, the water contained in a product through evaporation, generally by the combined action of heat and an airflow. It is one of the oldest and most widely used preservation techniques, particularly suited to agro-food products such as fruits, vegetables, aromatic and medicinal plants, and cereals.

The moisture state of a product is characterized by two complementary parameters: the moisture content, X (kg of water per kg of dry matter), which quantifies the amount of water present, and the water activity, Aw (ranging from 0 to 1), which reflects the availability of water for biochemical reactions and microbial growth. The primary objective of drying is to reduce both parameters below their critical thresholds. A water activity below 0.6 inhibits the growth of nearly all microorganisms, while a final moisture content of 10–15% ensures satisfactory stability for long-term storage without refrigeration [4].

### I.3.2 Heat and Mass Transfer Mechanisms

Convective drying of an agro-food product results from two simultaneous and coupled transfer processes: heat transfer from the hot air to the product, which supplies the energy required for water evaporation, and mass transfer of moisture from the product to the surrounding air, which removes the generated water vapor.

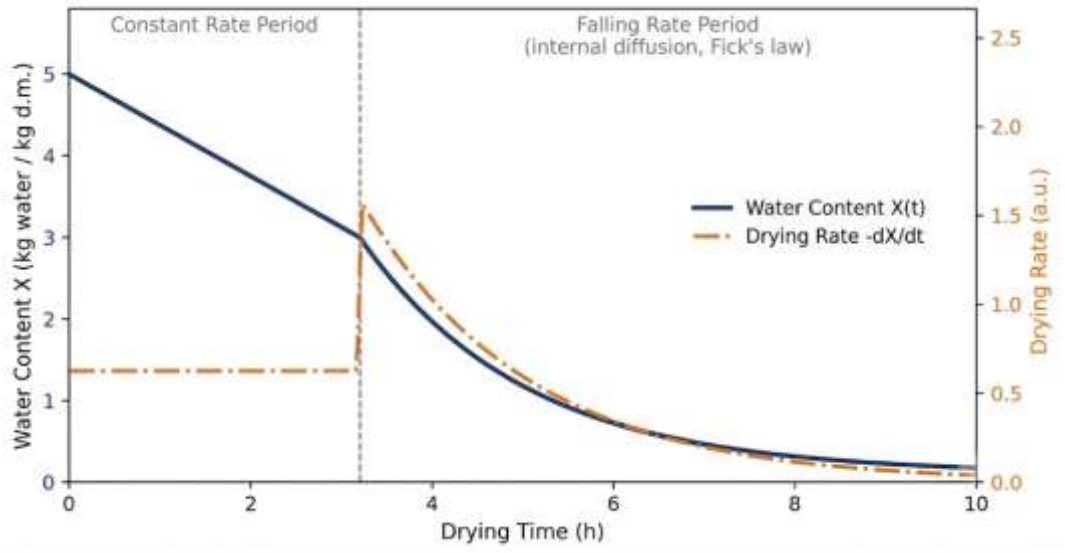



***Fig I. 1 Typical Drying Curve for Convective Drying***

The kinetics of this process are conventionally represented by the drying curve (Fig 1.1) [5]. Two characteristic drying periods are generally distinguished:

- Constant-rate drying period: During this stage, the free water present on the product surface evaporates at a rate controlled by the external drying conditions, namely the air temperature, relative humidity, and velocity. Under these conditions, the product behaves similarly to a free water surface.
- Falling-rate drying period: This stage begins when the migration of internal moisture to the product surface can no longer compensate for surface evaporation. The drying process then becomes controlled by the internal diffusion of bound water through the solid matrix.

### I.3.3 Operating Parameters Influencing Drying Kinetics

The drying rate and quality of solar drying are governed by five main operating parameters: air temperature, relative humidity, air velocity, product slice thickness, and the physicochemical properties of the product. These parameters strongly interact with one another, making a multi-objective optimization approach more appropriate than adjusting each factor independently.

a) Air temperature

Air temperature is the most influential parameter affecting drying kinetics. It accelerates both surface evaporation and the internal diffusion of moisture by increasing the kinetic energy of water molecules and reducing air viscosity.

b) Relative humidity

Relative humidity is the second most important parameter and, in some cases, may have a greater influence than solar irradiance itself. It directly determines the evaporation potential of the drying air: the drier the air, the greater its moisture-removal capacity.

c) Air velocity

Air velocity mainly affects the external convective heat and mass transfer coefficient between the drying air and the product surface, thereby influencing the duration of the constant-rate drying period.

d) Slice thickness

The thickness of the product directly determines the internal moisture diffusion path and, consequently, the duration of the falling-rate drying period, in accordance with Fick's law, according to which the drying time is proportional to the square of the diffusion distance (i.e., the slice thickness).

e) Product nature and structure

Each agro-food product possesses specific cellular structures, an initial moisture content, and a unique biochemical composition, all of which determine its drying behavior and response to the drying process.

***Table I. 1*** *Optimal Solar Drying Conditions for Typical Algerian Agro-Food Products [6–9]*

| Product | Optimal Temperature | Optimal Air Velocity | Recommended Thickness | Reference / Key Result |
|---|---|---|---|---|
| Tomato | 60–70°C (up to 68°C in parabolic dryer) | 1.0–1.5 m/s | 4–6 mm | Final moisture content 6% at 4 mm / 1.0 m/s; drying time reduced by 40% through relative humidity control |
| Fig | 55–65°C (up to 80°C at high flow rate) | Flow rate 150–300 $m^3/h$ | Whole slices or halved | Drying time reduced to 200 min at 80°C / 300 $m^3/h$, with preserved physical quality |
| Chilli / Red Pepper | 50–60°C | 1.3–1.5 m/s | 3 mm slices | Optimal velocity 1.31–1.5 m/s for maximum extractable colour |
| Apricot | 55–65°C | 0.01–0.015 kg/s (mass flow rate) | 5–8 mm slices | Collector efficiency 45.6–56.8% with matt black painted absorber |
| Orange / Citrus *(supplementary reference)* | 50–60°C | Adaptive natural/forced convection | 4 mm (optimum) | $D_{eff}$ 4.5–15 × $10^{-8}$ $m^2/s$; 48% reduction in drying time at 4 mm vs 8 mm |

### I.3.4 Solar Drying Systems

#### a) Direct Solar Drying

In a direct solar dryer, the product is exposed directly to solar radiation, usually beneath a transparent cover that creates a greenhouse effect and enhances water evaporation. This configuration offers the advantages of simple construction and very low cost. However, it also has several significant drawbacks, including the risk of localized overheating, degradation of pigments and vitamins due to direct ultraviolet (UV) exposure, possible contamination by dust

or insects if the enclosure is not perfectly sealed, and complete dependence on prevailing weather conditions.

**b) Indirect Solar Drying**

In an indirect solar dryer, ambient air is heated by a separate solar air collector and then conveyed to an independent drying chamber containing the product. The product is therefore never directly exposed to solar radiation. This separation between the heat collection unit and the drying chamber allows much better control of the drying air temperature, effective protection against insects and adverse weather conditions, and significantly improved sanitary and organoleptic quality of the dried product.

**c) Mixed and Hybrid Solar Drying**

Mixed solar dryers combine the two previous modes by exposing the product partially to direct solar radiation while simultaneously supplying preheated air from a separate solar collector. Hybrid solar dryers, on the other hand, integrate a solar drying system with an auxiliary energy source, such as an electric heater or biomass burner, to ensure continuous drying during periods of low solar radiation or at night.

**d) Active and Passive Solar Dryers**

Solar dryers can also be classified according to the method used to circulate the drying air. In passive solar dryers, air circulation occurs solely through natural convection, driven by the density difference between warm and cool air (the stack effect or chimney effect). Although this solution is inexpensive and does not require any auxiliary energy source, it generally provides low and variable airflow rates that strongly depend on weather conditions. In active solar dryers, a fan provides forced air circulation, allowing precise control of the airflow rate, more uniform temperature distribution within the drying chamber, and a significant reduction in the overall drying time.

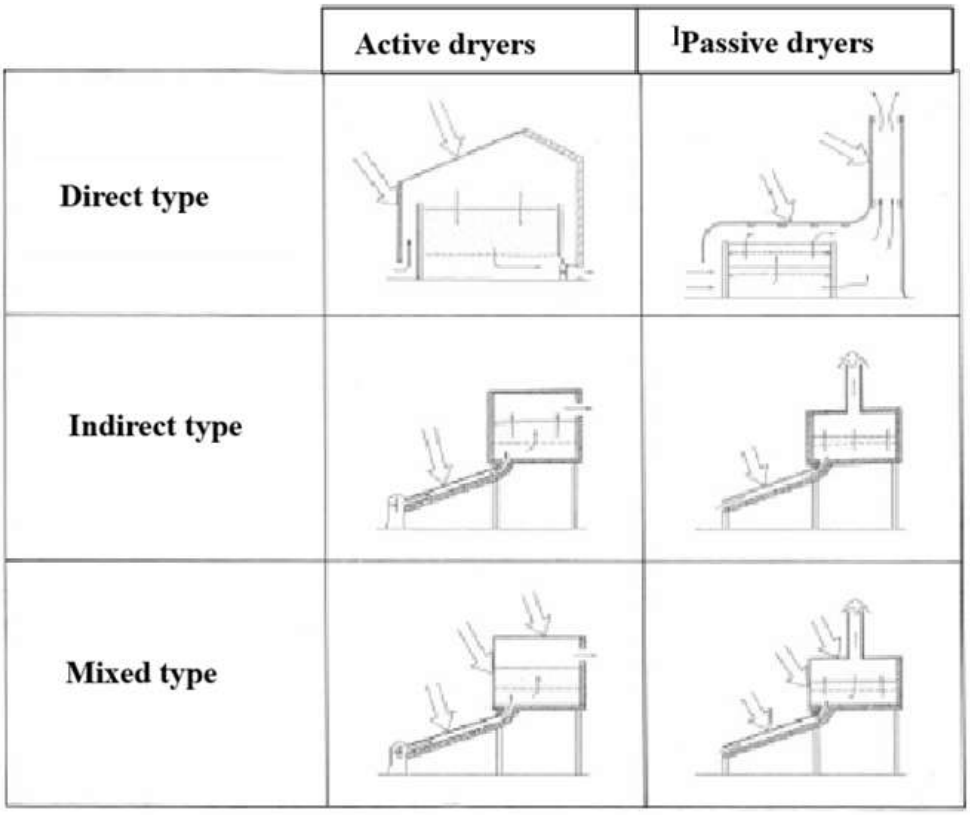



***Fig I. 2 Types of solar dryers***

## I.4 Solar Air Collectors (SAC)

### I.4.1 Justification for the Selection of an Indirect-Circulation Solar Air Collector

The convergence of several factors—namely the promotion of solar thermal energy applications, the abundance of solar resources at the selected study site, and the significant post-harvest losses associated with conventional drying methods—justifies the choice of an indirect solar air dryer. This technology offers several advantages. It protects agricultural products from direct solar radiation and external contamination, thereby preserving their quality. The use of air as the heat transfer fluid simplifies the system design and reduces maintenance costs. In addition, forced air circulation provides better control of the drying conditions and ensures greater process uniformity. Finally, the system is based on simple, low-cost materials that are readily available locally, making it particularly suitable for the local context.

### I.4.2 General Operating Principle and Components

A solar air collector is a flat-plate heat exchanger that absorbs the incident solar radiation and transfers the captured thermal energy to a flowing stream of air (Fig. I.3).

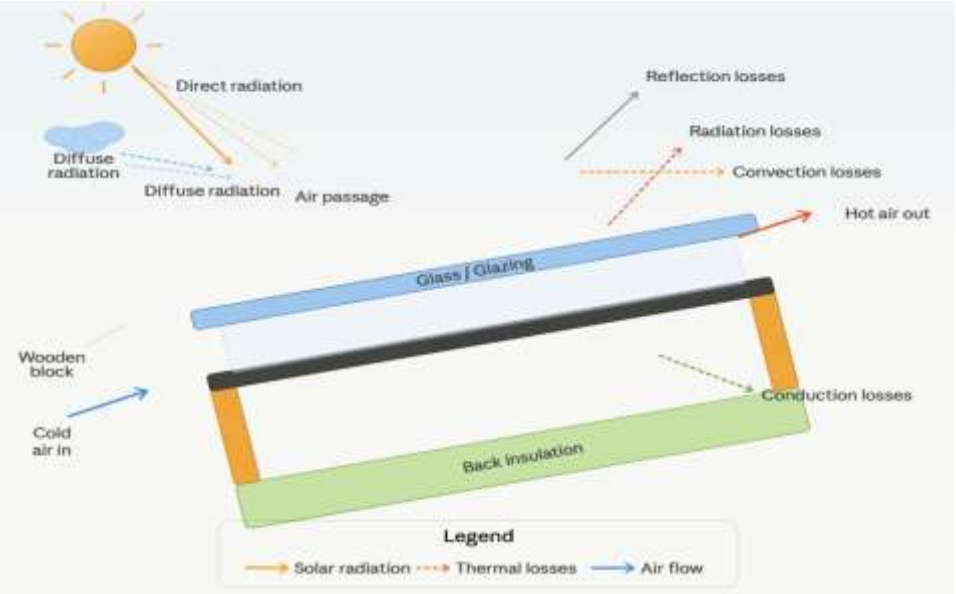



***Fig I. 3 Schematic cross-section of a solar air collector (steady-state regime)***

A solar air collector consists essentially of four functional components: a transparent glazing, which reduces convective heat losses to the surroundings while creating a greenhouse effect; an absorber, generally a flat metal sheet coated with a matte black surface, which converts incident solar radiation into thermal energy; an air channel, through which the heated air is conveyed to the intended application; and thermal insulation located at the back and along the sides of the collector to minimize conductive heat losses to the ambient environment (Fig. I.4).

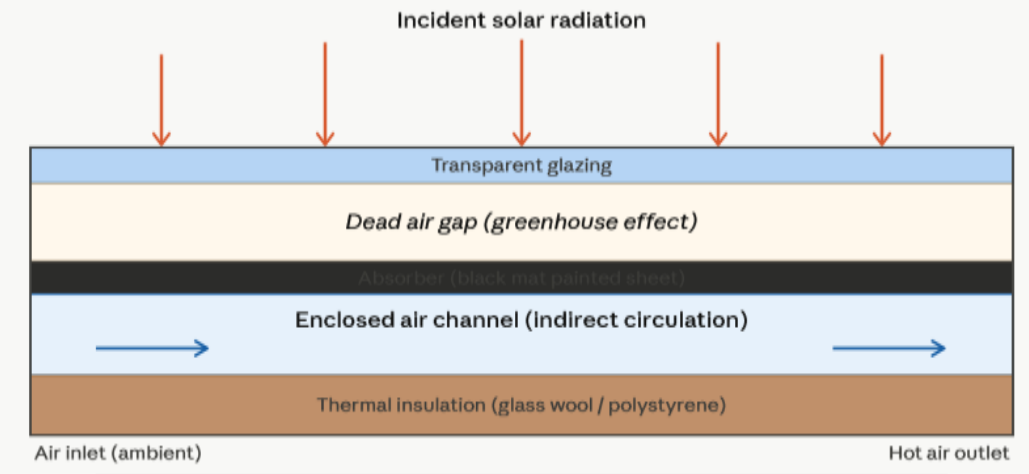



***Fig I. 4 Schematic cross-section of a solar air collector with indirect circulation***

Solar air collectors are commonly classified into three main configurations (Fig. I.5):

**a) Single-Pass Solar Air Collector**

In a single-pass solar air collector, the air flows through a single channel, either between the glazing and the absorber plate or between the absorber plate and the insulation. The underflow configuration, in which the air passes beneath the absorber, is generally considered the most efficient because it provides better heat transfer and reduces thermal losses. According to the literature, the thermal efficiency of single-pass collectors typically ranges from 30% to 55%, depending on the operating conditions.

**b) Double-Pass Solar Air Collector**

In a double-pass solar air collector, the air flows successively above and below the absorber plate. This double-pass arrangement increases the contact time between the air and the heated surfaces, thereby enhancing heat transfer and improving the collector's thermal efficiency. Several studies have reported significant performance improvements compared with single-pass collectors, with thermal efficiencies reaching up to 65%.

**c) Indirect-Flow Solar Air Collector**

An indirect-flow solar air collector employs a closed air duct that allows the air to circulate without direct contact with the absorber plate. This configuration provides improved sanitary safety by preventing any contamination of the product being dried. Although its heat transfer

performance is slightly lower than that of direct-contact systems, this limitation can be compensated for through appropriate collector sizing and optimization of the air duct design.

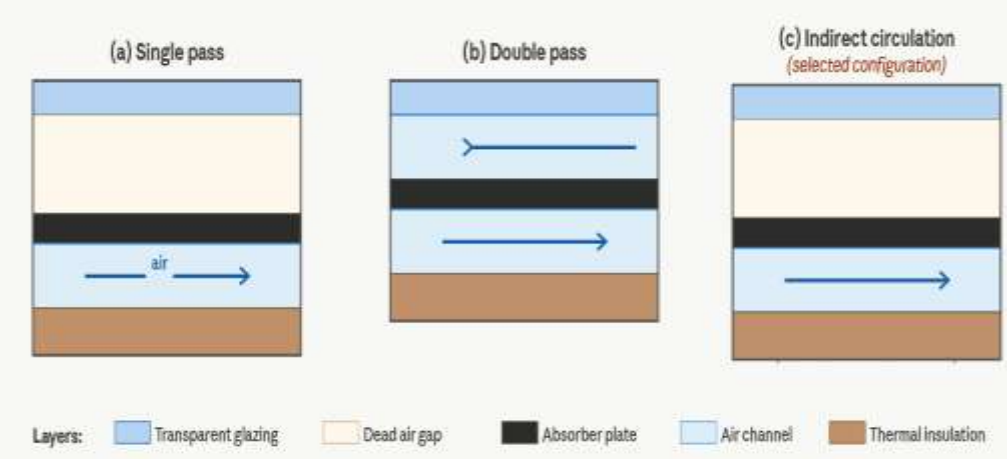



***Fig I. 5 Schematic comparison of the main air circulation configurations in solar air collectors***

### I.4.3 Design Parameters and Operating Conditions

The performance of a solar air collector depends on both the climatic conditions at the installation site and the collector's design parameters. Table 1.4 summarizes the main design and operating parameters commonly reported in the literature, together with their typical ranges. These values will serve as a reference for the design decisions adopted during the sizing procedure presented in Chapter 2.

***Table I. 2 Typical Design Parameters of a Solar Air Collector [10]***

| Parameter | Usual Range | Remark |
|---|---|---|
| Incident Solar Flux | 0 to 1200 W/m² | Primary energy source, variable according to time of day and season |
| Tilt Angle | 35° to 45° | Optimized according to site latitude to maximize solar energy capture |
| Orientation | Due South | Minimizes shading and maximizes daily solar exposure |
| Typical Dimensions | ≈ 2 m × 1 m | Compromise between thermal uniformity and space requirements |
| Air Gap (absorber–glazing) | 5 to 10 cm | Allows air circulation and insertion of baffles |
| Baffles / Fins | Variable according to design | Increase turbulence and convective heat transfer coefficient |
| Fan | Forced convection | Enables precise and reproducible control of air flow rate |
| Absorber Coating | Matt black paint or selective coating | Maximizes absorptivity α and minimizes emissivity ε |

### I.4.4 Techniques for Enhancing Thermal Performance

Several approaches can be employed to improve the thermal performance of solar air collectors. Geometric modifications, such as the incorporation of artificial roughness, fins, or baffles, enhance convective heat transfer by increasing both airflow turbulence and the heat transfer surface area. The radiative properties of the absorber can also be improved through the use of selective coatings, which reduce thermal losses. However, matte black paint remains the most widely used solution in low-cost systems because of its simplicity, low cost, and high solar absorptivity. Finally, the choice of glazing has a direct impact on the collector's thermal efficiency. Single glazing is the most economical option, whereas tempered glass, double glazing, and multiwall polycarbonate glazing provide greater reductions in heat losses, although at a higher cost.

## I.5 Literature Review:

In their study, N. Madhwesh et al. [11] investigated improving the thermal performance of a solar air heater by adding capsule-shaped flow enhancers to the absorber

plate. The study aimed to improve heat transfer by creating disturbance in the laminar sublayer formed within the air duct, which typically reduces the heat transfer coefficient.

Numerical analysis was performed using various Reynolds numbers, ranging from 3000 to 21000, with the flow enhancer orientation angle varying from 0° to 90°. The results showed that a 45° orientation angle achieved the best overall thermal performance, while larger angles increased flow resistance and pumping force. Additionally, the effects of the number of flow enhancer rows, spacing ratio, and height ratio were investigated to determine the optimal configuration.

The study revealed that a two-row flow enhancer configuration, with a spacing ratio of 0.05 and a height ratio of 0.006, achieved the highest thermal improvement. Compared to a conventional smooth collector, the optimized design resulted in an overall thermal performance improvement of approximately 15.76% and an increase in available energy efficiency of approximately 52.64%.

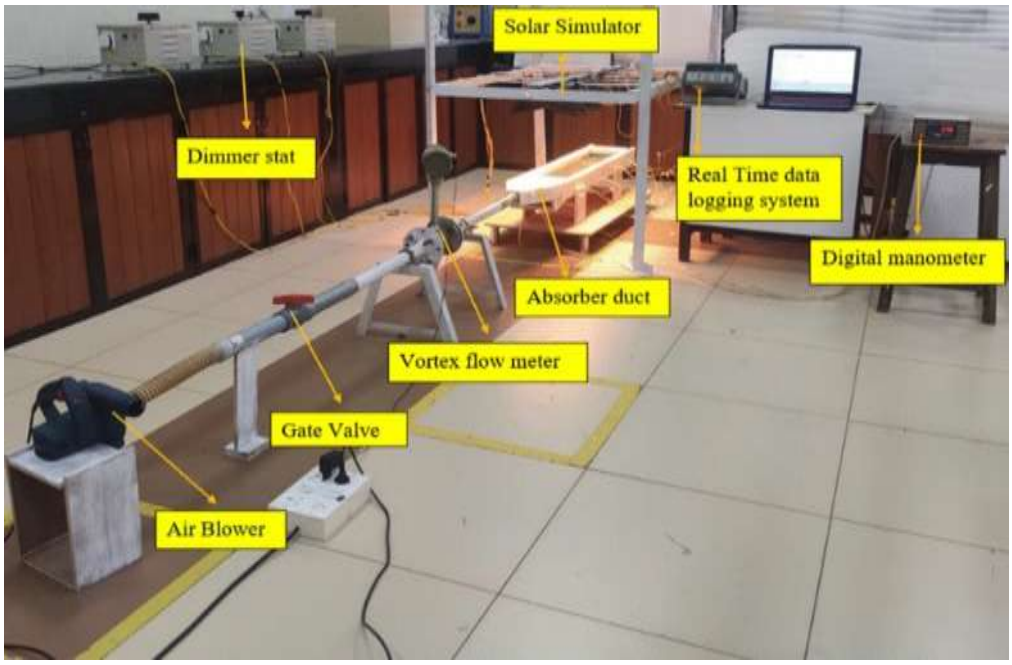



***Fig I. 6 Experimental setup used for the validation studies.[11]***

In their work, C. Foued et al. [12] experimentally investigated the effect of rectangular baffles on the thermo-hydraulic performance of a solar thermal collector under moderate weather conditions. Six different configurations were analyzed, including several baffled arrangements and a smooth plate used as a reference case.

The results demonstrated that the number and positioning of the baffles have a significant influence on heat transfer enhancement and overall thermal performance. Among the tested configurations, cases IV and V exhibited the best heat transfer characteristics, reaching maximum heat transfer coefficients of 15.84 W/m²·K and 17.46 W/m²·K, respectively. The study also revealed that heat transfer is more intense at the entrance of the channel and gradually decreases along its length.

Furthermore, the highest thermal efficiency was achieved in the 18M135 configuration, with a maximum efficiency value of 0.73, confirming the positive effect of rectangular baffles on

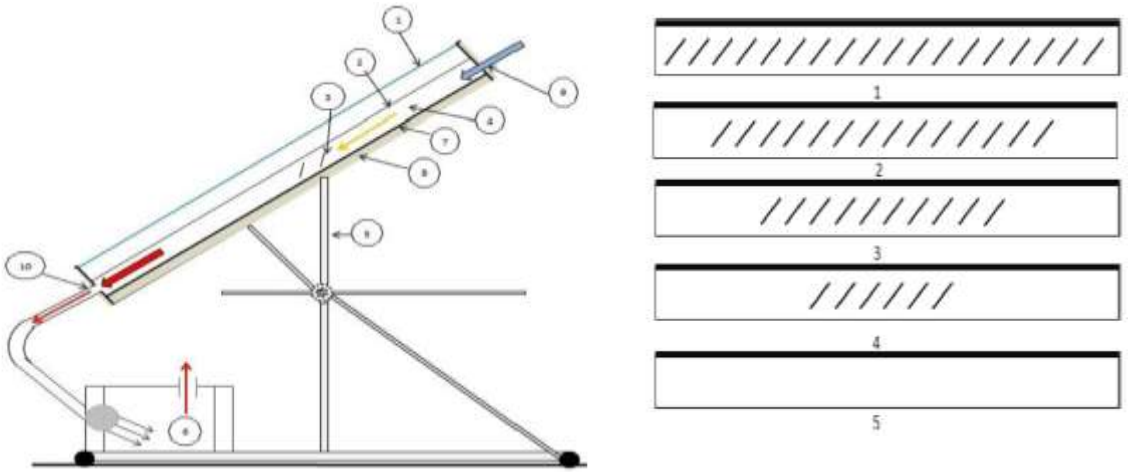



***Fig I. 7 schematic diagram: (1 transparent cover, 2 absorber plate, 3 baffles,4 air duct, 5 iron support, 6 aspirator, 7 bottom plate, 8 in- sulation, 9 inlet, 10 outlet. And Different cases[12].***

improving the thermal behavior of solar collectors.

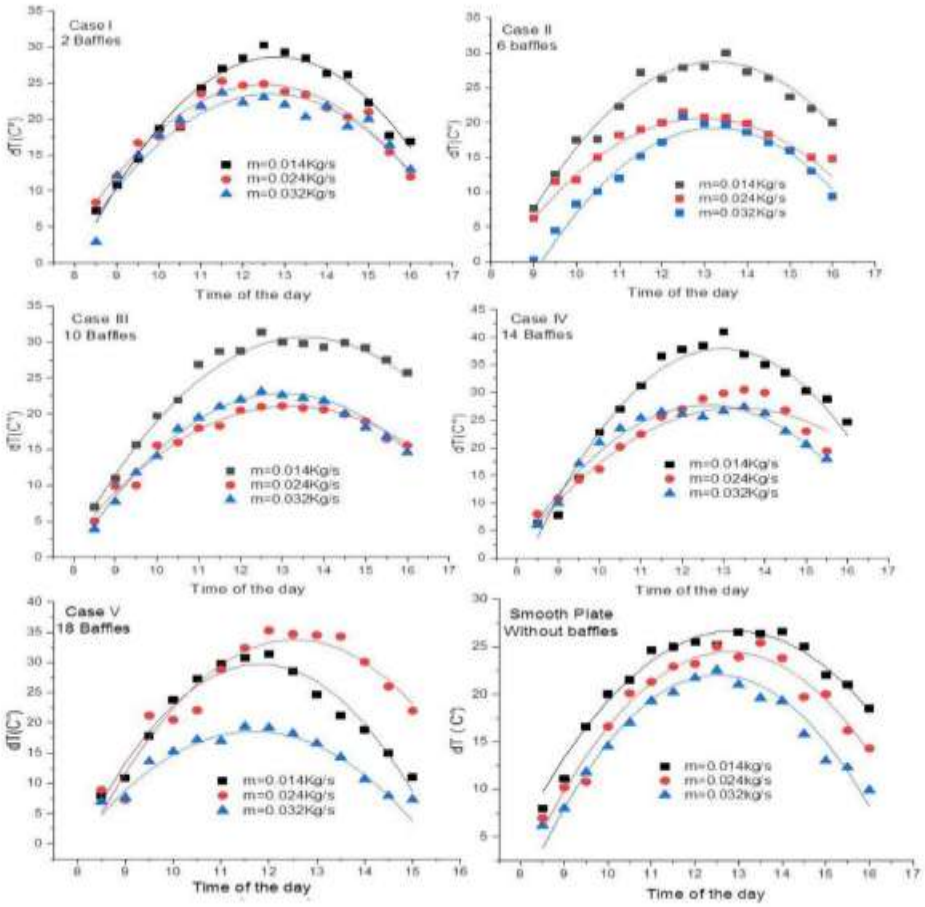



***Fig I. 8 Change in the temperature difference in terms of hours of the day at different mass flows for all cases[12].***

N.J. Yusaidi et al. [13] conducted a theoretical and experimental study on the performance of a dual-path solar air heater with diamond-shaped overlapping fins. The study aimed to enhance convection heat transfer and improve the heater's thermal efficiency by incorporating specially designed fins mounted on the absorber plate.

Forty diamond-shaped fins were mounted on the absorber plate, and various mass flow rates and solar irradiance intensities were tested to evaluate their impact on system performance. Numerical simulations using COMSOL Multiphysics 5.6.1 software were performed to analyze the fluid flow and thermal behavior prior to the experimental study.

The results showed that both the mass flow rate and solar irradiance intensity significantly affect the outlet temperature and the overall system efficiency. The highest thermal efficiency achieved was 59.34% experimentally and 62.01% numerically at a mass flux rate of 0.0261

kg/s and a solar irradiance of 1000 W/m², confirming the effectiveness of the diamond-shaped overlapping fins in improving the thermal performance of the DPSAH system.

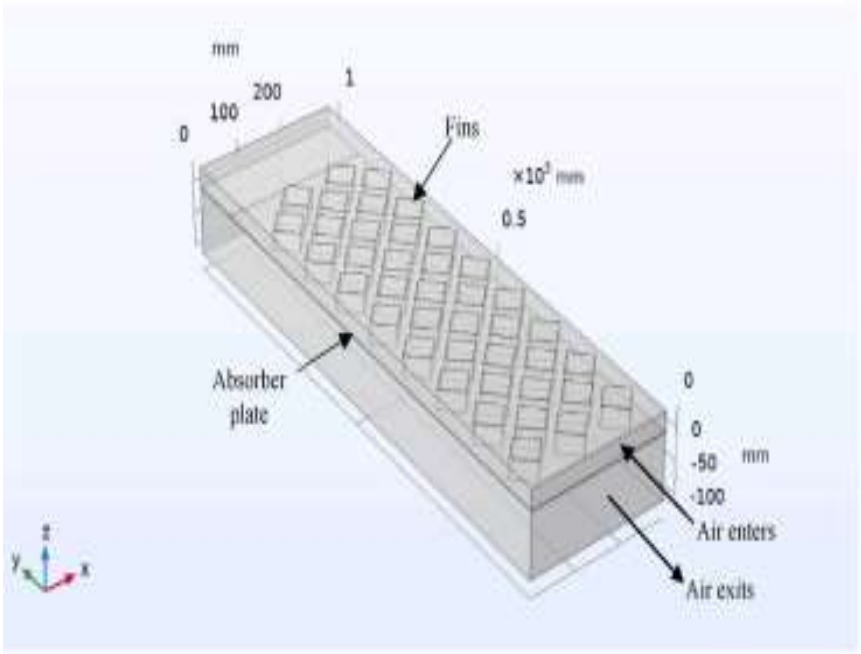



***Fig I. 9 Proposed design concept of double pass solar air heater with diamond shaped fins.[13]***

M. Abhinand and al [14] experimentally investigated the thermal, exergetic, economic, and environmental performance of solar air heaters (SAHs) equipped with different open-cut fin geometries, namely V-shaped, semi-circular, and rectangular fins. The study aimed to improve convective heat transfer, which is a major limitation in conventional SAHs, and to provide a systematic comparison under identical operating conditions.

The experimental setup consisted of four parallel channels, including one plain absorber and three finned configurations, all tested under two mass flow rates during daytime operation. The results showed that fin geometry significantly influences performance. Among the tested designs, V-shaped fins achieved the best overall results, with a maximum outlet temperature of 58°C, an energy efficiency of 66%, and a heat transfer coefficient enhancement of 70.3% compared to the plain absorber. Semi-circular fins showed moderate improvement, while rectangular fins exhibited the lowest performance gain.

In addition, the economic and environmental analyses revealed that V-shaped fins provided the shortest energy payback period (2.82 years), the lowest levelized cost of energy, and the highest $CO_2$ mitigation potential over the system lifetime. Overall, the study confirmed that

V-shaped open-cut fins offer superior thermo-economic and environmental performance compared to the other tested configurations.




***Fig I. 10 Experimental setup components: (a) SAH with Fin Arrangements, (b) Weather Monitoring Station, (c) Outdoor Installation of the SAH Unit, and (d) Data Acquisition System with Data Logger.[14]***

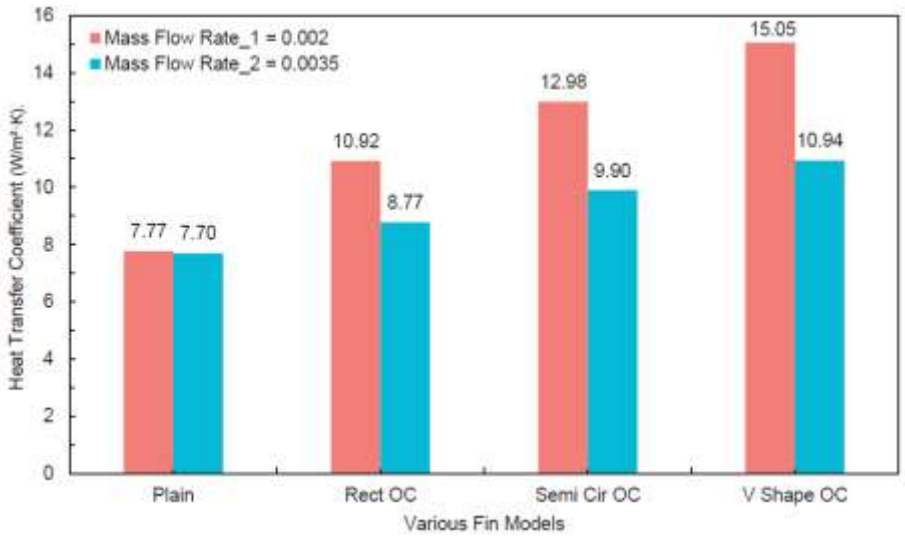



***Fig I. 11 Heat transfer coefficient variation for different mass flow rates.[14]***

H. Abou-Ziyan et al. [15] investigated the relationship between the storage orientation and the performance of single-stage latent heat thermal energy storage systems (LHTESS). The

study focused on evaluating several performance indicators, including charging capacity, charging time, charging rate, and average effectiveness under different inclination angles and charging levels.

A three-dimensional transient numerical model based on the enthalpy-porosity technique was developed to analyze the thermal behavior of the storage system. The results revealed that the optimal inclination angle strongly depends on both the charging level and the selected performance parameter. It was found that charging time and charging rate are more sensitive to orientation changes than charging capacity or effectiveness.

Furthermore, the study showed that the maximum charging capacity is always achieved in the horizontal position, regardless of the charging level. At complete charging conditions, the inclination angle of 60° provided the best overall performance, yielding the shortest charging time, the highest charging rate, and the greatest average effectiveness. These findings demonstrate the significant influence of storage orientation on the thermal performance of latent heat energy storage systems.

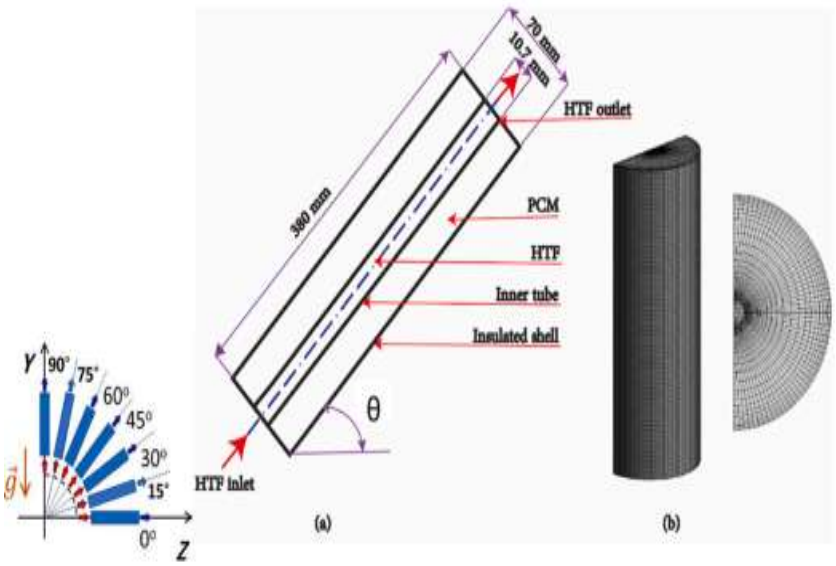



***Fig I. 12 (a) Geometry of LHTESS, (b) Computational mesh domain.[15]***

In their work, O. Murat [16] experimentally investigated the enhancement of photovoltaic-thermal (PVT) collectors by integrating surface modifications, nanotechnology, and thermal energy storage systems. The study aimed to improve both thermal and electrical performance while considering sustainability and environmental impacts.

Three different PVT configurations were developed and tested simultaneously: a V-grooved PVT collector (V-PVT), a nano-enhanced V-grooved PVT coated with graphene nanoparticles (NE/V-PVT), and a V-grooved PVT integrated with a thermal energy storage unit using phase change material technology (TS/V-PVT). The systems were equipped with airflow fans and low-cost insulation materials to ensure practical and economical operation.

The experimental results demonstrated that the nano-enhanced and thermal storage modifications significantly improved the collector performance. The thermal efficiencies reached 40.60%, 54.01%, and 53.90% for V-PVT, NE/V-PVT, and TS/V-PVT, respectively. In addition, the coefficient of performance (COP) increased considerably for the modified systems, confirming the positive effect of graphene nanoparticle coatings and thermal energy storage integration on the efficiency and sustainability of solar collectors.

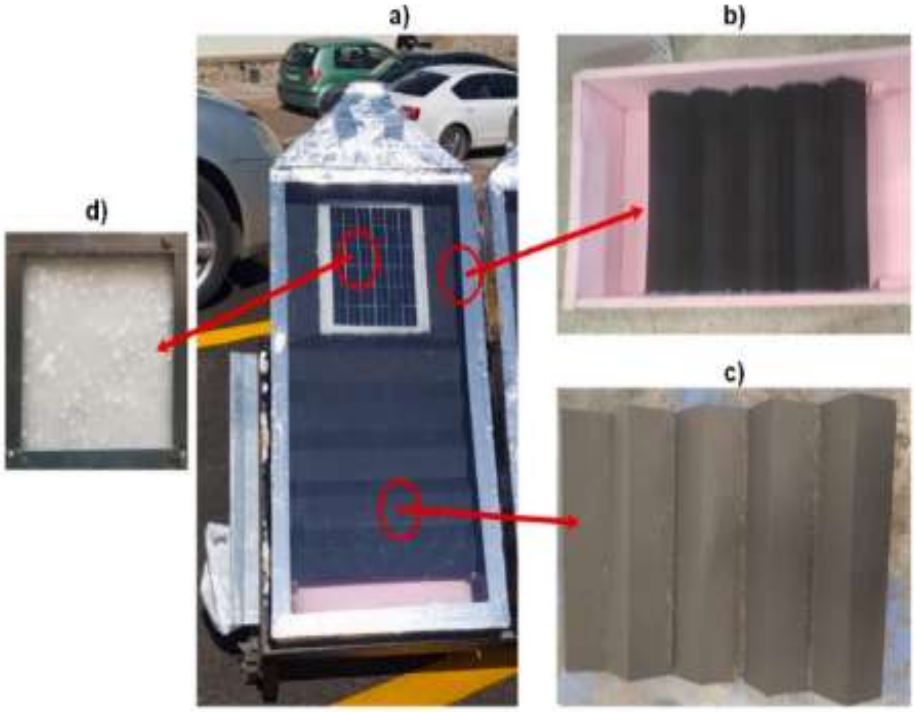



***Fig I. 13 Detailed photographs of the (a) designed collector, (b, c) absorber plate,and (d) thermal energy storage unit.[16]***

N. Embarek et al. [17] experimentally investigated a novel hybrid double-pass solar air heater equipped with wavy fins with air gaps and a latent heat thermal storage unit, aiming to improve the stability of outlet air temperature under fluctuating weather conditions. The study focused on enhancing thermal performance and reducing energy consumption through design optimization.

Initially, indoor experiments were conducted to determine the optimal fin inclination angle among 30°, 45°, and 60°, with results indicating that 45° provides the best thermal performance. Subsequently, outdoor experiments were carried out to evaluate the effect of the electric auxiliary heater position, comparing its placement at the U-turn section and at the outlet section of the system.

The results showed that placing the auxiliary heater at the outlet section (configuration 2) ensured better temperature stability, achieving an outlet temperature of 54 ± 1.3°C, a maximum temperature rise of 32°C, and reduced heat losses. This configuration also reduced electrical energy consumption by 4.2% and achieved a higher thermal efficiency of 68.1% compared to 65.6% for the first configuration. Overall, the study confirmed that the proposed hybrid system offers improved thermal stability, efficiency, and energy savings, making it suitable for agricultural and industrial applications.

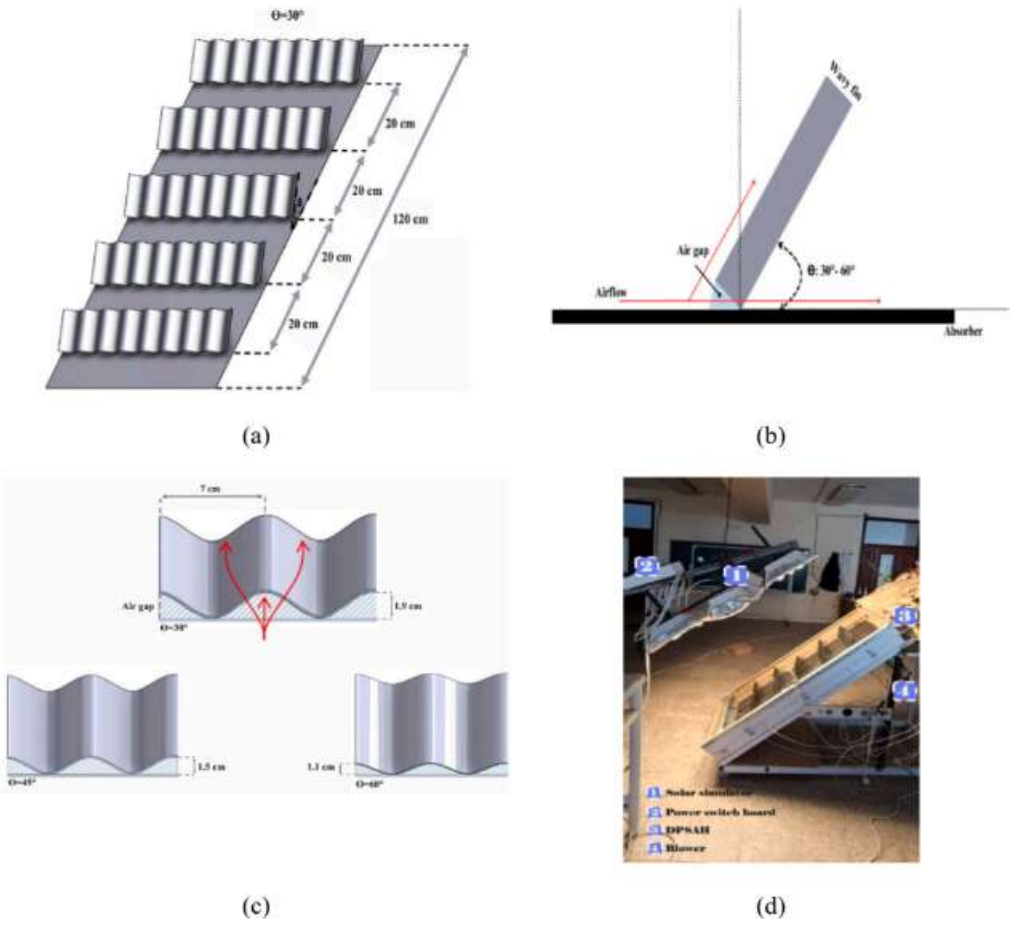



***Fig I. 14 (a–c) Illustrative design of fin arrangements with varying inclination angles (30◦, 45◦, and 60◦); (d) indoor experimental setup.[17]***

A. Lingayat et al. [18] provided a recent reference synthesis on the state of the art of solar air collectors (SACs), supplying comparative quantitative values of the thermohydraulic performance parameter (THPP) for a wide range of geometric configurations, making it a particularly valuable source for contextualizing and justifying design choices in any work related to solar thermal systems. The thermohydraulic performance parameter (THPP) is used as the main indicator. The comparative results showed:

***Table I. 3 comparative results [18]***

| Geometry / Configuration | THPP Obtained |
|---|---|
| Multiple C-shaped ribs | **3.48** *(maximum)* |
| Multiple broken transverse ribs | 3.24 |
| V-pattern ribs with combined grooves | 3.14 |
| Inclined twisted baffles (ITBs) | 1.98 |
| Chamfered square ribs (α = 20°, P/e = 7.14) | 2.047 |
| V-shaped ribs | 1.435 – 2.45 |
| Arc-shaped roughness | 2.33 |
| Hybrid rib roughness | 2.33 |
| Sinusoidal wave baffles | 2.05 |
| Hollow trapezoidal baffles | 1.93 |
| Sinusoidal protrusion ribs | 1.48 *(minimum)* |

The authors conclude that geometric modifications to the absorber plate represent the most effective lever for improving SAC performance, while emphasizing the need to strike a balance between thermal gain and pressure penalty. They recommend for future research: long-term durability assessments, integration of advanced thermal energy storage, development of standardized evaluation methods, and the combined use of computational fluid dynamics (CFD) simulation and experimental validation.

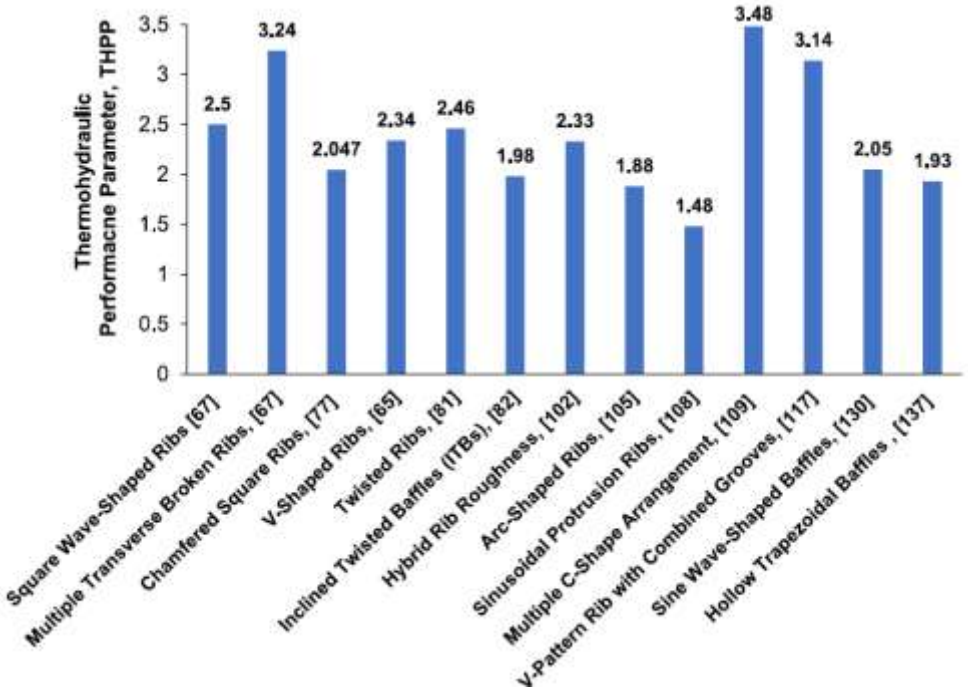



***Fig I. 15 THPP for different geometries/configurations used in SACs.[18]***

S. Muhammad et al. [19] experimentally investigated the thermal performance of a double-pass solar air heater integrated with phase change materials (PCMs) stored inside metallic finned tubes. The objective of the study was to enhance both thermal energy storage capacity and heat transfer rate in the solar air heater system.

Three different configurations were analyzed. The first configuration operated without PCM, while the second incorporated RT44HC phase change material inside semi-circular finned tubes placed in the upper air passage. The third configuration combined RT44HC in the upper passage with RT18HC, having a lower melting temperature, placed in circular finned tubes in the lower passage to further improve thermal storage performance.

The experimental results demonstrated that the integration of PCMs significantly improved the charging and discharging characteristics of the system. Among all tested designs, the third configuration showed the best thermal performance, confirming that the combined use of RT44HC and RT18HC effectively enhances the energy storage and overall efficiency of the double-pass solar air heater.



***Fig I. 16 Finned tubes and actual experimental configurations[19].***

O. Oulad Belkhier and al [20] studied the improvement of the performance of an indirect solar dryer by integrating a latent heat thermal energy storage system and a drying air recirculation device. The authors conducted an experimental study on the drying of chard and moringa leaves, evaluating parameters such as moisture content, drying kinetics, and effective diffusivity.

A comparative analysis between different drying configurations demonstrated the significant contribution of these improvements to the system's performance. Furthermore, the application of several mathematical models showed that the Midilli-Kucuk, Two-Terms, and Diffusion Approximation models are the most suitable for describing the drying kinetics.



***Fig I. 17 Collectors with cans and with baffles.[20]***

O. Murat et al. [21] investigated the design and performance of novel double-flow solar air collectors (SACs) aimed at improving clean energy production. The study focused on enhancing thermal performance and sustainability indicators by replacing conventional absorber plates with flexible aluminum air ducts and incorporating nano-enhanced coatings.

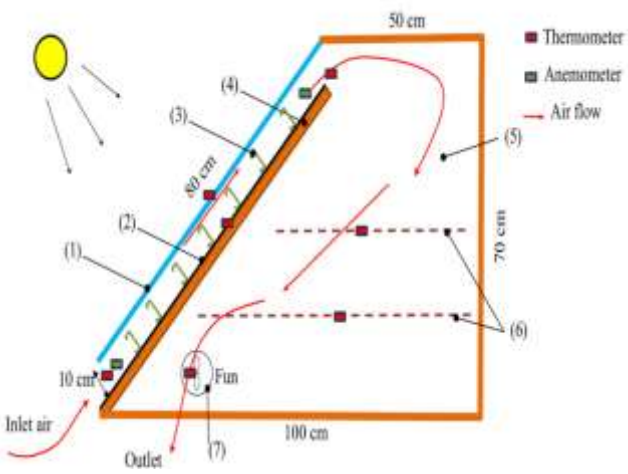
Two main configurations were experimentally tested under identical environmental conditions: a double-flow solar air collector with flexible aluminum air ducts coated with black matte paint (DSAC/FAD), and a similar system enhanced with graphene nanoplatelet-infused coating (DSAC/NFAD). All systems were operated using identical 40 W fans to ensure fair comparison. The study also evaluated energy, exergy, waste exergy ratio (WER), and sustainability index (SI) for each configuration.

The results showed that the nano-enhanced system (DSAC/NFAD) achieved the best overall performance, with a maximum thermal efficiency of 73.94%, a mean exergy efficiency of 37.73%, and the highest COP value of 5.22. In comparison, the conventional DSAC system showed significantly lower performance levels. Additionally, DSAC/NFAD exhibited superior sustainability indicators, confirming the positive effect of graphene nanoplatelet coatings and flexible duct design on improving both efficiency and environmental performance of solar air collectors.




***Fig I. 18 Flexible aluminum air ducts used in the system, a) original and b) painted versions.[21]***

A.I.N. Korti et al. [22] experimentally and thermodynamically evaluated a compact forced-convection indirect solar dryer equipped with three different absorber configurations, with the aim of identifying the optimal design combining energy and exergy efficiency for small-scale agricultural drying applications.




| Configuration | Description |
|---|---|
| WTF (baseline) | Absorbeur lisse, sans ailettes ni isolation |
| WFI | Ailettes en C décalées + isolation arrière (35 mm polystyrène) |
| RGI | Ailettes en C décalées + isolation + entrefer réduit (9 cm → 4,7 cm) |

***Fig I. 19 Schematic of the compact indirect sola dryer. The diagram shows key components: (1) glass cover, (2) absorber plate, (3) C-fins, (4) back insulation, (5) dryer chamber, (6) product trays, (7) DC fan [22]***

The authors highlight a critical design trade-off:

- The **RGI configuration** is the best thermal collector (ηc = 88.77 %) but exhibits a very low drying process exergy efficiency (16.6 %) due to airflow restriction that limits air renewal within the drying chamber.
- The **WFI configuration** offers the most balanced overall performance, combining enhanced heat transfer with adequate airflow renewal, resulting in the highest drying rate and the shortest drying time.
- The **exergy analysis** demonstrates that maximizing raw thermal energy capture at the collector level is not sufficient; the process exergy efficiency (ηex,evap) is the decisive indicator for evaluating the true effectiveness of a solar dryer.

***Table I. 4 Energy and Exergy Performance Results [22]***

| Parameter | WTF (Baseline) | WFI | RGI |
|---|---|---|---|
| Collector Efficiency ηc (%) | 46.02 | 72.78 (+58 %) | 88.77 (+93 %) |
| Dryer Efficiency ηd (%) | 20.71 | 27.97 (+35 %) | 50.58 (+144 %) |
| Collector Exergy Efficiency ηex,c (%) | 0.61 | 2.30 (+277 %) | 3.96 (+549 %) |
| Chamber Exergy Efficiency ηex,d (%) | 42.59 | 54.24 (+27 %) | 32.91 (−23 %) |
| Process Exergy Efficiency ηex,evap (%) | 16.04 | **54.77 (+242 %)** | 16.60 (+4 %) |
| Average Drying Rate (g/min) | 0.24 | **1.34 (+458 %)** | 0.45 (+88 %) |
| Total Drying Time (h) | 16 | **11 (−31 %)** | 15 (−6 %) |

B. Mbaye et al. [23] experimentally evaluated the performance of an indirect forced-convection solar dryer equipped with a hot air recycling system, applied to the drying of mango slices under Senegalese climatic conditions, by analysing heat and mass transfer mechanisms as well as drying kinetics.

***Table I. 5 Thermal and Exergetic Performance Results [23]***

| Parameter | Value Obtained |
|---|---|
| Maximum Solar Irradiance | 1000–1010 W/m² |
| Maximum Temperature in the Drying Chamber | 56–58 °C |
| Thermal Gradient Chamber/Ambient | ~20–25 °C |
| Maximum Collector Thermal Efficiency | **80 %** |
| Efficiency Gain due to Recirculation | **+37.59 %** |
| Exergy Efficiency without Recirculation | 1.7 % → 3.1 % |
| Exergy Efficiency with Recirculation | up to **5.3 %** |
| Exergetic Gain (Recirculation ON vs OFF) | **+53.3 %** |
| Total Drying Time | **13 hours** |
| Effective Moisture Diffusivity (Deff) | $3.54 \times 10^{-11}$ to $1.22 \times 10^{-10}$ m²/s |

The authors conclude that:

- Hot air recirculation significantly improves thermal and hygrometric uniformity within the drying chamber, thereby reducing thermodynamic irreversibilities.
- This approach constitutes an economical and robust solution well-suited to tropical conditions, without requiring phase change material (PCM) thermal storage or auxiliary energy input.
- The heat transfer coefficient (hc) and mass transfer coefficient (hm) confirm a strong correlation with solar irradiance, validating the heat-mass transfer analogy (Chilton-Colburn).
- The identified limitations are the risk of humidity saturation under very hot conditions and the absence of thermal storage for nighttime operation.

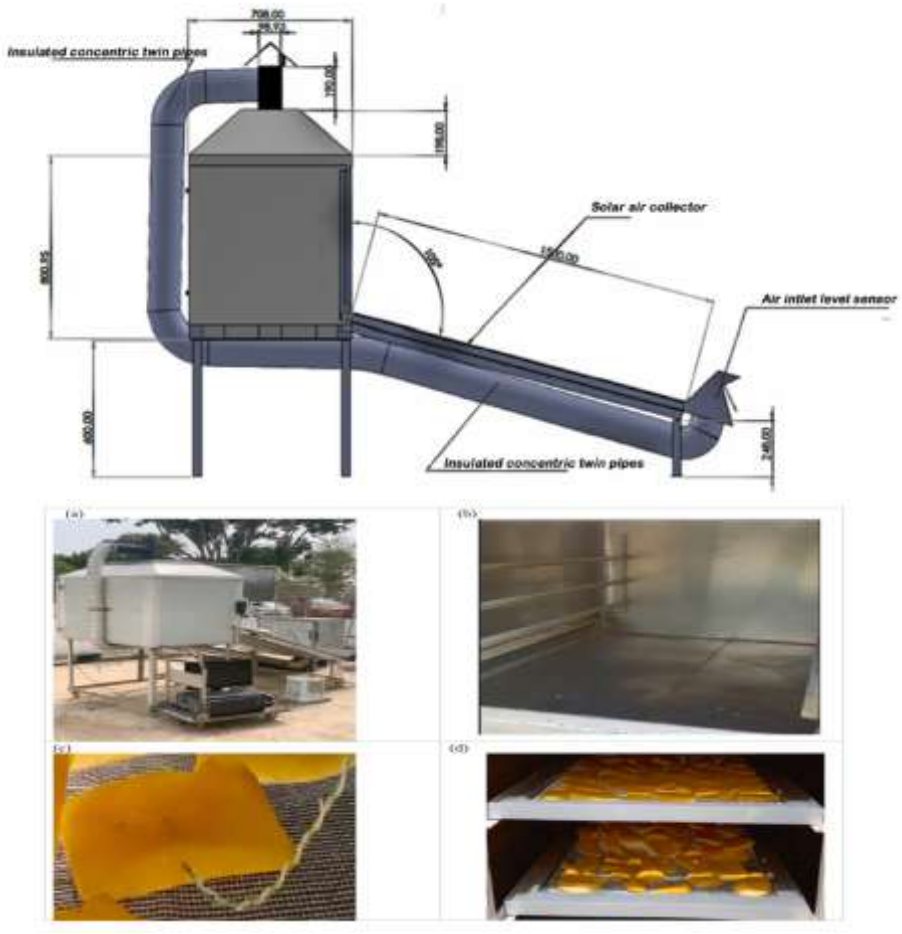



***Fig I. 20 (a) Schematic diagram of the dryer; (b) Interior of the dryer; (c) Measurement of the product temperature; (d) Dryer under load.[23]***

The master's thesis work of N. Midoun and al [24] aims to design, fabricate, and experimentally evaluate a mixed-mode forced-convection solar dryer intended for drying agricultural food products, using locally sourced low-cost materials, within the ETAP laboratory of the University of Tlemcen. Unlike traditional solar dryers that use a flat metal plate as an absorber, this prototype innovates by using flexible and metallic tubes as an absorber, whose cylindrical shape increases the air-absorber contact surface area and improves heat exchange. The authors conclude that the mixed-mode forced-convection solar dryer with a tubular absorber constitutes an effective and economical solution for drying agricultural products at a small scale. The use of tubes as an absorber significantly improves heat exchange and represents an accessible innovation well-suited to the local Algerian



***Fig I. 21 (a) Schematic diagram of the mixed Mode dryer and indirect Mode dryer [24]***

context.

***Table I. 6 Thermal Behavior of the Solar Collector [24]***

| Parameter | Indirect Mode | Mixed Mode |
|---|---|---|
| Maximum Absorber Temperature | 89.3 °C | 84.7 °C |
| Maximum Air Outlet Temperature | 69.8 °C | 67.4 °C |
| Inlet/Outlet Air Temperature Difference ΔT | 38.9 °C (+77.2 %) | 41.5 °C (+89 %) |
| Average Ambient Air Velocity | 1.31 m/s | 2.3 m/s |

## I.6 Conclusion

This chapter has established the theoretical and bibliographical foundations of the present study. The analysis of Algeria's energy context confirms the strategic relevance of solar drying as a means of harnessing the country's abundant solar resource while reducing post-harvest losses. The review of the fundamental principles of drying has shown that the quality and efficiency of the process depend on the interaction between the thermal properties of the drying air and the characteristics of the product, highlighting the superiority of forced-convection indirect solar dryers. Furthermore, the review of solar air collectors has identified geometric modifications of the absorber such as fins, artificial roughness, and baffles as the main approaches for enhancing thermal performance. Hot-air recirculation has also been identified as an effective strategy for improving temperature uniformity within the drying chamber without the need for costly thermal energy storage. These findings provide the scientific and technical foundation for the design of the prototype presented in the following chapter.

# CHAPTER II

# EXPERIMENTAL PROCEDURES

## II.1 Introduction

Faced with growing energy demand and contemporary environmental imperatives, the use of renewable energies has emerged as a sustainable alternative to conventional energy sources. Among these alternatives, solar thermal energy is of particular interest due to its availability, low operating cost, and limited environmental impact. The solar air collector, owing to its simple design and numerous applications in the fields of heating, drying, and ventilation, represents one of the most promising technologies in this context.

This chapter is devoted to the design, fabrication, and experimental characterization of a single-pass solar air collector, developed with a view to its integration into an indirect solar dryer intended for the processing of agri-food products. The device is designed to supply the necessary thermal energy in the form of hot air, thereby contributing to improving drying efficiency, preserving the quality of the treated products.

In order to optimize the thermal performance of the collector, several improvements were made to its basic configuration, notably the integration of flexible aluminum tubes onto the absorbing surface to increase the heat exchange area, as well as the implementation of high-performance thermal insulation aimed at minimizing energy losses to the external environment.

This chapter successively presents the description of the experimental setup, the fabrication and assembly stages of the collector, the measuring instruments used, the theoretical framework for performance evaluation, and the experimental tests conducted under two distinct operational configurations.

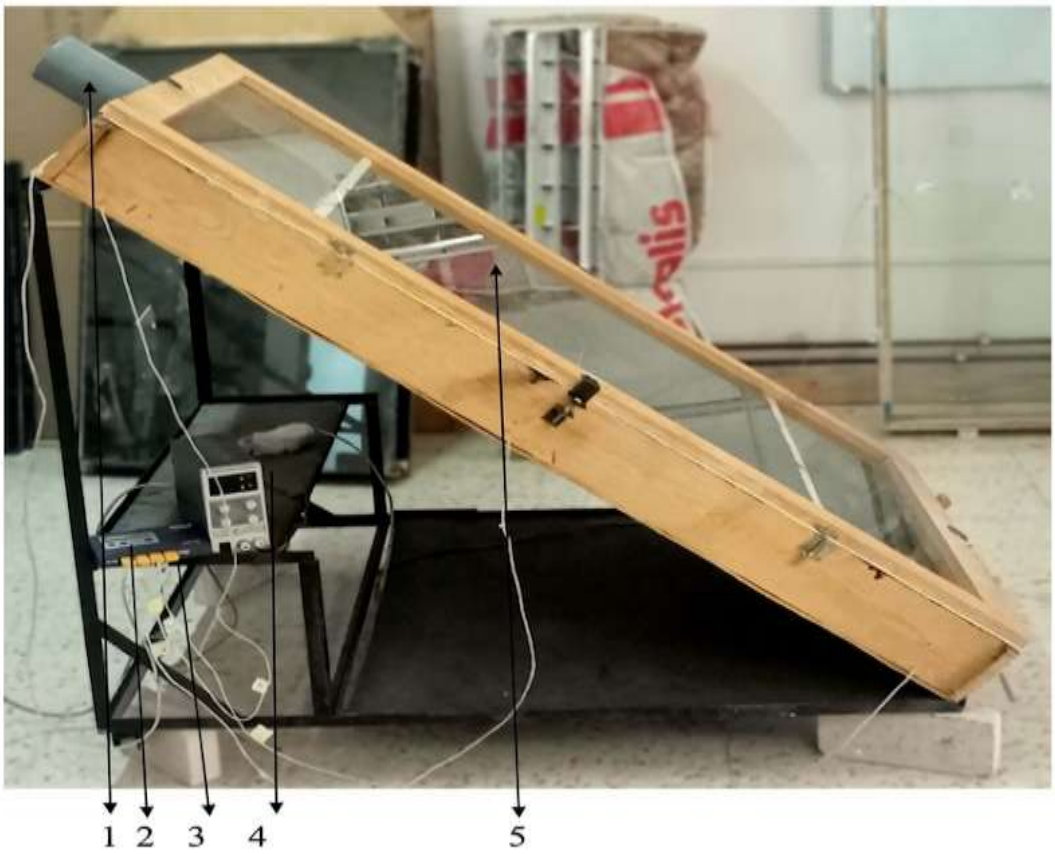
## II.2 Presentation of the Experimental Setup :

The experimental system investigated in this study is a single-pass solar air collector designed and optimized to convert solar energy into thermal energy in the form of heated air. This collector, developed as a functional experimental test bench, was entirely designed and

manufactured at the ETAP Research Laboratory of the University of Tlemcen. The overall design of the system emphasizes the use of readily available materials, low manufacturing

cost, and ease of reproduction, while incorporating significant improvements aimed at enhancing heat transfer and minimizing thermal losses.

The flat-plate solar air collector has a collecting surface area of 1.5 × 0.90 m² and is installed at an inclination angle of 45°. The main structure consists of a sturdy wooden enclosure that provides mechanical support for all the components while protecting the system from external environmental conditions. The upper surface of the collector is covered with a 3 mm thick transparent glass sheet, which allows incident solar radiation to reach the absorber while reducing convective heat losses to the ambient air, thereby creating an effective greenhouse effect above the absorber surface. To minimize heat losses to the surroundings, particularly under varying ambient temperature conditions, the bottom and inner side walls of the wooden enclosure are lined with a high-performance thermal insulation layer. The absorber plate is coated with matte black paint to maximize solar radiation absorption and minimize the reflection of incident light (Fig II.1).




1 - solar capture outlet tube.
2 - Recorder.
3 - Type K sensor with flat heads.
4 - Voltage and current controller. 5 Solar collector glass

***Fig II. 1 Experimental setup of a flat-plate solar collector 45° inclined***

Airflow through the collector is maintained by a mechanical ventilation system consisting of four fans installed at the air inlet (Fig II.2 and Fig II.3). Fresh air is continuously supplied through the inlet opening, flows in a forced convection mode along the heated absorber and through the aluminum tubes, and exits through the outlet after absorbing thermal energy (Fig II.4). Five thermocouples are installed at strategic locations (air inlet, air outlet, and absorber surface) to provide accurate real-time measurements of temperatures. In addition, the airflow rate and air velocity are monitored under different operating conditions to evaluate the thermal performance of the collector



*Fig II. 2 Inlet flat-plate solar collector External face*



*Fig II. 3 Inlet flat-plate solar collector Internal face (4 fans)*



*Fig II. 4 Outlet flat-plate solar collector*

## II.3 Description of the Solar Collector :

The solar collector used is rectangular in shape and has external dimensions of 152.8 cm in length, 93.6 cm in width, and 15 cm in height. The active surface of the collector measures approximately 139 cm in length and 76 cm in width (Fig II.5).

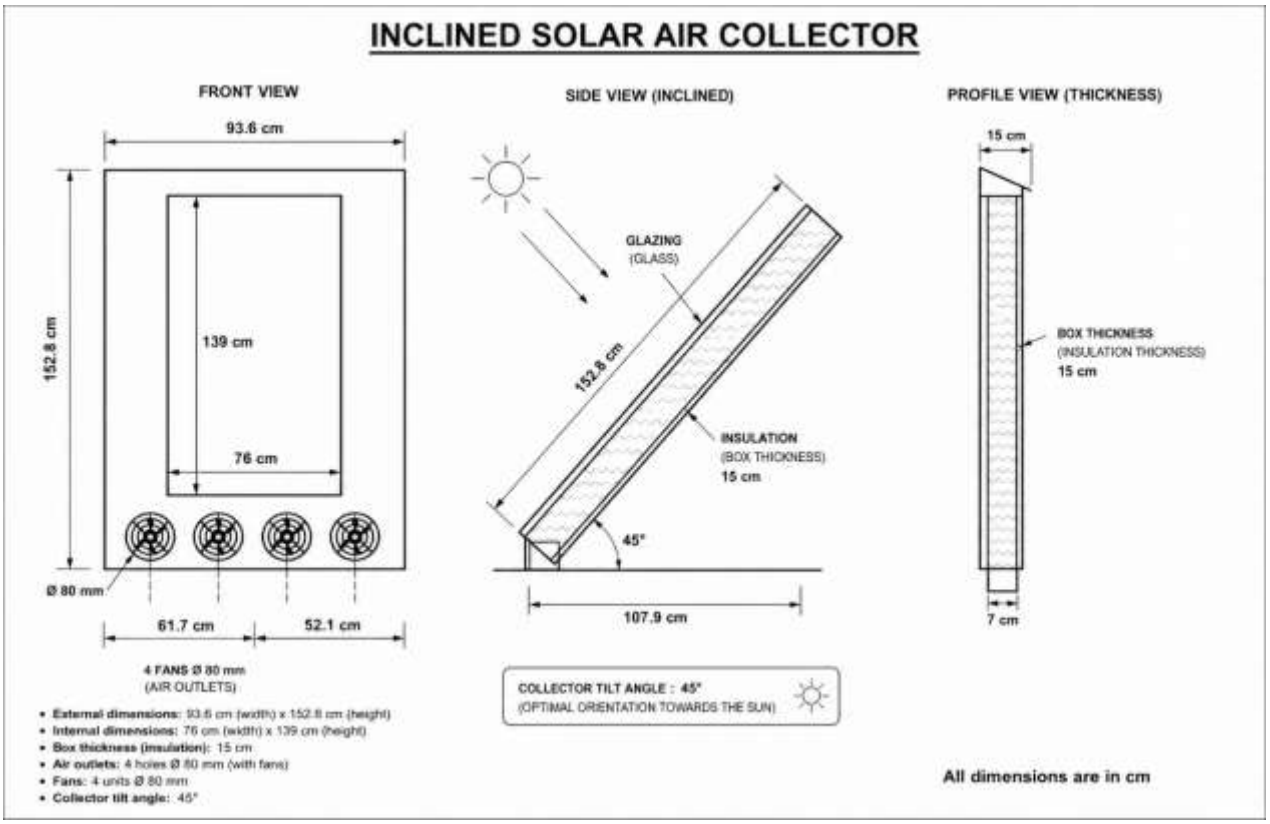



***Fig II. 5 Solar collector diagram***

The construction of the air solar collector required several successive operations, from the fabrication of the basic structure to the final assembly of the experimental setup. Each step was carried out carefully to obtain a robust, functional system capable of providing reliable experimental results. The various operations performed are described below.

### II.3.1 Construction of the Structure

The collector structure was constructed from wooden panels cut according to the specified design dimensions and assembled using screws to form a rigid enclosure. A layer of thermal insulation was installed on the bottom and inner walls of the collector to reduce heat losses to the surrounding environment.

### II.3.2 Fan Installation

Four openings were made in the collector housing to install the fans, ensuring continuous forced airflow through the collector. After preparing the openings, the fans were securely mounted. An appropriate electrical circuit with soldered connections was then constructed to provide a reliable and durable power supply.This step ensured the proper functioning of the electrical system and the safety of the installation (Fig II.3).

### II.3.3 Absorber Preparation

The absorber is the main component of the solar collector, as it converts solar radiation into heat. Before installation, its surface was thoroughly cleaned and then coated with a uniform layer of matte black paint to increase its solar radiation absorption capacity (Fig II.6).



***Fig II. 6 Internal view of the collector showing the matte black absorber plate and the fans.***

To overcome the inherently low thermal conductivity of air, nine rough-surfaced aluminum tubes, each 0.90 m long and 8 cm in diameter, were mounted in parallel directly onto the absorber plate. Owing to the high thermal conductivity of aluminum, these tubes significantly increase the effective heat transfer surface area between the absorber plate and the working fluid, thereby considerably enhancing the outlet air temperature of the collector (Fig II.7).



***Fig II. 7 flexible aluminum tubes***

### II.3.4 Glazing Installation

The top surface of the sensor was then closed with a transparent glass plate cut to the dimensions of the enclosure. The glazing was carefully positioned to ensu^ù re proper coverage of the entire collection surface.

### II.3.5 Thermocouple positions

Five thermocouples were strategically installed to monitor the temperature distribution within the system. The thermocouple $T_{in}$ measures the air temperature at the collector inlet, while $T_{out}$ measures the air temperature at the collector outlet. The thermocouples $Tp_1$, $Tp_2$, and $Tp_3$ are positioned at the lower, middle, and upper sections of the absorber, respectively, enabling the characterization of the temperature distribution along the absorber (Fig II.8).

### II.3.6 Final Assembly

After all components were installed, the various parts of the sensor were checked and then permanently assembled. A tube was attached to the sensor outlet to facilitate the exhaust and recovery of the heated air.

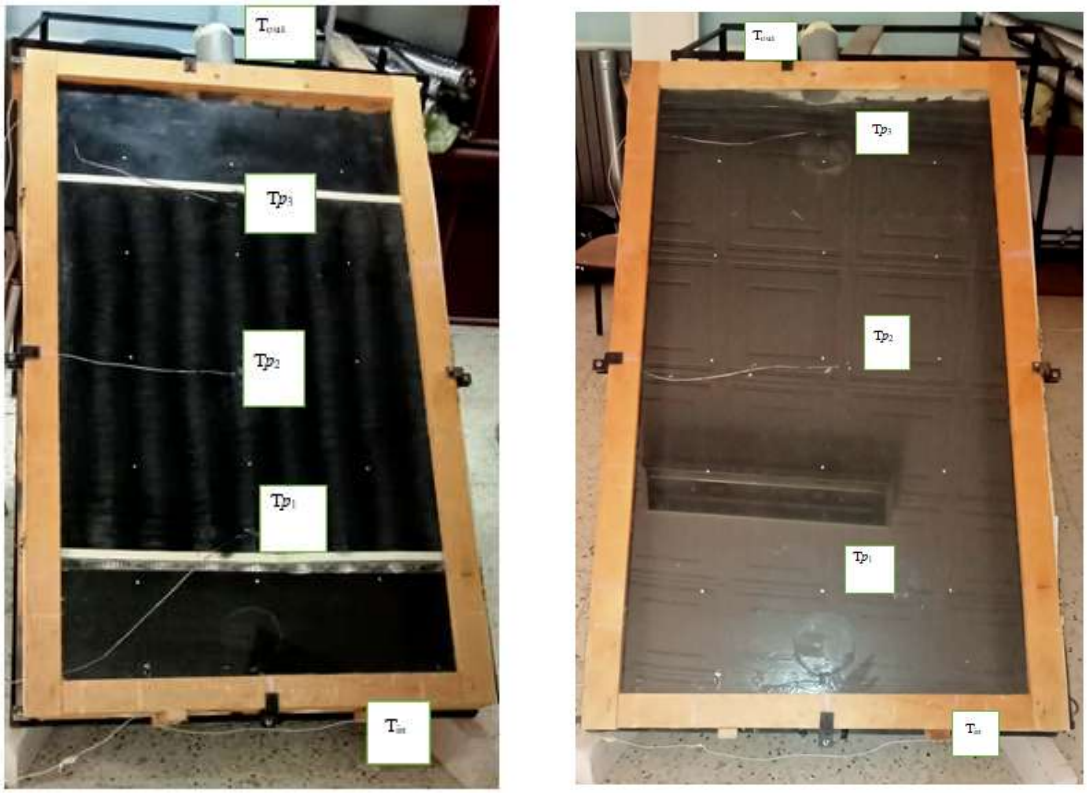


***Fig II. 8 Solar collector with and without flexible aluminum tubes***

Finally, the experimental setup was prepared for testing by installing an artificial light source capable of reproducing the sunlight conditions required for the study. This source allowed the experiments to be conducted under controlled and reproducible conditions. All the operations carried out led to the development of a functional single-pass air solar collector, intended for the experimental evaluation of its thermal performance and the influence of improvements made on its efficiency.

## II.4 Construction of an Artificial Heat Source

To provide a controlled thermal radiation source for the solar collector, an artificial heat source was designed according to the dimensions of the collector's absorbing surface. This source consists of a panel made of gypsum boards (BA13 type) on which 28 halogen lamps**,** each rated at 100 W, are mounted. The underside of the panel is covered with reflective aluminum sheets, whose purpose is to redirect the emitted light and thermal

radiation toward the collector, reduce energy losses, and ensure a more uniform distribution of the incident heat flux (Fig II.9)



***Fig II. 9 Artificial heat source***

## II.5 Measurement Instruments

### II.5.1 Measurement of Solar Radiation

The incident solar radiation is measured using a solarimeter placed directly on the glazing of the solar collector. This instrument is designed to accurately measure the solar irradiance received by a surface. Equipped with sensitive sensors, it quantifies the incident solar radiation flux, expressed in watts per square meter ($W/m^2$).



*Fig II. 10 Solarimetre*

### II.5.2 Air Velocity Measurement

The **9160SI digital thermo-anemometer** is used to measure the air velocity at the inlet of the solar collector by means of an internal vane sensor. The measured air velocity is displayed in meters per second (m/s).

The ambient air velocity is measured using an **AERCUS WS 2083 professional wireless weather station**. In addition to wind speed, this station also provides measurements of ambient relative humidity, ambient temperature, and direct solar radiation



*Fig II. 11 Digital Thermo-Anemometer*



*Fig II. 12 Automatic Weather Station*

### II.5.3 Temperature Measurement

To ensure thermal monitoring and data acquisition for our solar capture system, we equipped our experimental setup with a Grant Squirrel Series 600 data logger. This self-contained, portable device is connected to five type K temperature sensors, known for providing high-precision measurements with excellent responsiveness to even the slightest temperature variations. The thermocouples provide a measurement accuracy of approximately **0.1 to 0.2 °C**.




***Fig II. 14 Type K thermocouple*** ***Fig II. 13 Temperature recorder***

### II.5.4 Voltage and Current Controller

The **WANPTEK KPS3010D** voltage and current controller is an adjustable DC power supply capable of delivering an output voltage ranging from **0 to 30 V** with a maximum output current of **10 A**. Designed for use in laboratories, educational institutions, and industrial environments, this equipment provides precise control of both the output voltage and current. Owing to its high stability and accuracy, it is particularly well suited for powering electronic devices and conducting tests and experiments that require reliable control of electrical parameters.

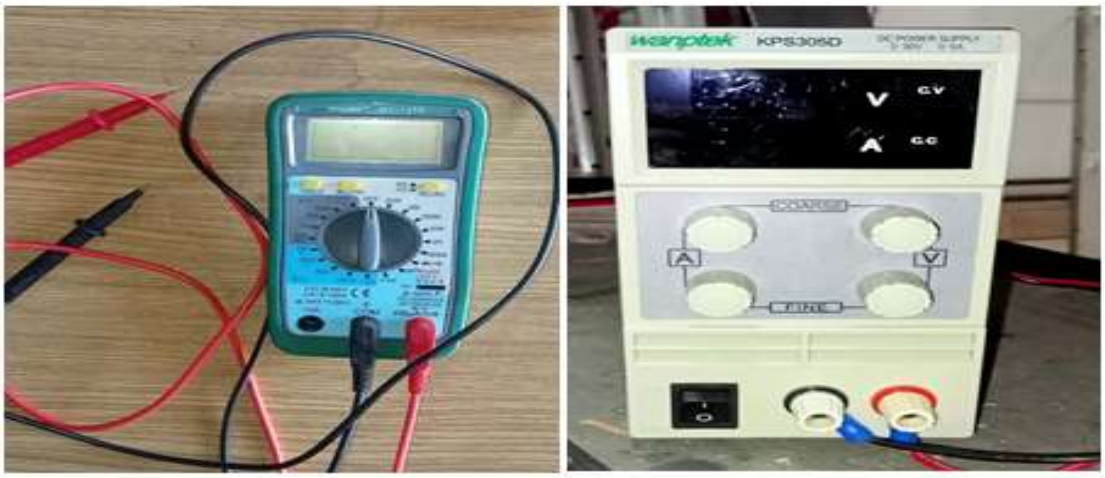



***Fig II. 15 Digital Multimeter and Voltage and amperage controller***

## II.6 Experimental Procedure

Two configurations of the solar air collector, designed for the drying of agri-food products, were investigated and compared in this experimental study. The first configuration was equipped with a flat absorber, while the second incorporated flexible tubes intended to enhance heat transfer. The experiments were carried out under carefully controlled laboratory conditions to ensure the repeatability of the measurements and to provide a reliable comparison of the thermal and energy performance of the two configurations.

The tests were conducted under different levels of irradiance generated by an artificial solar radiation source, allowing various solar exposure conditions to be simulated. In addition, several air flow rates were imposed at the collector inlet to investigate their influence on heat transfer, air temperature rise, thermal efficiency, and the overall performance of the system. The experiments were performed on the solar collector alone, without the drying chamber, in

order to evaluate its thermal performance before its integration into a solar dryer intended for drying agri-food products. For each combination of irradiance and air flow rate, the tests were carried out for 45 minutes, allowing the system to reach steady-state conditions.

During each experiment, temperatures, solar irradiance, air velocity, and other operating parameters were continuously recorded. The collected data were then analyzed to evaluate and compare the thermal and energy performance of the two collector configurations and to identify the configuration exhibiting the best thermal behavior under the investigated operating conditions. The results of this study provide the basis for selecting the most efficient collector configuration prior to its integration into a solar drying system for agri-food products.



***Fig II. 16 Experimental Setup Used in the Laboratory***

## II.7 Assembly and Experimental Evaluation of the Solar Drying System

The **solar air collector** developed in this study was coupled with a **drying chamber** designed, fabricated, and experimentally validated by Master's students in the same laboratory. The work on the drying chamber was carried out simultaneously with our study and under the same experimental conditions, ensuring the compatibility of the two systems.

After their fabrication, the solar air collector and the drying chamber were assembled to form a complete **solar drying system** intended for the drying of agri-food products. The connection between the collector and the drying chamber was made using a flexible aluminum duct. To minimize heat losses during the transfer of heated air from the collector to the drying chamber, the duct was covered with a thermal insulating sleeve. This insulation reduces heat exchange with the surrounding environment and helps maintain a higher air temperature before it enters the drying chamber, thereby improving the overall thermal performance of the solar drying system.

The experimental investigation was carried out under actual outdoor operating conditions using natural solar radiation. Two different system configurations were evaluated to assess the influence of the connecting duct on the overall thermal performance of the solar dryer. During the first experimental campaign, the solar collector was tested in its original configuration, in which the collector was directly coupled to the drying chamber without the flexible connecting duct. This configuration served as the reference case for performance evaluation.

In the second experimental campaign, the flexible insulated aluminum duct was installed between the collector and the drying chamber. This modified configuration made it possible to investigate the effect of the connecting duct on hot air transport, heat losses, and the overall thermal efficiency of the drying system. To ensure a meaningful comparison, both experimental campaigns were performed under similar meteorological conditions.

The drying performance of the system was evaluated using two agricultural products, namely mint leaves and banana slices. Each product was dried under identical operating conditions in both configurations, allowing the influence of the collector configuration on the drying process to be assessed and compared.

Throughout the experiments, the temperatures, solar irradiance, air velocity, and other operating parameters were continuously monitored and recorded. The collected data were subsequently analyzed to evaluate the thermal performance of the solar collector and the overall efficiency of the solar drying process. The experimental results, together with their analysis and discussion, are presented in detail in Chapter 4



***Fig II. 19 Experimental Setup of the Solar Drying System.***



***Fig II. 17 banana slices***



***Fig II. 18 mint leaves***

## II.8 Theoretical analysis

### II.8.1 The energy $Q_{out}$

The energy $Q_{out}$ output from the solar sensor:

$$Qout = \dot{m}\ cp\ (T_{out} - T_{in}) \quad \text{..... (II.1)}$$

$$\Delta T = T_{out} - T_{in} \quad \text{.....(II.2)}$$

### II.8.2 Energy efficiency

Energy efficiency $\boldsymbol{\eta_{th}}$ is the ratio between the useful energy captured by a solar collector and the total solar energy received.

$$\eta_{\text{th}} = \frac{Q_{out}}{Q_{total}} \quad \text{.....(II.3)}$$

$$\eta_{\text{th}} = \frac{\dot{m}\ C_p\ \Delta T}{I\ A_c} \quad \text{.....(II.4)}$$

## II.9 Conclusion

This chapter presented the experimental methodology adopted throughout this study, including the design, fabrication, instrumentation, and testing of the solar air collector, as well as the development of the complete solar drying system. The proposed collector, incorporating flexible aluminum tubes and enhanced thermal insulation, was designed to improve heat transfer and reduce thermal losses while remaining simple, low-cost, and easy to manufacture. A comprehensive experimental protocol was established to compare the conventional and modified collectors under controlled laboratory conditions. Subsequently, the optimized collector was integrated with a drying chamber and evaluated under real outdoor conditions using mint leaves and banana slices. The experimental results and performance analysis of both collector configurations and the complete drying system are presented in the following chapter.

# CHAPTER III

# PARAMETRIC COLLECTOR ANALYSIS

## III.1. Introduction

This chapter aims to characterize and evaluate the thermal performance of two distinct solar air collector configurations under controlled laboratory conditions. The first configuration corresponds to a conventional flat-plate solar collector (PSC), which serves as the baseline reference design, while the second incorporates a tube-integrated geometry, referred to as the Solar air Collector with Tubes (SCT), specifically developed to enhance internal convective heat transfer.

The thermal behavior of solar air collectors is inherently governed by the complex interaction between the incident solar irradiance, the convective heat transfer at the absorber-fluid interface, and the parasitic heat losses dissipated through the glazing cover to the surrounding environment. A fundamental understanding of these coupled phenomena is essential to identify the limiting factors of conventional flat-plate designs and to assess the potential improvements introduced by geometric modifications of the flow channel.

In this context, the experimental campaign was structured around two primary parametric studies, conducted independently for each collector type. The first study examines the influence of solar irradiance on the thermal response at a fixed air mass flow rate, while the second investigates the effect of varying the mass flow rate under constant irradiance conditions. For each configuration, the transient and steady-state temperature distributions, outlet air temperature rise, and overall thermal efficiency are systematically recorded and analyzed.

The chapter is organized as follows. Section III.1 presents the thermal behavior and efficiency of the PSC under varying irradiance and mass flow rate conditions. Section III.2 then introduces the SCT configuration and provides a comparative performance analysis against the PSC baseline, focusing on heat transfer enhancement mechanisms attributed to the tube geometry. The chapter concludes with a quantitative summary table consolidating the key performance metrics for both systems.

## III.2 Plate solar collector PSC

### III.2.1 Thermal Behavior of PSC

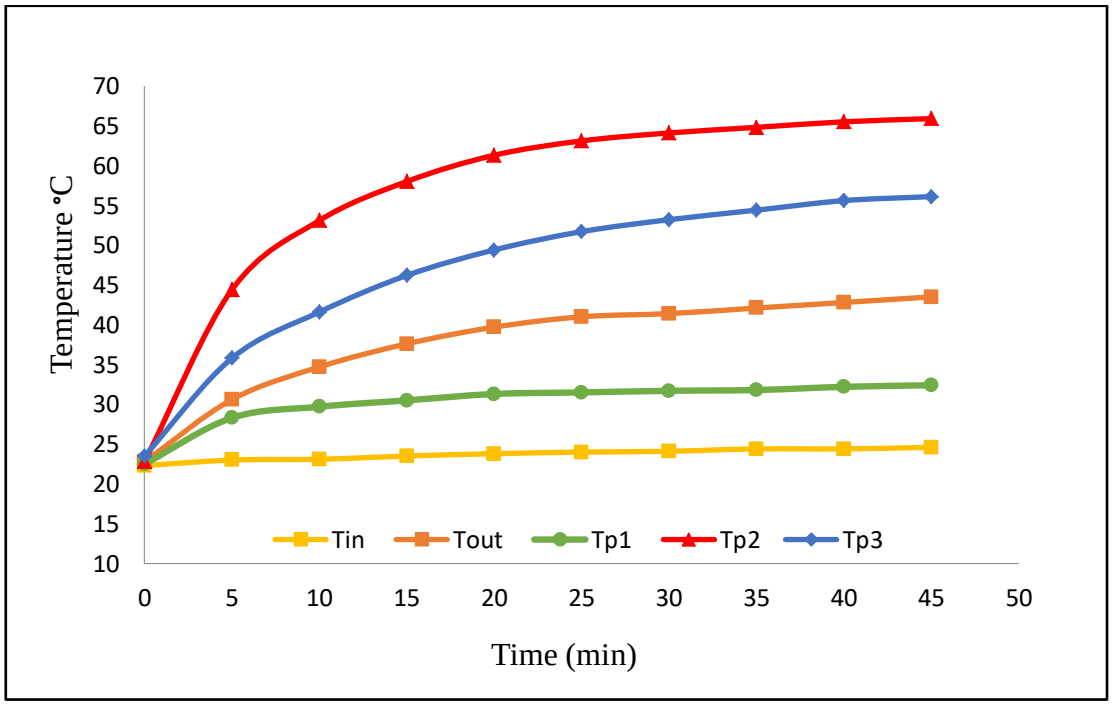



***Fig III. 1 Temperature Evolution (Tin to Tp1) of PSC as a Function of Time at mass flow rate m ≔ 0.015 kg/s and solar irradiance I = 323.55 W/m²)***

Figure III.1 shows the experimental temperature curves of a conventional flat-plate solar air collector as a function of time over a 45 (min) test period, with a mass flow rate of 0.015 kg/s and a solar irradiance of 323.55 W/m². It includes the inlet air temperature ($T_{in}$), the outlet air temperature ($T_{out}$), as well as the absorber plate temperatures measured in the lower ($Tp_1$), middle ($Tp_2$), and upper ($Tp_3$) zones.

At t = 0, all curves originate from nearly the same point, between 22.3°C and 23.5°C, confirming that the system starts in thermal equilibrium with the surrounding ambient air. As solar exposure begins, two distinct thermal regimes appear on the graph:

The first 25 (min) correspond to a transient phase, visible as steep, exponential-like rises in all five curves, most notably $Tp_2$ and $Tp_3$. During this period, the absorbed solar energy far exceeds the heat being transferred to the air, so most of the energy is stored as sensible heat within the absorber plate, producing the sharp slopes.

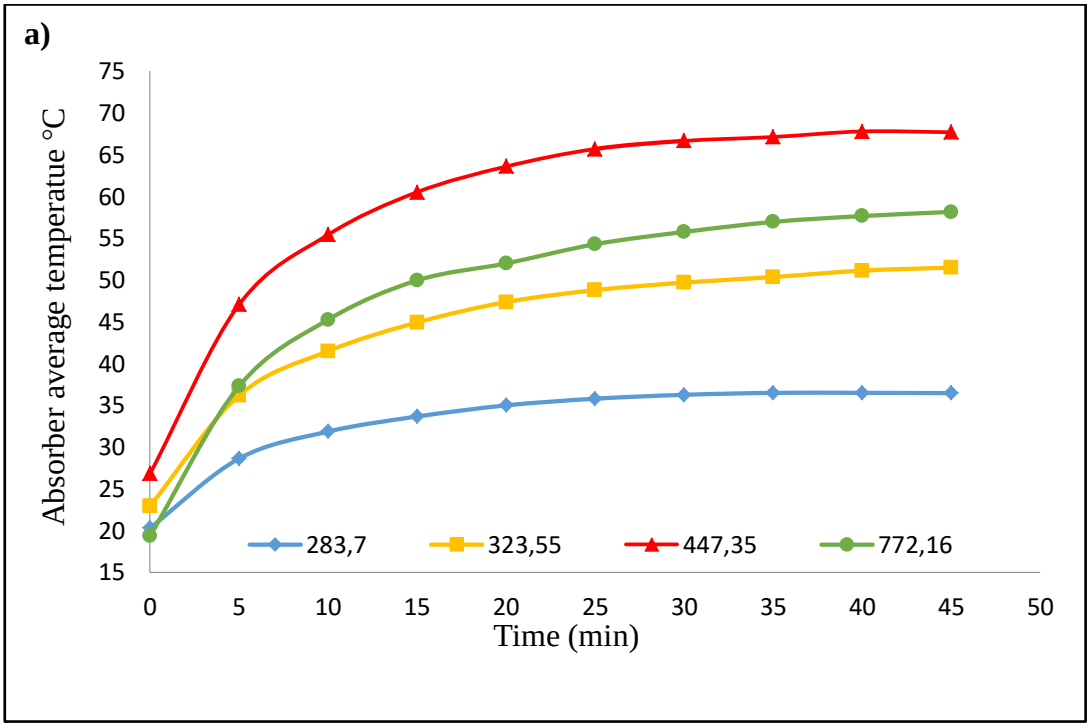
From minute 25 to 45, the curves flatten markedly, marking a semi-steady state. The slope reduction is most evident for $Tp_2$, which rises only 2.8°C in the last 20 (min) versus 40.3°C in the first 20. This plateauing reflects an energy balance where incoming solar

radiation is now mainly split between useful heat transfer to the air and losses to the environment, rather than being stored in the plate.

The vertical spacing between curves at steady state reveals the spatial temperature distribution across the absorber plate. $Tp_2$ (middle zone) sits highest at 65.9°C, since this region is farthest from the edges and inlet, minimizing both edge losses and convective cooling by incoming air. $Tp_3$ (upper/outlet zone) follows at 56.1°C, slightly lower than $Tp_2$ because the air, having absorbed heat along its path, now removes some energy from this zone as it exits. $Tp_1$ (lower/inlet zone) remains lowest at 32.4°C, since this is where the coolest incoming air ($T_{in}$) first contacts the plate and extracts heat most aggressively, creating a strong local cooling effect.

$T_{in}$ stays nearly flat near 23 to 24.6°C throughout, as expected for an ambient-fed inlet stream. $T_{out}$, the outlet air temperature, rises steadily to 43.5°C, tracking the overall heating trend but lagging well behind the plate temperatures.

### *A. Radiation effect*



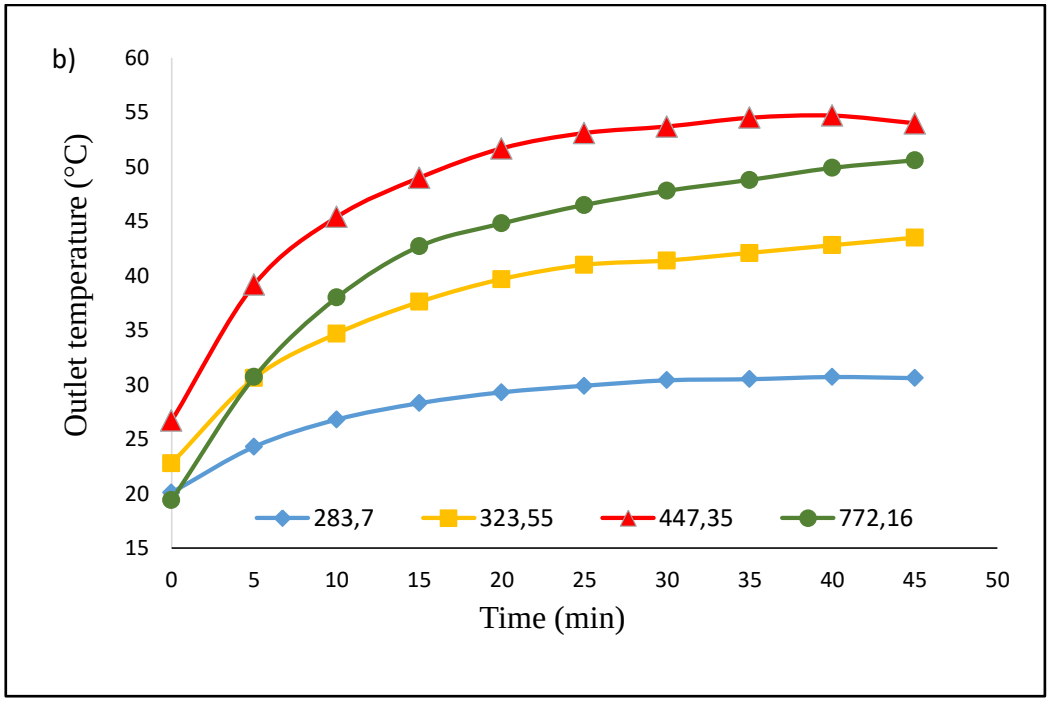



***Fig III. 2 Temporal evolution of temperature at a mass flow rate of ṁ= 0.015 kg/s under different solar irradiance levels (283.7, 323.55, 447.35 and 772.16 W/m²).***

***a) Average temperature of a plat absorber Tp = average (Tp1 Tp2, Tp3)***

***b) Outlet air temperature (Tout).***

Figure III.2.a shows temporal evolution of average temperature of a plat absorber T*p* = average of (T$p_1$ T$p_{2,}$ T$p_3$)and Figure III.2.b shows temporal evolution Outlet air temperature ($T_{out}$) at a mass flow rate of 0.015 kg/s under different solar irradiance levels (283.7, 323.55, 447.35 et 772.16 W/m²).

Both graphs show temperature rising rapidly during the first from 10 to 15 min, and then gradually approaching steady-state plateaus by around from 30 to 45 min, for all four irradiance levels.

In Figure III.2.a, the absorber plate temperature reaches higher values overall, ranging from about 37, 52 , 68 and 58.13°C of 283.7, 323.55, 447.35 and 772.16 W/m² respectively at steady state

It is observed that the absorber plate reaches a maximum steady temperature of 67.67 °C at an average irradiance of 447.35 W/m², whereas the absorber plate temperature decreases significantly to 58.13 °C at a higher irradiance value of 772.16 W/m².

**This behavior is governed by the overall structural heat loss equation:**

$$\mathbf{Q_{loss} = h\ A_p\ (T_p - T_{amb})} \quad \textbf{(III.1)}$$

At 772.16 W/m², the higher incident flux drives a steeper initial temperature rise, but since h (convection coefficient in the empty channel) and the air mass flow rate stay fixed, the fluid can't carry away the extra energy proportionally. The elevated $T_p$ then increases top losses ($Q_{loss} = h \cdot A_p \cdot (T_p - T_{amb})$, plus radiation through the glass cover) disproportionately, so the system re-equilibrates at a lower steady-state $T_p$ = 58.13°C than at I = 447.35 W/m² $T_p$=67.67 °C i.e., the loss term grows faster than the gain term as irradiance increases, producing the inversion.

In figure III.2.b the outlet air temperature follows the same trend but with lower magnitudes, ranging from at a current intensity of 283.7 W/m²: The air outlet stabilizes at 30.60°C, resulting in a net air temperature rise of 10.5°C. At a current intensity of 323.55 W/m²: The air outlet rises to 43.50°C, increasing the temperature rise to 20.7°C. At an irradiation intensity of 447.35 W/m²: The system achieves its highest heat output. The quality reaches 54.00 °C and achieves temperature rise of ΔT = 27.3 °C. When irradiance is maximized to 772.16 W/m², the air outlet temperature drops sharply to 50.60 °C and achieves a maximum temperature rise of ΔT = 31.2 °C, reproducing the same inversion seen in figure III.2.a. Because the air mass flow rate is constant (ṁ = 0.015 kg/s), the internal convection heat transfer coefficient (h) remains constant and is constrained by the smooth channel geometry. The liquid side cannot keep pace with the massive solar flux, allowing energy to bypass the passing air and escape as heat loss from the top of the glass envelope instead of being converted into perceptible enthalpy of the liquid. This decline clearly demonstrates that conventional flat panel designs require artificial roughness or flow enhancers to improve heat transfer performance at high irradiance levels.

### B. *Mass flow effect*

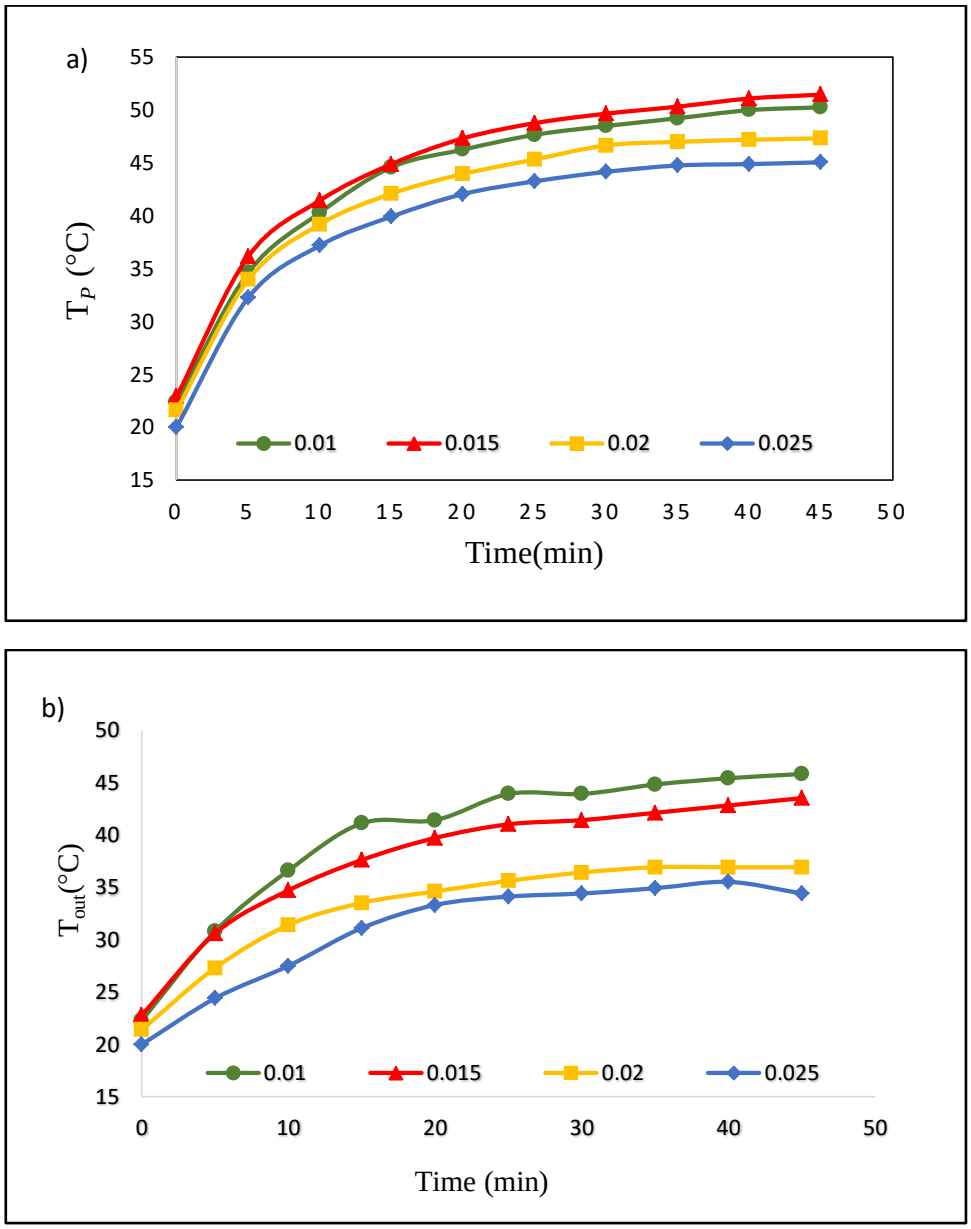



***Fig III. 3 Temporal evolution of temperature at a solar irradiance I= 323.55 W/m² under different mass flow rate (0.01, 0.015, 0.02, 0.025 kg/s )***

a) **Average temperature of a plat absorber T*p* = average of (T$p_1$ T$p_2$, T$p_3$)**
b) **Outlet air temperature ($T_{out}$).**

Figure III.3.a shows temporal evolution of average temperature of a plat absorber (T$p_1$ T$p_2$, T$p_3$) and Figure III.2.b shows temporal evolution Outlet air temperature ($T_{out}$) at a solar irradiance I = 323.55 W/m² under different mass flow rate levels (0.01, 0.015, 0.02, 0.025 kg/s ).

In Figure III.3.a, the plat absorber temperature reaches steady state around 45 to 52°C, with values decreasing as masse flow rate increases: 0.015 kg/s gives the highest plat absorber temperature T*p* = 51.5°C, followed closely by 0.01 kg/s with T*p* = 50.3°C, then 0.02 kg/s T*p* = 47.3°C and 0.025 kg/s the lowest T*p*= 45.1°C.

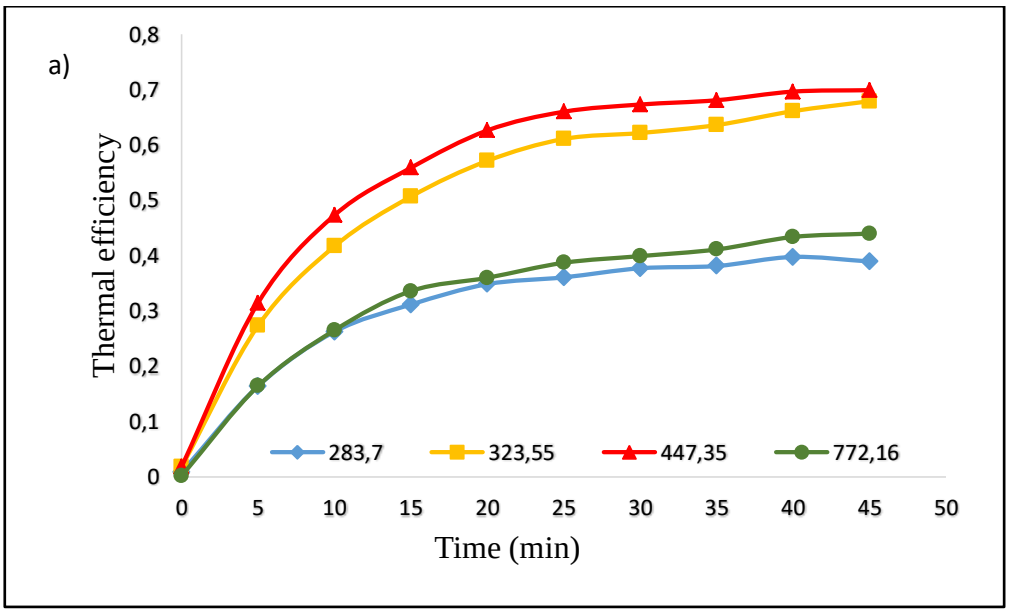
In Figure III.3.b, the outlet air temperature shows a different ordering: 0.01 kg/s reaches the highest plat absorber temperature $T_{out}$ = 46°C, followed by 0.015 kg/s with $T_{out}$ = 43.5°C, then 0.02 kg/s $T_{out}$ = 37°C and 0.025 kg/s $T_{out}$= 34.4°C.

This reflects the classic trade-off in solar air heaters: lower flow rates give the air more residence time to absorb heat, raising $T_{out}$ = 46°C (hence 0.01 kg/s leads in figure III.3.b), but the slower flow also means heat is removed from the plat absorber less efficiently, allowing the plat absorber temperature T*p* itself to run hotter (hence 0.015 kg/s edges out 0.01 kg/s in figure III.3.a), though both top plate values are close, suggesting a balance point near this flow rate.

As mass flow rate increases from 0.02 to 0.025 kg/s, both T*p* and $T_{out}$ decrease consistently, since the higher convective coefficient h removes heat faster from the plate absorber temperature (lowering T*p*) but the shorter residence time per air parcel limits the temperature rise (lowering $T_{out}$) an overall efficiency reduction in terms of absolute outlet temperature gain.

### III.2.2 Thermal efficiency Behavior of PSC

#### A. Radiation effect



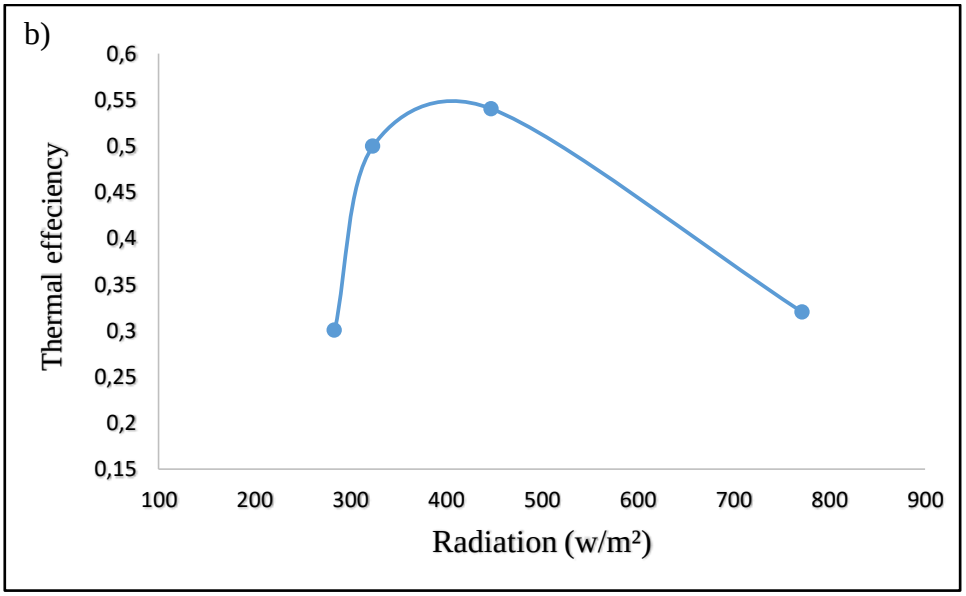



***Fig III. 4 a) Temporal evolution of Thermal efficiency at ṁ= 0.015 kg/s under different solar irradiance levels (283.7, 323.55, 447.35 and 772.16W/m²), b) Thermal efficiency as a function of irradiance at constant mass flow***

Figure III.4 shows the transient and steady-state thermal efficiency (η) performance of a conventional solar air collector. The test was carried out over a continuous period of t=45min, at a constant fluid mass flow rate of ṁ = 0.015 kg/s, across four separate levels of solar irradiance (283.7, 323.55, 447.35 W/m², and 772.16 W/m²).

In Figure III.4.a, the four curves show rapid exponential asymptotical growth during the initial operating phase (from t = 0 to 20 min). This initial sharp rise indicates that upon startup, the useful heat extraction rate ($\dot{m}\, C_p\, (T_{out} - T_{in})$) increases rapidly as the fluid channel in the convection heat transfer system stabilizes. Between t = 20 and 35 (min), the efficiency growth rate ($d\eta/dt$) slows down due to a concurrent increase in the steady-state updraft. After t= 35 min, the curves reach a perfectly steady level, confirming that the system has reached a fully stable thermodynamic equilibrium.

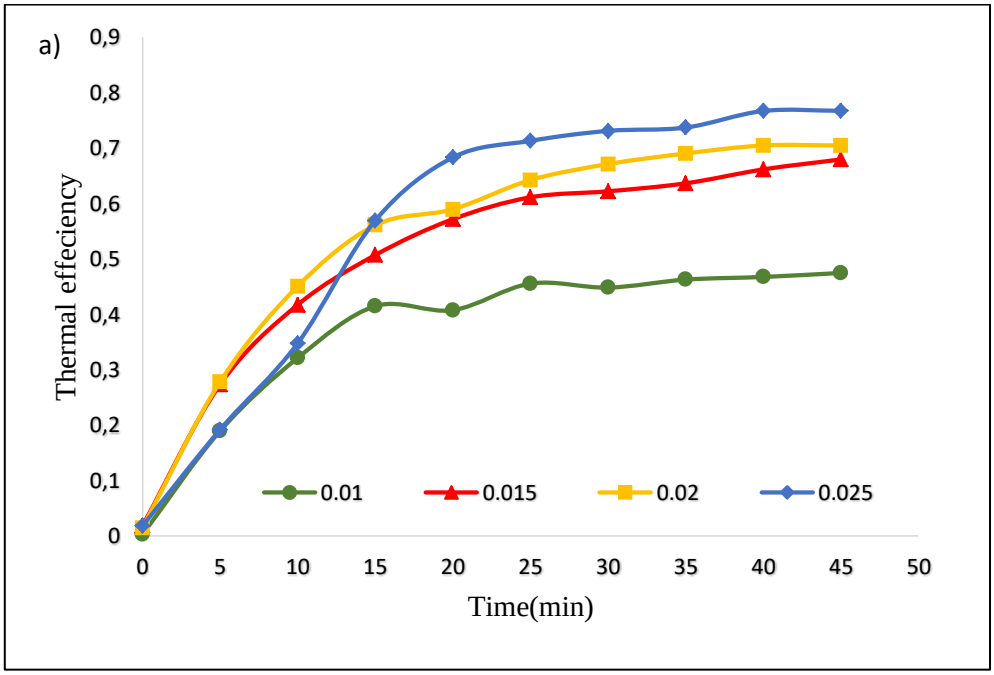
Figure III.4. b. Steady-state heat conversion efficiency versus solar irradiance ($\eta = f(I)$). The discrete data points extracted at the steady-state limit t = 45 minutes show a parabolic nonlinear performance trend as a direct function of incident solar irradiance: at the baseline solar irradiance level (I = 283.7 W/m²), the collector operates at a steady-state heat conversion efficiency of 29.99%. Increasing the irradiance flux to I = 323.55 W/m² results in a sharp rise in performance, raising the conversion efficiency to 49.94%. The heat conversion capacity stabilizes and reaches its absolute peak at an average irradiance of I = 447.35 W/m², resulting in a maximum heat efficiency of 54%. Beyond this optimum heat flux region, intensifying the

irradiance source to 772.16 W/m² leads to a significant drop in performance, forcing the power efficiency down to 31.96%.This behavior is primarily governed by the main thermodynamic efficiency equation for a solar air collector:

$$\eta = \frac{\dot{m} \cdot Cp \cdot (Tout - Tin)}{I.Ap} \quad \text{.....(III.2)}$$

Physically, the initial upward trajectory (from 283.7 to 447.35 W/m²) represents an efficient operating system, as the increasing temperature gradient between the absorber plate and the air facilitates the transfer of useful convection heat to the fluid stream. However, the sharp drop in efficiency to 31.96% at a peak solar irradiance of 772.16 W/m² highlights the aerodynamic limitations of an unmodulated, smooth, empty channel.

**B. Mass flow effect**



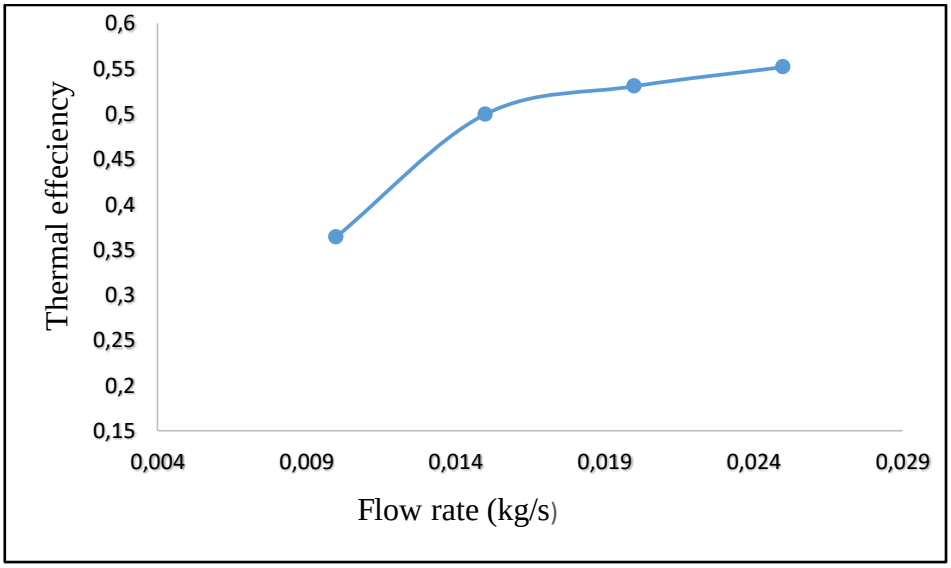



***Fig III. 5 a) Temporal evolution of Thermal efficiency at constant solar irradiance I=323.550 W/m² under different mass flow levels, b) Thermal efficiency as a function of mass flow at constant solar irradiant***

Figure III.5 shows the transient and steady-state thermal efficiency (η) performance of a conventional solar air collector. The test was carried out over a continuous period of t=45min, at a constant solar irradiance of I = 323.55 W/m², across four separate air mass flow rates (0.01, 0.015, 0.02, and 0.025 kg/s).

In Figure III.5.a. All four parametric curves show a rapid and sharp exponential rise during the initial startup period (from t = 0 to 20 minutes). This behavior indicates that the convection heat extraction rate $\dot{m}$ Cp ($T_{out}$ – $T_{in}$) increases rapidly upon startup of the flux channel. Between t = 20 and 35 (min), the efficiency curves begin to curve as the system approaches thermodynamic equilibrium. After exceeding 35 (min), the curves plateau, indicating the attainment of a fully steady-state equilibrium.

In Figure III.5.b. Steady-state thermal efficiency versus fluid mass flow rate (η = f($\dot{m}$)). Discrete data points extracted at the steady-state limit t = 45 min show a continuous and monotonous upward performance trajectory as a direct function of the fluid mass flow rate: at the minimum mass flow rate ($\dot{m}$ = 0.01 kg/s), the collector operates at the lowest steady-state thermal efficiency of 36.41%. Increasing the fluid flow rate to $\dot{m}$ = 0.015 kg/s results in a significant jump in performance, raising the efficiency to 49.94%. Raising the mass flow rate to $\dot{m}$ = 0.02 kg/s leads to a continuous increase in conversion power, reaching 53.03%. At the maximum experimental flow configuration ($\dot{m}$ = 0.025 kg/s), the system achieves peak performance, registering a maximum steady-state efficiency of 55.15%.

This relative growth is governed by the standard collector efficiency relation:

$$\eta = \frac{\dot{m}.Cp.(Tout - Tout)}{I.Ap} \text{.....(III.3)}$$

Physically, this behavior represents a classic heat transfer optimization in fluid dynamics. Low mass flow rates (0.01 kg/s) produce low velocities within the smooth channel, resulting in a thick thermal boundary layer and a restricted convection heat transfer coefficient (h). Since the passing air cannot efficiently dissipate the trapped heat flux, the absorber plate heats up excessively, leading to significant heat losses at the top

$$Q_{loss} = h\ Ap\ (Tp - Tamb) \text{ .....(III.4)}$$

Through the glass cover, maintaining the foundation efficiency at 47.43%. In contrast, increasing the mass flow rate to 0.025 kg/s accelerates the fluid transfer velocity, reducing the thickness of the lamellar boundary layer and significantly increasing the convection heat transfer coefficient (h). This forced loading cools the boundaries of the solid absorber plate, lowering the plate's steady-state temperature (T*p*). By reducing the temperature gradient impacting the external environment, the top heat losses are significantly suppressed. Consequently, although the net rise in fluid temperature (ΔT) is lower due to the increased volume of flowing fluid, the absolute rate of energy extraction increases, raising the net steady-state efficiency to a peak of 55.15%.

## III.3 Solar air collector with a metallic tubular absorber (SCT)

To enhance the convective heat transfer between the absorber surface and the drying air, a modified absorber design was developed and integrated into the solar collector. The conventional flat-plate absorber was replaced with an assembly of nine rough-surfaced aluminum tubes. The outer surfaces of the tubes were coated with matte black paint, selected for its high solar absorptivity and low reflectivity, in order to maximize the absorption of incident solar radiation while minimizing optical losses.

Compared with a conventional flat absorber, the cylindrical geometry of the tubes provides a larger effective heat transfer area, thereby promoting stronger convective heat exchange between the absorber and the flowing air. In addition, this configuration ensures a more uniform distribution of the absorbed heat flux along the collector length, reducing localized overheating and improving the overall temperature uniformity.

Furthermore, the rough surface of the aluminum tubes plays a key role in enhancing the collector's thermal performance. It further reduces surface reflectivity, thereby increasing the amount of absorbed solar energy. At the same time, the roughness disrupts the thermal boundary layer developing along the tube walls and promotes local turbulence in the airflow. These effects enhance the convective heat transfer coefficient, resulting in more efficient heat

transfer from the absorber to the drying air and, consequently, improving the overall thermal efficiency of the solar collector.

### III.3.1 Comparative Thermal Performance of Flat-Plate and Tube-Integrated Absorbers

***A.*** ***Radiation effect :*** **at a constant mass flow rate of ṁ = 0.015 kg/s**

**Absorber temperature**

***Fig III. 6 Temporal evolution of the absorber average temperature for the PSC***

**Figure III.6** presents the temporal evolution of the average absorber plate temperature (**Tp**) for the

collectors exhibit a rapid temperature increase during the initial heating period, followed by a gradual stabilization toward a quasi-steady state as thermal equilibrium is reached.

At both investigated solar irradiance

). Under the lower irradiance level of 278.15 W/m², the absorber plate temperature reaches a steady state at the end of the transient period (t = 45 min).

***Table III. 1 Comparative Thermal Performance of PSC and SCT Collectors Under Low and High Solar Irradiance Conditions***

| Parameter | Low Irradiance G = 278.15 W/m² | High Irradiance G = 447.35 W/m² |
|---|---|---|
| Tp PSC (°C) | 48.93 | 67.67 |
| Tp SCT (°C) | 51.90 | 72.47 |
| ΔTp (°C) | +2.97 | +4.80 |
| Relative thermal gain (%) | +6.07 % | +7.09 % |

The superior thermal performance of the **tube-integrated solar collector (SCT)** compared with the **conventional flat-plate collector (PSC)** is attributed to its larger effective heat transfer area and the disruption of the thermal boundary layer by the rough tubes, which enhances the convective heat transfer coefficient (**h)**. Increasing the solar irradiance from **278.15 to 447.35 W/m²** improves the thermal performance of both collectors; however, the temperature difference between the SCT and the PSC increases from **2.97 °C to 4.80 °C**, demonstrating that the tube-integrated design utilizes high solar irradiance more efficiently by significantly reducing convective and radiative heat losses through the glass cover.

1. Air temperature rise ΔT

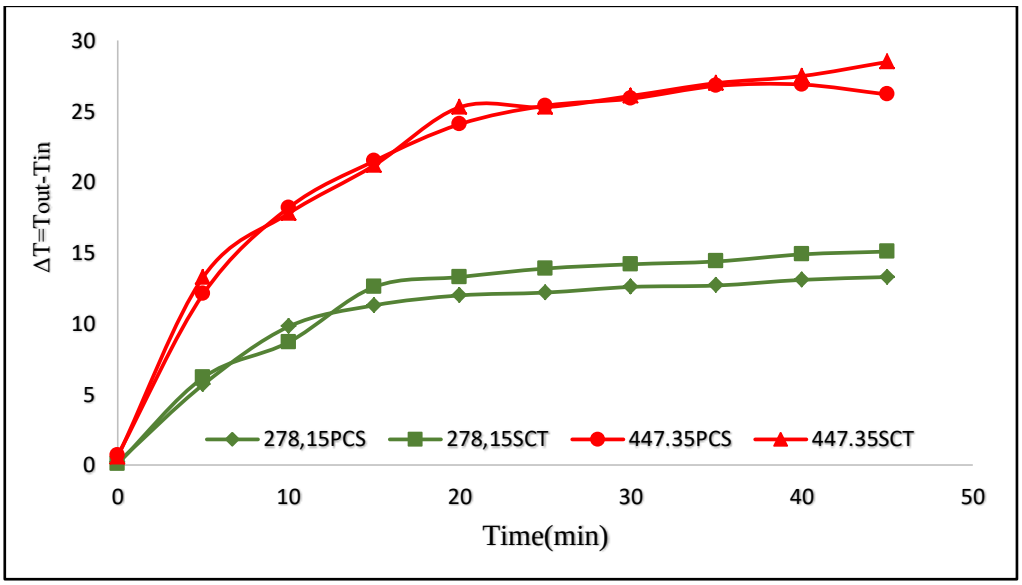



***Fig III. 7 Temporal evolution of the air temperature rise (ΔT = Tout − Tin) across the PSC and SCT collectors under two solar irradiation levels (278.15 W/m² and 447.35 W/m²) at a constant mass flow rate of ṁ = 0.015 kg/s***

Figure III.7 illustrates the temporal evolution of the air temperature rise ($\Delta T = T_{out} - T_{in}$) for the PSC and SCT collectors under two solar irradiance levels (278.15 and 447.35 W/m²) at a constant air mass flow rate of 0.015 kg/s, highlighting their transient thermal behavior

A comparative analysis of the system's performance at a low solar irradiance level of 278.15W/m² shows that the temperature differential trends for both collector designs remain relatively similar throughout the tracking period. At the end of the transient test cycle (t=45min), the air temperature rise stabilized at 15.10 °C for the pipe-integrated SCT configuration, while the conventional flat PSC design reached 13.30 °C. This indicates a clear improvement in net thermal performance of 1.80 °C in favor of the SCT, demonstrating that even under low irradiance, the pipe arrangement facilitates a more efficient conversion of the captured flux into a perceived fluid enthalpy.

***ar irradiance***

| Parameter | Low Irradiance<br>G = 278.15 W/m² | High Irradiance<br>G = 447.35 W/m² |
|---|---|---|
| ΔT PSC (°C) | 13.30 °C | 26.20 °C |
| ΔT SCT (°C) | 15.10 °C | 28.50 °C |
| Relative thermal gain (%) | +1.80 °C | +2.30 °C |

The results confirm the thermal superiority of the SCT collector over the PSC under all tested conditions, with an advantage that becomes more pronounced as solar irradiation increases. The temperature rise ΔT represents a direct indicator of the useful thermal power output, according to the relation $Q = \dot{m}\ Cp\ \Delta T$, and its enhancement through the SCT

configuration directly translates into an improvement of the overall thermal efficiency of the system.

## 2. **Thermal efficiency**

***Fig III. 8***

Figure III.8 presents temporal evolution of the thermal efficiency ($\eta_{th}$

***Table III. 3***

***solar irradiance***

| Parameter | Low Irradiance<br>G = 278.15 W/m² | |
|---|---|---|
| $\eta_{th}$ PSC | 55.59 % at 45 min | |
| $\eta_{th}$ SCT | 63.11 % at 45 min | |
| gain (%) | **+7.52 %** | **+5.98 %** |

At low irradiance (278.15 W/m²), the SCT achieves a net efficiency gain of +7.52 %, demonstrating superior solar flux conversion even under reduced solar input.

At high irradiance (447.35 W/m²), the PSC exhibits a notable efficiency drop of −1.82% between t = 40 and t = 45 min, while the SCT continues to improve, widening the performance gap to +5.98 % at the end of the operating period.

This behavior highlights the vulnerability of conventional flat-plate collectors to thermal degradation under prolonged high-intensity solar exposure, a limitation effectively mitigated by the SCT tube-integrated design.

**B.** ***Mass flow effect:*** **at a constant solar irradiance of I=447.35 W/m²**

## 1. Absorber temperature

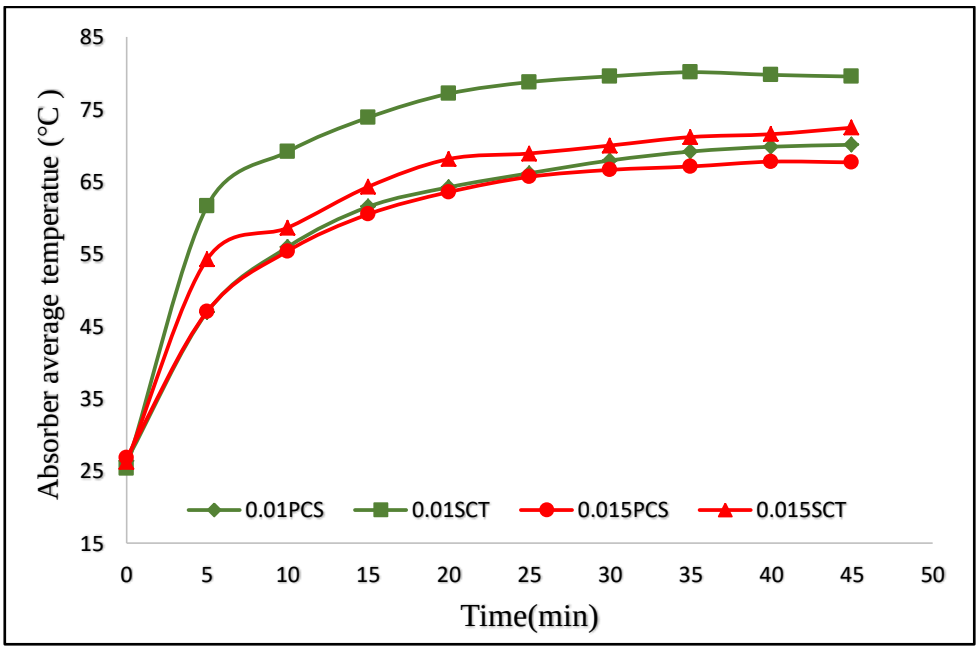



***Fig III. 9 Temporal evolution of the absorber average temperature TP for the PSC and SCT collectors under two mass flow rate levels (ṁ = 0.01 kg/s and 0.015 kg/s) at a constant solar irradiation I= 447.35 W/m²***

Figure III.9 shows how the absorber average temperature evolves over 45 minutes for two collector types PSC and SCT at two mass flow rates (ṁ = 0.01 kg/s and 0.015 kg/s), under a constant irradiation of 447.35 W/m².

.

At the same flow rate, the SCT collector consistently reaches higher absorber temperatures than PSC:

This thermal enhancement is directly attributed to the geometric modification of the SCT collector (incorporating flexible aluminum tubes on the absorber plate). The corrugations significantly increase the effective heat exchange surface area and generate local turbulence in the air flow, which disrupts the thermal boundary layer and enhances the heat transfer rate.

A higher mass flow rate increases the fluid velocity inside the channel, which elevates the convective heat transfer coefficient. Consequently, heat is extracted more rapidly from the absorber plate by the passing air stream, cooling the plate down while simultaneously increasing the thermal energy carried away by the fluid.

### 1. Air temperature rise ΔT

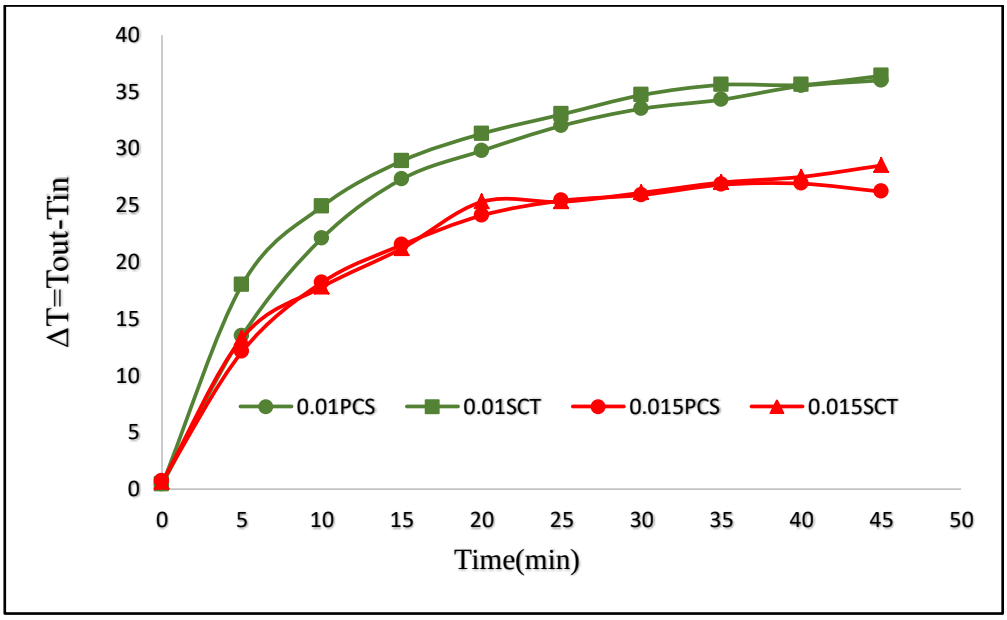



***Fig III. 10 Temporal evolution of ΔT=Tout-Tin for the PSC and SCT collectors under two mass flow rate levels (ṁ = 0.01 kg/s and 0.015 kg/s) at a constant solar irradiation I= 447.35 W/m²***

Figure III.10 the evolution of the air temperature difference, ΔT = Tout − Tin, as a function of time for the two solar collector configurations (PSC and SCT) at two mass flow rates (0.01 and 0.015 kg/s) shows under a constant irradiation of 447.35 W/m².

tube-integrated geometry enhances heat transfer more effectively at higher airflow rates.

Overall, increasing the mass flow rate from 0.01 to 0.015 kg/s reduces the air temperature difference for both collectors. Nevertheless, the SCT consistently maintains a higher $\Delta T$ than the PSC, confirming its superior heat transfer capability due to the increased internal heat exchange surface and the enhanced convective heat transfer.

## 2. **Thermal efficiency**

***Fig III. 11 Temporal evolution of the thermal efficiency***

***I= 447.35 W/m²***

Figure III.10 shows the evolution of the **thermal**

constant irradiation of 447.35 W/m².

At a mass flow

.5%, compared with 62.8% for the PSC, indicating a slight improvement resulting from the tube-integrated design.

Increasing the mass flow rate

%, whereas the PSC attains about 69.8% at 45 min. This corresponds to an efficiency improvement of approximately 4.2 percentage points in favor of the SCT.

Overall, increasing the mass flow rate

convective heat transfer and improves the overall thermal efficiency of the solar air collector, particularly at higher airflow rates.

***Table III. 4 Comparison of thermal efficiency ηth between PSC and SCT configurations under low and high mass flow rate.***

| Parameter | $\dot{m}$ =0.01 kg/s | |
|---|---|---|
| $\eta_{th}$ PSC | 62.8 % at 45 min | |
| $\eta_{th}$ SCT | 63.5 % at 45 min | |
| gain (%) | **+0.7 %** | |

## III. 4 Summary of key performance indicators for both configurations

| Parameter | Condition | PSC (flat-plate) | SCT (tubular) | Δ |
|---|---|---|---|---|
| **ABSORBER TEMPERATURE** | **quasi-steady state (t = 45 min)** | | | |
| Tp at I = 278.15 W/m², ṁ = 0.015 kg/s | Quasi-steady state | | | |
| Tp at I = 447.35 W/m², ṁ = 0.015 kg/s | Quasi-steady state | | | |
| Tp at I = 447.35 W/m², ṁ = 0.01 kg/s | Quasi-steady state | | | |
| Tp at I = 447.35 W/m², ṁ = 0.015 kg/s | Quasi-steady state | | | |
| **AIR TEMPERATURE RISE ΔT = Tout – Tin** | **quasi-steady state** | | | |
| ΔT at I = 278.15 W/m², ṁ = 0.015 kg/s | Quasi-steady state | | | |
| ΔT at I = 447.35 W/m², ṁ = 0.015 kg/s | Quasi-steady state | | | |
| ΔT at I = 447.35 W/m², ṁ = 0.01 kg/s | Quasi-steady state | | | |
| ΔT at I = 447.35 W/m², ṁ = 0.015 kg/s | Quasi-steady state | | | |
| **THERMAL EFFICIENCY ηth** | **effect of irradiance (ṁ = 0.015 kg/s)** | | | |
| η at I = 278.15 W/m² | Quasi-steady | | | |

| Parameter | Condition | PSC (flat-plate) | SCT (tubular) | Δ |
|---|---|---|---|---|
| | state | | | |
| η at I = 447.35 W/m² (optimal) | Quasi-steady state | 68.08 % | 74.06 % | +5.98 % |
| η at I = 283.7 W/m² (PSC only) | Quasi-steady state | | | |
| η at I = 772.16 W/m² (PSC only) | Quasi-steady state | | | |
| PSC efficiency drop (t=40→45 min, 447.35 W/m²) | Transient | | | |
| **THERMAL EFFICIENCY ηth effect of mass flow rate (I = 447.35 W/m²)** | | | | |
| η at ṁ = 0.01 kg/s | Quasi-steady state | | | |
| η at ṁ = 0.015 kg/s | Quasi-steady state | 69.8 % | 74.0 % | +4.2 % |
| **THERMAL EFFICIENCY ηth PSC baseline, effect of mass flow (I = 323.55 W/m²)** | | | | |
| η at ṁ = 0.01 kg/s | Quasi-steady state | | | |
| η at ṁ = 0.015 kg/s | Quasi-steady state | | | |
| η at ṁ = 0.02 kg/s | Quasi-steady state | | | |
| η at ṁ = 0.025 kg/s (peak) | Quasi-steady state | | | |
| **BEHAVIOURAL RESPONSE** | | | | |
| Optimal irradiance | — | | | |
| Optimal mass flow rate | — | | | |
| Overall average efficiency (comparable cases) | — | | | |

## III.4 Conclusion

The experimental investigation conducted in this chapter has provided a comprehensive comparative characterisation of two solar air collector configurations: a conventional flat-plate design (PSC) and a modified design integrating an array of aluminum tubes on the absorber surface (SCT), tested under varying mass flow rates and solar irradiance levels. The key findings of this study can be summarised as follows:

1. Flat-plate configuration (PSC):

- The collector achieved a maximum thermal efficiency of 68.08% under optimal irradiance conditions

  = 0.025 kg/s

  under I = 323.55 W/m².
- The thermal efficiency exhibited a bell-shaped response to solar irradiance, with a well-defined optimum

  driven by the disproportionate growth of thermal losses from the overheated absorber surface.
- At low irradiance levels (283.7 W/m²), efficiency dropped significantly to

  n the absorber and the fluid, limiting convective heat extraction.
- At high irradiance (772.16 W/m²), the absorber plate temperature decreased from 67.67°C to 58.13°C, confirming that the smooth-channel geometry is unable to handle elevated heat fluxes efficiently, as thermal losses through the glazing increase faster than the useful energy gain.
- A notable efficiency decline of −

  instability under prolonged high-intensity solar exposure.

2. Tube-integrated absorber configuration (SCT):

- Absorber temperatures were consistently higher than those of the PSC across all tested conditions: at ṁ =

  a gain of +11°C, confirming enhanced heat retention by the tube geometry.

- The longitudinal thermal gradient along the absorber was more effectively managed by the SCT, with the temperature difference between the two collectors increasing from +2.97°C at low irradiance (278.15 W/m²) to +4.80°C at high irradiance (447.35 W/m²), indicating that the tube-integrated design utilises high solar flux more efficiently.
-

a gain of +4.2 percentage points.

- Unlike the flat-

superior thermal robustness.

- The most significant improvement was recorded at low irradiance (I = 278.15 W/m²), where the SCT achieved 63.11% compared to only 55.59% for the PSC — an absolute gain of +7.52% — demonstrating that the tube geometry enhances heat transfer even under reduced solar input.
- Over all directly comparable test cases, the SCT achieved an

confirming the systematic and reliable superiority of the tube-integrated design regardless of the operating condition considered.

3. Over all conclusion:

These results confirm that the integration of aluminum tubes onto the absorber surface constitutes a meaningful and effective thermal enhancement strategy, simultaneously improving heat extraction efficiency, absorber temperature uniformity, and operational robustness across a wide range of flow rate and irradiance conditions. The SCT configuration demonstrated a consistently superior thermal response compared to the conventional flat-plate design, with particular advantages at high irradiance levels and elevated mass flow rates, where the limitations of the smooth-channel geometry are most pronounced. The tube-integrated absorber is therefore validated as a superior design for solar air heating applications, offering broader optimal operating conditions and greater resilience to thermal degradation under varying environmental inputs.

# Chapter IV

# Thermal Capture Analysis

## IV.1 Introduction

Experimental validation constitutes an essential step in evaluating the actual thermal performance of a solar air collector under real outdoor operating conditions. While laboratory experiments conducted using a solar simulator provided an initial characterization of the system's thermal behavior in a controlled environment, outdoor testing offers a more comprehensive assessment of its thermal response under the natural variability of meteorological conditions, particularly solar irradiance and ambient temperature.

The primary objective of this chapter is to investigate the performance of the solar air collector in its application to the drying of agricultural products. Following the thermal characterization of the two collector configurations—a conventional smooth absorber plate collector (PSC) and a solar air collector incorporating metallic tubes (SCT)—under laboratory conditions using a solar simulator, the collector was integrated into a complete solar drying system to evaluate its performance under real outdoor operating conditions.

## IV.2 Description of the Experimental Setup

The experimental setup consisted of a solar air collector coupled to an active-wall drying chamber through a

the atmosphere, while airflow throughout the system was maintained by a mechanical fan operating under forced convection conditions.

The outdoor experimental tests were conducted at the University of Tlemcen (34.9° N latitude, 1.3° W longitude) during

The following two days were dedicated to drying agricultural products using the two collector configurations successively: the conventional smooth absorber plate collector (PSC) on June 18 and the collector with a tubular absorber

(SCT) on June 22. This experimental approach enabled a rigorous assessment of the influence of the absorber geometry on the thermal performance of the solar drying system under real operating conditions. The experimental data collected included incident solar irradiance, ambient temperature, and the temperatures of both the absorber and the air at different locations throughout the system.

## IV.3 Experimental Results

The results presented in this section correspond to the experimental tests conducted over two separate days:

- June 18, 2026 (PSC): The experiment was carried out from 09:09 to 16:09 using a conventional flat-plate solar collector (PSC) with a smooth absorber and without integrated tubes.
- June 22, 2026 (SCT): The experiment was conducted from 09:09 to 17:25 using a solar collector with integrated tubes (SCT).

The comparison of the results obtained from these two experimental campaigns makes it possible to evaluate the effect of tube integration on the thermal performance of the solar collector, as well as its influence on the overall efficiency of the drying process.

### IV.3.1 Diurnal Variation of Solar Irradiance

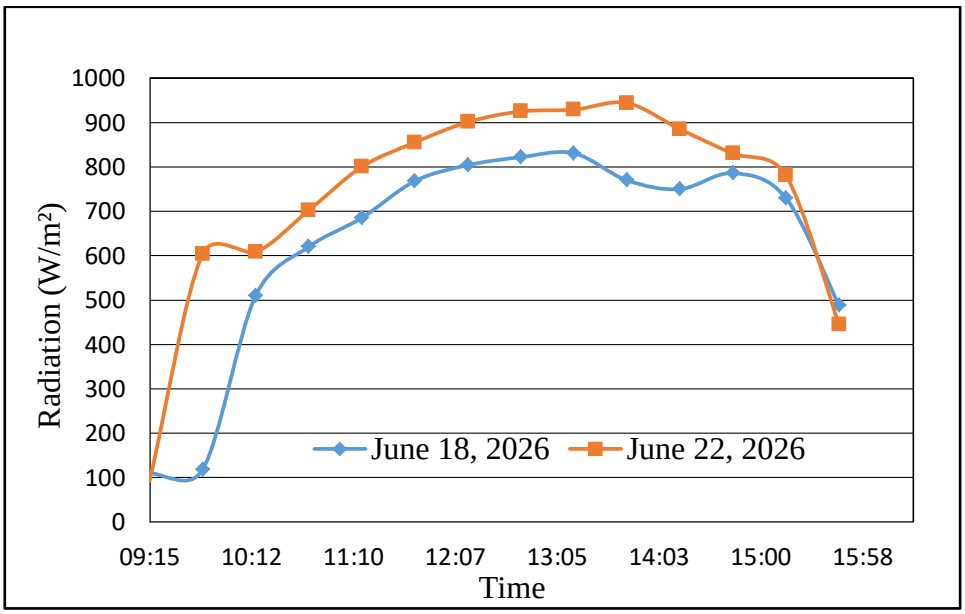



***Fig IV. 1 Temporal variation of solar irradiance on June 18th, and 22nd, 2026.***

Figure IV.1 illustrates the temporal evolution of the global solar irradiance (I) measured at the outdoor experimental site during the two test days, June 18 and June 22, 2026. These measurements highlight the different meteorological conditions to which the solar collector and the drying system were exposed, as well as their influence on the availability of solar energy.

- On June 18, 2026, the experiments started under unfavorable weather conditions characterized by low solar irradiance, with values of only 109.6 W/m² at 9:15 a.m. and 118 W/m² at 9:45 a.m., due to cloud cover or morning fog. Between 9:45 a.m. and 10:15 a.m., a rapid improvement in atmospheric conditions resulted in a significant increase in solar irradiance, rising from 118 W/m² to 510 W/m². Thereafter, the irradiance increased progressively, reaching a maximum value of 831 W/m² at 1:15 p.m. This evolution demonstrates the ability of the system to operate despite significant meteorological fluctuations and allows its thermal response to be evaluated under transient solar radiation conditions.
- June 22, 2026, corresponded to a day of intense sunshine, characterized by the highest solar irradiance levels recorded during the experimental campaign. Although the irradiance was low at the beginning of the measurements (92.8 W/m² at 9:15), it increased rapidly to 604 W/m² at 9:45. It then continued to rise, exceeding 900 W/m² at 12:15. (901 W/m²) and reaching a peak value of 944 W/m² at 1:45. These conditions provided a particularly favorable environment for the operation of the solar collector and enabled the evaluation of its performance under high solar irradiance.

For both test days, a gradual decrease in solar irradiance was observed from the beginning of the afternoon onward, as a result of the decreasing solar elevation angle and the corresponding increase in the solar zenith angle. Nevertheless, between 11:15 and 14:15, the solar irradiance remained above 750 W/m² during both experimental campaigns, ensuring a sufficient energy supply to provide effective air heating and promote the heat transfer required for the solar drying process.

### IV.3.2 Ambient Temperature Evolution

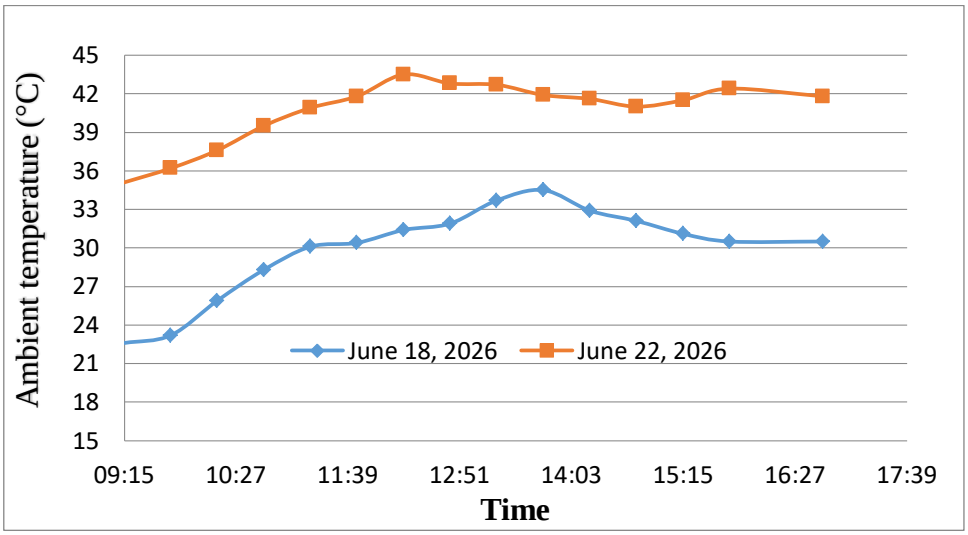



***Fig IV. 2 Ambient temperature profiles for June 17th, 18th, and 22nd, 2026.***

**Figure IV.2** compares the temporal evolution of the ambient temperature $T_{amb}$ recorded on **June 18 and June 22, 2026**

June 18, 2026: Reflecting the cloudy morning conditions, June 18 began with an initial low ambient temperature of 22.6°C at 9:15 and remained low at 23.2°C during the first 30 minutes. Following a rapid atmospheric clearing, the ambient temperature experienced a sharp and sustained rise. Interestingly, unlike the solar radiation, which peaked at minute 13:15, the ambient temperature continued to rise gradually, reaching its global daily peak of 34.5°C later at 13:45. This shift in the peak value demonstrates classic atmospheric inertia, where the surrounding air retains heat from the Earth for a considerable period after the peak of solar radiation has passed.

June 22, 2026: This campaign was conducted under a very hot thermal regime, representing the peak of summer weather. The initial morning temperature was remarkably high, reaching 35.1°C at 9:15. Due to the strong solar flux that day, the ambient temperature rose rapidly, exceeding 40.0°C by 11:15 (40.9°C) and reaching a maximum peak of 43.5°C at 12:15. Throughout the remainder of the afternoon, the ambient temperature remained consistently high, hovering above 41.5°C.

From an aerodynamic and thermodynamic perspective, the high ambient temperatures recorded on June 22 (over 41°C) and June 18 (over 33°C) play a significant role in reducing heat loss from the top and edges of the solar collector by lowering the temperature gradient

($\Delta T = T_{abs} - T_{amb}$). This significantly reduced environmental impact limits radiative and convection heat dissipation from the glass cover, thereby increasing the net heat energy transferred to the working fluid flowing through the metal pipes before entering the connected drying chamber.

## IV.4 Thermal performance and temperature profile of the solar collector

### IV.4.1 Diurnal Variation of Collector Component Temperatures

***Fig IV. 3 Temporal evolution of***

***June 18, 2026.***

**Figure IV.3** presents the temporal evolution of the absorber plate temperature T*p* outlet air temperature $T_{out}$ and ambient

solar radiation, with the absorber plate exhibiting the strongest thermal response.

Initial Cloudy Phase (9:15 to 9:45): During the first 30 minutes of the campaign, the solar collector operates under very limited thermal conditions due to the dense morning cloud cover and low radioactive flux (from 109.6 to 118 W/m²). At t 9:15 , the absorber plate temperature is close to the ambient temperature, at 30.7°C, while the air exiting the collector is 23.8°C compared to an ambient temperature of 22.6°C. This slight temperature difference confirms that the perceived heat buildup in the fluid is almost negligible during cloudy periods due to the insufficient incident energy on the unfanned absorber surface.

Rapid Transient Acceleration Phase (9:45 to 12:15): Following the rapid clearing of the atmosphere, the sudden increase in local solar irradiance leads to a massive thermal response in all components. The temperature of the absorber plate ($T_{abs}$) exhibits a sharp, almost vertical rise, increasing from 33.2°C at 9:45 to over 58.0°C at 10:15, and finally reaching 90.5°C at 12:15. In response to this intense plate heating, the incoming air successfully absorbs the heat energy via convection. The air outlet temperature ($T_{out}$) follows a parallel upward trajectory, steadily rising from 25.2°C (at 5:45) to a high operating temperature of 54.1°C at 12:15.

Midday Stabilization and Thermal System Peak (12:15 to 14:15): During this extended period, the solar collector reaches a near-steady operating state, with component temperatures hovering around their maximum values. The absorber plate temperature reaches its maximum of 92.3°C 13:15. Similarly, the air outlet temperature stabilizes at its highest thermal threshold, reaching a significant peak of 54.8°C at 13:45 This slight time lag between the absorber plate's maximum temperature and the air temperature peak highlights the thermal inertia of the inner liquid layer and the development of the plate's smooth boundary layer.

Late Afternoon Lag Phase (14:15 to 16:45): After 300 minutes, the natural decrease in the sun's azimuth angle causes a gradual decline in the incoming energy flow. As a result, the absorber plate temperature experiences a significant decrease, dropping from 90.2°C to 65.5°C at the end of the campaign (16:45). The air outlet temperature also decreases gradually and steadily, reaching 43.4°C.

From a purely thermodynamic perspective, the large temperature difference between the flat absorber plate and the flowing fluid ($\Delta T = T_{abs} - T_{out} \approx 35$ to 38°C during peak hours) indicates a major thermal bottleneck in simple flat plate designs. Because the smooth PSC design lacks extended heat transfer surfaces (fins) or internal turbulence inducers, the convection heat transfer coefficient between the absorber plate and the airflow remains essentially limited. The ordinary plate struggles to effectively dissipate the accumulated heat to the passing fluid, causing the absorber temperature to rise excessively to more than 92°C, which unnecessarily increases the radioactive and upper convection heat loss to the surrounding air ($T_{amb}$) and limits the final air outlet temperature to 54.8°C.

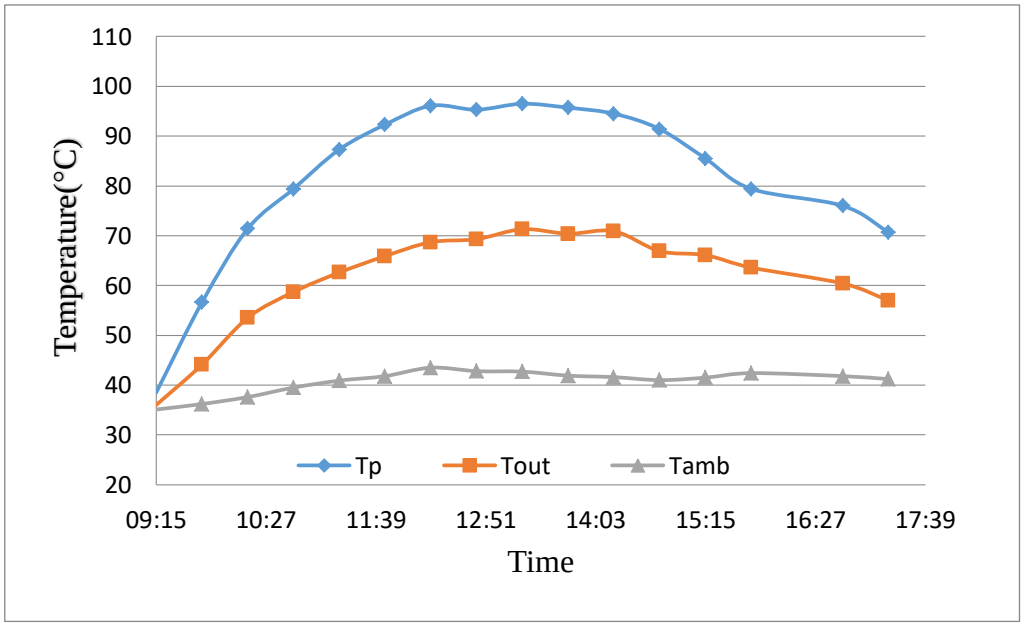



***Fig IV. 4 Temporal evolution of absorber plate, outlet air, and ambient temperatures for the SCT on June 18, 2026.***

**Figure IV.4** presents the temporal evolution of the absorber plate temperature T*p* outlet air temperature $T_{out}$ and ambient temperature $T_{amb}$ , recorded on **June 18, 2026**, for the SCT configuration.

The experimental curves show a highly responsive system characterized by rapid early morning heating, followed by an extended and highly efficient thermal production phase:

the initial sub-period and rapid thermal initialization (from 9:15 to 10:45). Thanks to exceptionally clear skies and strong local solar flux in the early morning, the solar collector exhibits an immediate thermal start-up. At 9:15, the initial conditions reflect a warm environment, with an ambient temperature of 35.1°C, an output temperature of 36.0°C, and an absorber temperature of 38.5°C. During the first 90 min, the absorber plate temperature undergoes a significant acceleration, rising by more than 40°C to reach 79.4°C. Importantly, the air outlet temperature corresponds to this rapid growth with a remarkable responsiveness, rising sharply to 58.7°C at 10:45. This slight initial delay indicates a highly reactive thermal coupling between the absorber matrix and the fluid stream.

The midday peak sustainable heating zone (11:15 to 14:15) During this central operating period, the integrated solar heating system (SCT) achieves its highest energy output under maximum local solar availability. The absorber plate temperature safely exceeds the 90°C threshold at 11:45 (92.3°C) and reaches its experimental maximum peak of 96.5°C at 13:15.

Simultaneously, the air circulating within these corrugated aluminum tubes captures this heat energy with exceptional efficiency, driving the air outlet temperature to a high maximum of 71.3°C at 13:15. The air outlet temperature remains constant above 70.0°C between 13:15 and 14:15, providing an ideal and highly stable inlet for the thermal fluid for the dual-drying application.

The late afternoon cooling and thermal storage phase (14:45 to 17:15): As the intensity of solar radiation decreases after minute 300, the component temperatures begin to gradually decrease. The temperature of the absorber plate drops from 94.5°C (at 14:15) to 70.7°C at the final measurement (17:15). Simultaneously, the air outlet temperature decreases from 70.9°C to 57.0°C. Remarkably, even at the end of the continuous 7.5-hour test, the air outlet temperature (57.0°C) remained significantly higher than the elevated ambient temperature (41.2°C), indicating continued heat conduction.

From a thermodynamic and fluid dynamics perspective, the remarkably narrow temperature difference between the absorber plate and the airflow ($\Delta T = Tabs - Tout \approx 25.2°C$ at peak hours) highlights the remarkable success of the compressed air cooling (SCT) system design compared to conventional smooth plates. The integration of flexible aluminum tubes acts as both a finned surface and an internal turbulence inducer. The corrugated tube shape breaks the laminar thermal layer of the passing air, inducing localized eddy currents that significantly increase the convection heat transfer coefficient. Consequently, instead of allowing the accumulated heat to stagnate on the absorber plate and escape via top loss, the SCT system rapidly harvests this energy and directs it to the working fluid, raising the usable air output to 71.3°C while keeping the plate temperature below 97°C.

### IV.4.2 Comparative Analysis of Temperature Gain and Thermal Efficiency for PSC and SCT Configurations

A. Temperature Gain ΔT

This section presents a comparative thermodynamic analysis of the air temperature rise ($\Delta T=T_{out} - T_{in}$) achieved by a smooth plate solar collector (PSC) and a solar collector with flexible aluminum tubing (SCT). The air temperature difference between the collector's inlet and outlet is a direct indicator of the net usable heat energy collected by the working fluid. By studying the concurrent data for both designs, the physical effect of integrating a corrugated

tubular absorber array over a conventional flat smooth plate can be determined with high precision under identical mass flow rate constraints (0.015 kg/s).

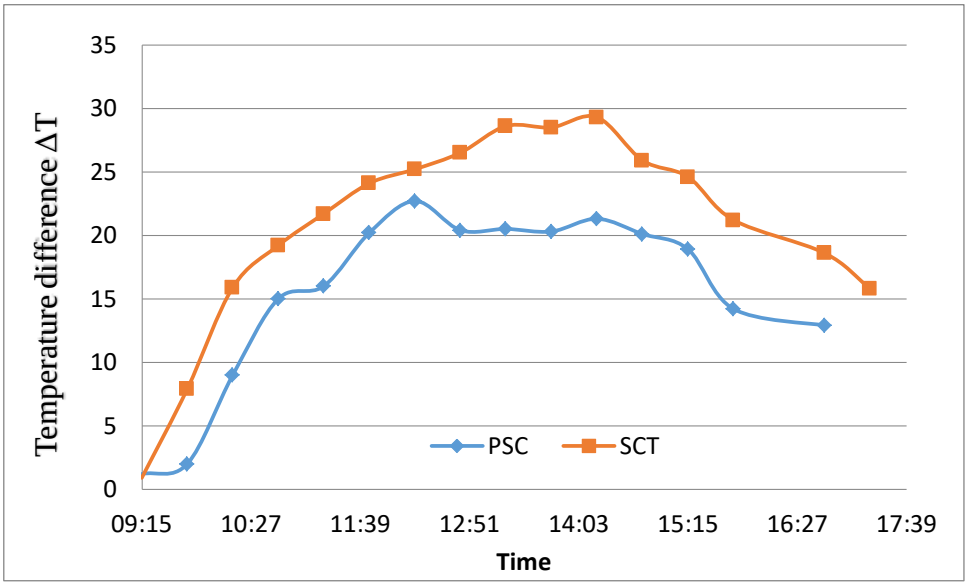



***Fig IV. 5 Daily variation of the temperature difference (ΔT) between PSC and SCT configurations.***

Figure IV.5 shows the temporal evolution of the temperature difference ΔT (°C), typically defined as the difference between the outlet and inlet air temperature (ΔT = T_outlet − T_inlet), for two collector configurations

The experimental data demonstrate a clear difference in heat collection performance, showing an immediate and sustained superiority of the finned tubular structure throughout the day-to-day tracking period.

Initial transition phase (from 9:15 to 10:15): At the start of field testing (9:15), both systems exhibited minimal fluid heating, with a temperature difference (ΔT) of 1.2 °C recorded for the PSC system and 0.9 °C for the SCT system. However, as local solar irradiance began to increase, the thermal response of the two systems diverged sharply. At 9:45, the air temperature rise in the SCT system jumped rapidly to 7.9 °C, while the smooth-flowing PSC system lagged significantly behind, reaching a minimum rise of 2.0 °C. At the one-hour mark (10:15), the SCT configuration produced a substantial performance gap, delivering an air temperature rise of 15.9 °C compared to only 9.0 °C produced by the PSC system.

Gradual growth and midday peak zone (10:45 to 14:15): During this period of high irradiance, the thermal gap between the two collectors stabilizes, demonstrating the high heat exchange

capacity of the finned tubular design. The air temperature rise within the PSC configuration exceeds the 20.0°C threshold at 11:45 (20.2°C), reaching an absolute experimental maximum of 22.7°C at 12:15, before stabilizing between 20.3°C and 21.3°C. In contrast, the SCT configuration exhibits a superior heating rate, exceeding the 20°C mark early at 11:15 (21.7°C) and maintaining a strong upward trajectory.

The SCT system exceeds the critical threshold of 25.0°C at 12:15 (25.2°C), and its maximum temperature rise reaches 29.3°C at 14:15, significantly outperforming the flat plate by 8.0°C. The late afternoon cooling phase (from 14:45 min to 15:45): As the solar flux decreases, both curves follow a parallel downward trend due to the decline in net felt heat input. At 15:45, the fluid temperature rise drops to 14.2°C in the PSC configuration. Remarkably, the SCT configuration maintains a highly efficient temperature rise of 21.2°C even during this late cooling period, which matches the absolute maximum performance that a normal flat plate can only achieve at midday peak.

From an aerodynamic and fluid mechanics perspective, the significant improvement in temperature difference ($\Delta T$) achieved by the SCT design is directly attributable to two interconnected physical mechanisms. First, the flexible aluminum tubes act as highly efficient extended fin surfaces, greatly increasing the net solid-to-fluid heat transfer area compared to the two-dimensional surface of the PSC. Second, the internal ripples and geometric curvature of the flexible tubes prevent the formation of a thick, insulating thermal boundary layer. Instead, these ripples generate local eddy currents and small secondary eddies that promote intensive fluid mixing. This fluid turbulence significantly increases the local convection heat transfer coefficient, ensuring that the heat energy absorbed by the metal matrix is rapidly extracted by the passing airflow rather than being lost to the surrounding environment through the top cover's dissipation.

B. Thermal Efficiency

This section presents a comparative analysis of the hourly thermal efficiency ($\eta$) profiles achieved by a smooth-panel solar collector (PSC) and a solar collector integrated with flexible aluminum tubes (SCT). Thermal efficiency is the critical indicator of a system's ability to convert incident solar radiation into usable sensible heat within a moving airflow. Examining these synchronous efficiency trajectories reveals the thermodynamic effect of using extended-finned geometries instead of standard smooth-panel solar collector systems.

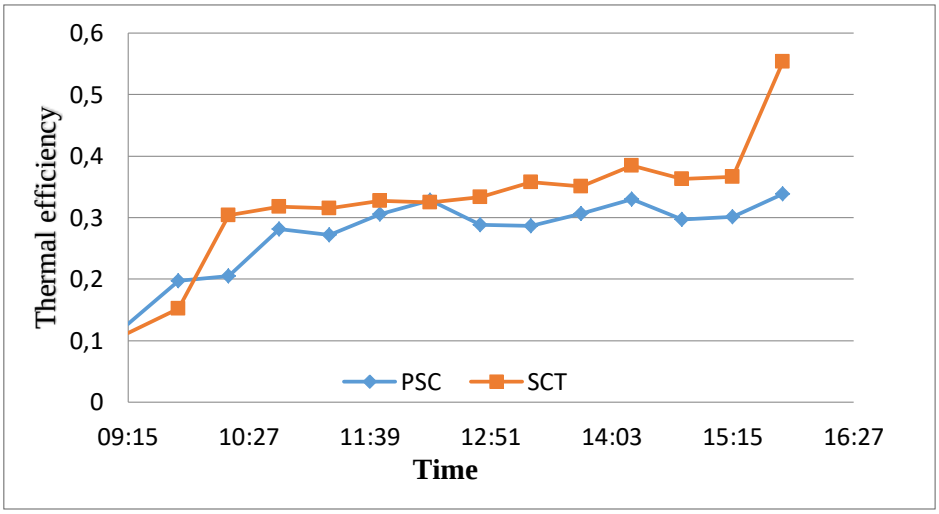



***Fig IV. 6 Temporal variation of thermal efficiency for both SCT and PSC configurations.***

Figure IV.6 shows the temporal evolution of the thermal efficiency typically for two collector configurations

The experimental data demonstrate a consistent and significant performance contrast between the two configurations, highlighting the immediate operational superiority of the tube structure:

Initial and Thermal Operation (9:15 to 9:45): At the start of testing (9:15), both collectors exhibited low efficiency, registering 12.7% for the PSC and 11.3% for the SCT, due to the cooled fluid and low initial solar irradiance.

At 9:44, as the collectors began to heat up, the PSC efficiency increased to 19.7%, while the SCT efficiency remained slightly lower at 15.2%. This short initial delay in SCT system configuration represents the time required for the aluminum tube block to accumulate sufficient internal heat before stable convection heat extraction could begin.

Convection Boost and Separation Phase (10:15 to 11:45): Once the initialization phase is complete, the SCT system exhibits an immediate and significant performance boost. At 10:15, the thermal efficiency of the SCT system rises to 30.4%, surpassing the conventional PSC system which stops at 20.5%. During the subsequent period up to 11:45, the SCT system maintains a consistent advantage over the ordinary plate collector, with its efficiency increasing sequentially from 31.8% (10:45) to 32.8% (11:45), while the smooth PSC configuration fluctuates less, ranging between 27.2% and 30.6%.Midday stability zone (from 12:15 to 14:15): Within this optimal operating range, the systems reach a quasi-thermodynamically stable state. At t = 180 min, the curves briefly converge as the

photovoltaic solar cell efficiency reaches a local peak of 32.8%, close to the SCT value of 32.5%. However, beyond this point, the smooth plate collector suffers increased heat dissipation due to the higher temperature of its plates, resulting in a decrease in efficiency to 28.7% at 13:15. In contrast, the SCT design maintains high heat extraction rates, keeping its efficiency above 33.3% (12:45) and gradually increasing to 38.5% at 14:15. The late afternoon slowdown and sudden peak phase (14:45 to 15:45): After 14:15, the natural breakdown of the solar radiation profile causes a rapid mathematical shift in the efficiency calculation

$$\eta = \frac{\dot{m}.Cp.(Tout-Tin)}{I.A} \quad \text{.....(VI.1)}$$

Since the incident solar radiation intensity (I) decreases much faster than the sensible heat stored within the metal structures, both designs show an upward trend in calculated efficiency near the end of the test. In the final hour (15:45), the efficiency of the PSC system reaches 33.8%, while the efficiency of the SCT system accelerates to an exceptional peak of 55.4%. From a fluid dynamics and energy conservation perspective, the high efficiency of the SCT system is directly dependent on the advanced heat removal factor ($F_R$). In a smooth-surfaced PSC system, the flat surface area of the plate limits the convective heat transfer coefficient from the solid to the fluid, causing the absorber plate to retain heat, thus increasing its temperature and amplifying radioactive and convective losses. In contrast, the flexible aluminum tubes in the SCT system act as large-area internal fins, increasing the contact area with the moving air. Simultaneously, the corrugated internal structure breaks down the thick insulating boundary layer, generating continuous mixing and minor secondary eddy currents. This fluid turbulence significantly increases the convective heat transfer coefficient, rapidly transferring the captured solar energy to the working fluid and resulting in a highly efficient and stable solar air collector.

## IV.5 Conclusion

The experimental investigation conducted under real outdoor conditions demonstrated the thermal performance of both the smooth plate solar collector (PSC) and the flexible aluminum tube solar collector (SCT). The

ambient temperatures above

**41 °C** on June 22, providing favorable conditions for solar heat collection.

The comparative analysis revealed the clear superiority of the **SCT** configuration over the conventional **PSC**. Owing to the combined effect of the flexible aluminum tubes acting as extended heat

plate and the outlet air confirmed a more efficient heat extraction process and lower thermal losses.

The SCT also

validate the proposed design concept and demonstrate that integrating corrugated flexible aluminum tubes into a flat-plate solar collector is an effective strategy for improving thermal performance, making the SCT a reliable heat source for solar drying applications under varying climatic conditions.

# General Conclusion

# General Conclusion

This work presents an experimental investigation of an indirect solar air collector designed for the drying of agri-food products. The main objective is to enhance the collector's thermal performance by modifying the absorber geometry. Two configurations were designed and compared: a conventional flat-plate solar air collector (PSC) used as the reference configuration, and an innovative solar air collector (SCT) incorporating flexible aluminum tubes attached to the absorber plate to increase the heat transfer surface area. The study consisted of two experimental phases: the first was conducted under controlled laboratory conditions using a solar simulator to characterize the thermal behavior of the collector, while the second involved outdoor experiments carried out at the University of Tlemcen in June 2026 under real meteorological conditions to evaluate the performance of the complete solar drying system.

**Laboratory experiments**

- The conventional flat-plate solar collector (PSC) achieved a maximum thermal efficiency of **68.08%** under a solar irradiance of **447.35 W/m²** and an airflow rate of **0.015 kg/s**, confirming this flow rate as the optimum operating condition.
- The solar collector equipped with

  **to +7.52%**.
- The tubular configuration systematically produced higher outlet air temperatures, with an average increase of **2.30 °C** compared with the flat-plate collector, indicating enhanced convective heat transfer between the absorber and the working fluid.
- The SCT collector maintained superior thermal performance as solar irradiance increased, demonstrating a greater capacity to capture incident solar energy while limiting absorber overheating and thermal saturation.
- The experimental results confirmed that integrating rough-surfaced flexible aluminum tubes is a simple, cost-effective, and efficient solution for improving the thermal performance of solar air collectors.

**Outdoor experiments**

The complete indirect forced-convection solar drying system was assembled by coupling the collector with

The SCT collector achieved a maximum outlet

- 

ign under real operating conditions.

- The smaller temperature difference between the absorber and the outlet air observed for the SCT configuration indicates more effective heat extraction and reduced thermal losses through the collector glazing.
- Drying experiments performed using

applications under the climatic conditions of the Tlemcen region.

**Recommendations and future work**

- Evaluate the system performance over a longer period and throughout different seasons in order to assess its behavior under a wide range of climatic conditions.
- Investigate the potential for large-scale manufacturing and industrial implementation of the proposed collector using locally available materials to further reduce production costs and promote its adoption in the agricultural sector.

# Reference

[1] Ministère de la Transition Énergétique et des Énergies Renouvelables (MTEER), Programme National des Énergies Renouvelables 2020–2030, Algérie. https://creg.gov.dz › la-production-de-lelectricite › Consulté le 10/06/2026

[2] International Energy Agency (IEA), Algeria Energy Profile, 2023. https://www.iea.org › energy-mix. Consulté le 09/06/2026.

[3] BP Statistical Review of World Energy, 2022. https://www.energyinst.org.. Consulté le 09/06/ 2026

[4] J. P. Nadeau, J. R. Puiggali. Séchage : des processus physiques aux procédés industriels.

Technique et Documentation, Lavoisier, Paris, France 1995.

[5] M. Daguenet, Les séchoirs solaires : théorie et pratique, Publications de l'UNESCO. Paris,

France. (1985).

[6] ELWAKEEL, A.E., GAMEH, M.A., EISSA, A.S. et MOSTAFA, M.B. Quality evaluation of dried tomato fruit and optimization of drying conditions using a modified solar dryer integrated with an automatic solar collector tracker. Scientific Reports (Nature Publishing Group), mars 2025. DOI : 10.1038/s41598-025-89248-x

[7] SANDALI, M., BOUBEKRI, A. et MENNOUCHE, D. Thermodynamic study of four environmental variables and their impact on the kinetics of solar drying of tomatoes during four seasons. Journal of Sustainable Development of Energy, Water and Environment Systems (JSDEWES), 2024, vol. 12, n° 2, art. 13-611. DOI : 10.13044/j.sdewes.d13.0611

[8] FADHIL, G.Q. et ABDUL HUSSEIN, S.A. Effect of air flow rate variation on the performance of an indirect solar dryer using flat and perforated absorber plates. ResearchGate Preprint, 2024.

[9] CASTRO, C. Solar dryers : heat transfer and air movement. Solar (MDPI), 2024, vol. 4, n° 2, p. 345–378. DOI : 10.3390/solar4020015

[10] El-Sebaii, A. A., & Shalaby, S. M., "Solar Drying of Agricultural Products: A Review", Renewable and Sustainable Energy Reviews, 2012.

[11] Madhwesh N., Vasudeva Karanth K., Shiva K ," Heat transfer enhancement of a solar air heater using capsule-shaped turbulators: a numerical analysis" , Scientific Reports , 2025

[12] Foued Chabane and Zouhair Aouissi, "Experimental investigations on the thermal efficiency of a solar air collector with transverse rectangular baffles inclined by an angle of 135°", Energy and Built Environment, 2024

[13] Yusaidi N.J. et al. , "Theoretical and experimental investigations on the effect of

double pass solar air heater with staggered-diamond shaped fins arrangement", Case Studies

in Thermal Engineering , 2024

[14] Maniyanthottil , Y. Srikanth , P. Balakrishnan , "Experimental comparison of thermal,

economic, and environmental outcomes in open-cut fin solar air heaters" , Solar Energy ,

2025

[15] Abou-Ziyan H. et al., "Optimal orientation of phase change material energy storage

systems for different performance indicators and charging levels" , Case Studies in Thermal

Engineering , 2025

[16] Murat Oztürk , Coskun Yüksel ,Erdem Çiftçi , "Energy, exergy and sustainability analysis of a photovoltaic-thermal solar system with nano-enhancement and thermal energy storage integration" , Process Safety and Environmental Protection , 2024

[17] Noureddine Embarek a, Hocine Guellil , Abdel Illah Nabil Korti , Ibrahim Sulimieh ," An experimental investigation on the influence of auxiliary heater position and wavy fin inclination on the performance of a novel hybrid solar air heater with phase change material" , Applied Thermal Engineering , 2026

[18] Lingayat, A., Das, P., & Chandramohan, V.P. , "A detailed review on performance

enhancement of solar air collector systems", Applied Thermal Engineering , 2025

[19] Muhammad Sajawal and al ," Experimental thermal performance analysis of finned

tube-phase change material based double pass solar air heater" , Case Studies in Thermal Engineering ,2019

[20] Oussama Oulad Belkhier and Abdelbasset Moulay Brahim , “Conception, Réalisation et investigation expérimentale d’un procédé de séchage solaire avec système de stockage d’énergie thermique “, Université Ghardaia ,2022

[21] Murat Oztürk , Erdem Çiftçi , “ Upgrading the performance of a solar air collector with flexible aluminum air ducts and graphene nanoplatelet-enhanced absorber coating”, Thermal Science and Engineering,2023

[22] Korti, A.I.N., & Khaldi, S. , “ Experimental and thermodynamic optimization of a compact indirect solar dryer using a staggered C-finned absorber: Balancing energy and exergy efficiency”,Energy,2026

[23] Mbaye, B.C., Le Bideau, P., Coly, M.L., Thiam, O.N., Magueresse, A., Sambou, V., Sow,M.L.,” Experimental performance of an indirect solar dryer with hot air recycling for mango drying”,Solar Energy , 2026

[24] Midoun, N., Kholkhal, B.,”Amélioration des performances d’un séchoir solaire a capteur plan “, 2024

**ملخص**

تقدم هذه الدراسة عملاً تجريبياً لمقارنة مجمّعين شمسيين للهواء غير مباشري الجريان ، ومصممين لتجفيف الأغذية الزراعية: المجمّع الشمسي التقليدي ذو اللوح المسطح (PSC)، ومجمّع شمسي مبتكر مزود بأنابيب ألومنيوم مرنة (SCT) تم تطويره لتعزيز انتقال الحرارة. أُجريت الاختبارات التجريبية في مختبر (ETAP) بجامعة تلمسان تحت مستويات إشعاع شمسي ومعدلات تدفق هواء مختلفة. وأظهرت النتائج تفوق المجمّع المزود بأنابيب مرنة (SCT) على المجمّع التقليدي (PSC)، حيث حقق متوسط زيادة في درجة حرارة الهواء قدره 2.30 درجة مئوية، وكفاءة حرارية أعلى بنسبة 5.98%.

بناءً على ذلك، تم ربط المجمّع بغرفة تجفيف لتشكيل نظام تجفيف شمسي متكامل يعمل بالحمل القسري غير المباشر. وأُجريت البحوث التجريبية في ظل ظروف مناخية حقيقية بجامعة تلمسان خلال شهر يونيو 2026 لكلا التصميمين (PSC و SCT). وأكدت النتائج التجريبية موثوقية النظام: حيث سجل المجمّع المبتكر (SCT) درجة حرارة للهواء الخارج بلغت 71.3 درجة مئوية، مقارنة بـ 54.8 درجة مئوية للمجمّع التقليدي (PSC)، ما يمثل زيادة في درجة الحرارة بمقدار 16.5 درجة مئوية، كما حقق كفاءة حرارية قصوى بلغت 55.4%، في حين حقق المجمّع التقليدي (PSC) نسبة 33.8%. وتثبت هذه النتائج أن دمج أنابيب الألومنيوم المرنة في مجمّعات الهواء الشمسية يعد حلاً بسيطاً، واقتصادياً، وفعالاً لتعزيز الأداء الحراري لمجمّعات الهواء الشمسية وتحسين الكفاءة العامة لأنظمة التجفيف الشمسية.

**الكلمات المفتاحية:** مجمّع هواء شمسي، التجفيف الشمسي، لوح ماص مستوٍ، أنابيب ألومنيوم مرنة، الكفاءة الحرارية، الطاقة المتجددة.

**Abstract**

This work presents an experimental study comparing two indirect forced-convection solar air collectors designed for agricultural food drying: a conventional flat-plate solar collector (PSC) and an innovative solar collector equipped with flexible aluminum tubes (SCT), developed to enhance heat transfer. Experimental tests were conducted at the ETAP Laboratory of the University of Tlemcen under various solar radiation levels and airflow rates. The results showed that the SCT outperformed the PSC, providing an average air temperature increase of 2.30 °C and a 5.98% higher thermal efficiency. The collector was subsequently coupled with a drying chamber to form a complete indirect forced-convection solar drying system. Experimental investigations were carried out under real climatic conditions at the University of Tlemcen during June 2026 for both configurations (PSC and SCT). The experimental results confirmed the reliability of the system: the SCT achieved an outlet air temperature of 71.3 °C, compared with 54.8 °C for the PSC, corresponding to a temperature gain of 16.5 °C, and reached a maximum thermal efficiency of 55.4%, whereas the PSC achieved 33.8%. These findings demonstrate that integrating flexible aluminum tubes into solar air collectors is a simple, cost-effective, and efficient solution for enhancing the thermal performance of solar air collectors and improving the overall efficiency of solar drying systems. **Keywords:** solar air collector, solar drying, smooth absorber plate, flexible aluminum tubes, thermal efficiency, renewable energy.

**Résumé**

Ce travail présente une étude expérimentale comparant deux capteurs solaires à air à circulation indirecte destinés au séchage agroalimentaire : un capteur plan conventionnel (PSC) et un capteur innovant à tubes flexibles en aluminium (SCT), conçu pour améliorer les échanges thermiques. Des essais expérimentaux ont été réalisés au niveau du laboratoire ETAP au sein de l'Université de Tlemcen sous différentes conditions de rayonnement solaire et de débit d'air. Les résultats ont montré que le SCT surpasse le PSC, avec une élévation de température de l'air plus élevée de 2,30 °C et un rendement thermique supérieur de 5,98 %.Le capteur a ensuite été couplé à une chambre de séchage afin de constituer un système complet de séchage solaire indirect à convection forcée. Des essais en conditions climatiques réelles ont été réalisés à l'Université de Tlemcen durant le mois de juin 2026 pour les deux configurations (PSC et SCT). Les résultats expérimentaux confirment la fiabilité du système : le SCT atteint une température de sortie d'air de 71,3 °C (contre 54,8 °C pour le PSC, soit un gain de 16,5 °C) et un rendement thermique maximal de 55,4 % (contre 33,8 % pour le PSC).Ces résultats prouvent que l'intégration de tubes flexibles en aluminium est une solution simple, économique et efficace pour

optimiser les capteurs solaires à air et les systèmes de séchage solaire **Mots-clés :** capteur solaire à air, séchage solaire indirect, absorbeur tubulaire, tubes flexibles en aluminium, transfert thermique, rendement thermique, énergie solaire.

REPUBLIQUE ALGERIENNE DEMOCRATIQUE ET POPULAIRE
Ministère de l'Enseignement Supérieur et de la Recherche Scientifique

Université Abou Bekr Belkaid Tlemcen

# Business Model Canvas

# BMC

Date de dépôt :

N° de projet :

Faculté/Institut :Technologie

Département :Génie mécanique

Nom du projet : Capteur Solaire à Air pour le Séchage des Produits Agricoles

Encadrant 1 : Guellil Hocine

Encadrant 2 : Khaldi Souhila

Co-encadrant 1 : Korti .A . Nabil

Co-encadrant 2 : Sari Hassoun Hind

Etudiants : - BEKKAYE AYMEN

- BEKHTI ADEM

Année universitaire : 2025/2026

## 1- Proposition de valeur (Value Proposition) القيمة المقترحة

a. Quels problèmes résolvons-nous pour nos clients ?

ما هي المشاكل التي نحلها لعملائنا ؟

Les pertes post-récolte sont importantes à cause de l'absence de moyens de séchage efficaces. Le séchage traditionnel à l'air libre est lent, dépendant de la météo et expose les produits à la poussière et aux insectes.
Les séchoirs électriques ou à gaz existants sont coûteux à l'achat et à l'usage pour les petits agriculteurs.
Notre capteur solaire à air résout ces problèmes en offrant un séchage rapide, propre et économique, grâce à une énergie solaire gratuite et renouvelable, sans recours à l'électricité ou aux combustibles fossiles.

b. Quels besoins de nos clients satisfont nos produits ou services ?

ما هي الاحتياجات التي يلبيها منتجاتنا أو خدماتنا لعملائنا؟

Nos clients ont besoin de conserver leurs produits agricoles plus longtemps, d'améliorer la qualité et l'hygiène du séchage, de réduire leurs coûts énergétiques et d'augmenter la valeur marchande de leurs produits grâce à un séchage maîtrisé et régulier.

c. En quoi notre offre est-elle différente de celle de nos concurrents ?

في ماذا تختلف عروضنا عن تلك التي يقدمها منافسونا؟

Contrairement aux séchoirs classiques, notre capteur solaire à air fonctionne sans électricité ni combustible, avec une conception simple, robuste et adaptée au contexte local, offrant un meilleur rendement thermique à un coût de fabrication très faible.

d. Quelles est notre proposition unique de valeur ?

ما هو العرض الفريد للقيمة لدينا؟

Un capteur solaire à air innovant, économique et écologique permettant aux agriculteurs de sécher leurs produits rapidement et hygiéniquement, en valorisant une énergie propre, gratuite et disponible localement.

## 2- Segments de clients (Customer Segment) انواع العملاء

a. Quels sont nos clients principaux?

من هم العملاء او الزبائن الرئيسيون ؟

Les petits et moyens agriculteurs ainsi que les coopératives agricoles locales.

b. Quels sont les différents segments de clients que nous visons ?

ما هي الفئات المختلفة من العملاء التي تستهدفها؟

Les agriculteurs individuels en zones rurales, les coopératives agricoles, les PME de transformation agroalimentaire (dattes, figues, tomates, plantes aromatiques et médicinales) et les institutions de développement rural.

c. Quels sont les besoins spécifiques de chaque segment de clients?
ما هي الاحتياجات الخاصة لكل فئة من العملاء؟
Les agriculteurs individuels recherchent une solution simple et abordable, les coopératives ont besoin d'une capacité de séchage plus importante, et les transformateurs recherchent une qualité constante et traçable.

d. Comment pouvons-nous catégoriser nos clients en groupes distincts?
كيف يمكن تصنيف عملائنا الى مجموعات مختلفة؟
En les classant selon la taille de l'exploitation, le type de produit à sécher, la localisation géographique (zones à fort ensoleillement) et la capacité d'investissement.

## 3- Relation avec les clients (Consumer Relationships) علاقة مع العملاء :

a. Quel type de relation chaque segment de clients attend il de nous ?
اي نوع من العلاقة يتوقعه كل فئة من العملاء منا؟
Un accompagnement technique personnalisé, une formation à l'utilisation et à l'entretien du séchoir, ainsi qu'un support après-vente de proximité.

b. Comment entretenons-nous actuellement les relations avec nos clients ?
كيف نحافظ حاليًا على العلاقات مع عملائنا؟
Par un contact direct sur le terrain, des démonstrations pratiques et un suivi régulier via les coopératives agricoles locales.

c. Comment pouvons-nous améliorer ou personnaliser nos interactions avec nos clients ?
كيف يمكننا تحسين أو تخصيص تفاعلاتنا مع عملائنا؟
En mettant en place un service après-vente, des supports pédagogiques (guides, vidéos) et un suivi via les réseaux sociaux et les groupes communautaires locaux.

## 4-Canaux de distribution ( Channels) قنوات التوزيع

a- Par quels canaux nos clients veulent-ils être atteints ?
من خلال أي قنوات يفضل عملاؤنا أن يتم التواصل معهم؟
Par la vente directe sur site, les démonstrations dans les foires agricoles, le bouche-à-oreille et les coopératives agricoles.

b- Quels canaux sont les plus efficaces pour atteindre chaque segment de clients ?

ما هي القنوات الأكثر فعالية للوصول إلى كل فئة من العملاء؟

Les démonstrations sur le terrain, les foires agricoles et le partenariat avec les chambres d'agriculture.

c- Comment pouvons-nous intégrer différents canaux pour améliorer l'expérience clients ?

كيف يمكننا دمج مختلف القنوات لتحسين تجربة العملاء؟

En combinant la présence physique (salons, démonstrations) avec une présence numérique (réseaux sociaux, site internet) pour assurer un parcours client cohérent.

## 5-Partenaires clés (Key Partnerships) : الشراكة الرئيسية

a. Qui sont nos partenaires clés ?

من هم شركاؤنا الرئيسيون؟

Les fournisseurs de matériaux (tôle, isolant, vitrage), la chambre d'agriculture, l'université (encadrement technique et recherche) et les organismes de financement (NESDA,ANGEM,CNAC).

b. Quels sont les partenariats qui nous aident à réduire les coûts, à accéder à de nouvelles ressources ou à améliorer notre proposition de valeur ?

ما هي الشراكات التي تساعدنا على خفض التكاليف أو الوصول إلى موارد جديدة أو تحسين قيمتنا المقترحة؟

Les fournisseurs locaux de matériaux à prix réduit, l'université pour le développement technique, et les organismes publics pour les subventions et le financement.

c. Comment pouvons-nous aligner nos intérêts avec ceux de nos partenaires ?

كيف يمكننا مزامنة مصالحنا مع تلك لشركائنا؟

En établissant des accords gagnant-gagnant, en partageant les objectifs de développement durable et en impliquant les partenaires dans la conception et les retours d'expérience.

## 6-Activités clés (Key Activities) :الأنشطة الرئيسية

a. Quelles sont les actions principales que nous devons entreprendre pour livrer notre proposition de valeur ?

ما هي الأنشطة الرئيسية التي يجب علينا القيام بها لتقديم قيمتنا المقترحة؟

La conception et la fabrication du capteur solaire à air, les tests et l'optimisation thermique, l'installation chez les clients, et la formation des utilisateurs.

b. Quelles sont les opérations essentielles pour notre entreprise ?

ما هي العمليات الأساسية لشركتنا؟

L'approvisionnement en matériaux, la fabrication et l'assemblage, le contrôle qualité, la distribution et le service après-vente.

c. Quelles sont les activités qui créent le plus de valeur pour nos clients ?

ما هي الأنشطة التي تخلق أكبر قيمة لعملائنا؟

L'optimisation du rendement thermique du capteur, l'amélioration de la qualité du séchage, et la réduction du temps de séchage.

## 7- Ressources clés (Key resources) :الموارد الرئيسية

a. Quels sont nos actifs matériels, immatériels et humains essentiels ?

ما هي الأصول المادية وغير المادية والبشرية الأساسية لدينا؟

Matériels : atelier de fabrication, matériaux (absorbeur, vitrage, isolant, structure métallique). Immatériels : savoir-faire technique et innovation. Humains : équipe technique encadrée par l'université.

b. Quels sont les outils, les technologies ou les partenariats dont nous avons besoin pour réussir ?

ما هي الأدوات والتكنولوجيا أو الشراكات التي نحتاجها لتحقيق النجاح؟

Des instruments de mesure thermique (capteurs de température, anémomètre), des logiciels de simulation thermique, et un partenariat avec le laboratoire de recherche de l'université.

c. Quels sont les principaux avantages concurrentiels de nos ressources ?

ما هي المزايا التنافسية الرئيسية لمواردنا؟

La maîtrise technique acquise par la recherche universitaire, le faible coût de fabrication avec des matériaux locaux, et l'expertise académique en énergie solaire.

## 8- Charges et coûts (Cost structure) :التكاليف

a. Quels sont les coûts fixes et variables associés à notre modèle économique ?

ما هي التكاليف الثابتة والمتغيرة المرتبطة بنموذجنا الاقتصادي؟

Coûts fixes : atelier, équipements de fabrication. Coûts variables : matériaux (tôle, vitrage, isolant), transport et installation.

b. Quels sont les coûts les plus importants pour notre entreprise ?

ما هي التكاليف الأكثر أهمية لشركتنا؟

Les matériaux de fabrication (vitrage, absorbeur, isolant) et la main-d'œuvre qualifiée.

c. Comment pouvons-nous réduire les coûts ou améliorer l'efficacité de nos opérations ?

كيف يمكننا خفض التكاليف أو تحسين كفاءة عملياتنا؟

En utilisant des matériaux locaux et recyclés, en optimisant la conception et en produisant en série.

## 9- Revenus (Revenue) مصادر الدخل:

a. Quels produits ou services nos clients sont-ils prêts à payer ?

ما هي المنتجات أو الخدمات التي يكون عملاؤنا على استعداد لدفع ثمنها؟

Le capteur solaire à air, son installation et sa mise en service, ainsi que la formation et la maintenance.

b. Quels sont les différents moyens par lesquels nous pouvons générer des revenus ?

ما هي الطرق المختلفة التي يمكننا من خلالها تحقيق الدخل؟

La vente directe des séchoirs solaires, les prestations d'installation et de maintenance, et les contrats de partenariat avec les coopératives.

c. Quel est notre modèle de tarification ?

ما هو نموذج التسعير لدينا؟

Un prix de vente fixé selon la capacité du séchoir, avec des tarifs préférentiels pour les achats groupés par les coopératives.

# Business Model Canevas : BMC

**Partenaires clés**
**Key Partnerships**
**الشراكة الرئيسية**

Fournisseurs de matériaux
Université (R&D)
Chambre d'agriculture
Organismes de financement

**Activités clés**
**Key Activities**
**الأنشطة الرئيسية**

Conception et fabrication
Installation
Formation
Maintenance

**Ressources clés**
**Key resources**
**الموارد الرئيسية**

Atelier de fabrication
Savoir-faire technique
Équipe encadrée (université)

**Proposition de valeur**
**Value Proposition**
**القيمة المقترحة**

Séchoir solaire à air
Économique et écologique
Rapide et hygiénique
Sans électricité

**Relation clients**
**Consumer Relationship**
**علاقة مع العملاء**

Accompagnement personnalisé
Formation à l'utilisation
Support après-vente

**Canaux de distribution**
**Channels**
**قنوات التوزيع**

Vente directe
Démonstrations terrain
Foires agricoles
Coopératives
Réseaux sociaux

**Segment client**
**Customer Segment**
**انواع العملاء**

Agriculteurs individuels
Coopératives agricoles
PME agroalimentaires

**Coûts**
**Coste structure**
**التكاليف**

Matériaux (bois 4 planches prix 9600DA ,peinture 400DA , 2 tôle 3000 DA , Tronçonneuse 7000DA 4 ventilateur 1000DA alimentation électrique 20000 DA , 9 tuyaux en aluminium 9000DA, 3m de laine de roche 3000DA , total =58000DA)
Main-d'œuvre
Atelier
Transport

**Revenus**
**Revenue**
**مصادر الدخل**

Vente des séchoirs
Services de séchage et de vente de produit agricoles .
Installation
Formation
Maintenance
Contrats coopératives

| Matériels | nombre | Prix Unitaire (DA) | Prix Total(DA) |
|---|---|---|---|
| bois | 4 | 1200 | 9600 |
| peinture | 1 | 400 | 400 |
| tôle | 2 | 3000 | 3000 |
| Tronçonneuse | 1 | 7000 | 7000 |
| ventilateur | 4 | 250 | 1000 |
| alimentation électrique | 1 | 20000 | 20000 |
| tuyaux en aluminium | 9 | 1000 | 9000 |
| laine de roche | 1 | 8000 | 8000 |
| PRIX TOTAL (DA) | | 58000DA | |